



**HAL**  
open science

# New bacterial transglutaminase Q-tag substrate for the development of site-specific Antibody Drug Conjugates

Eva Sivado

► **To cite this version:**

Eva Sivado. New bacterial transglutaminase Q-tag substrate for the development of site-specific Antibody Drug Conjugates. Immunology. Université de Lyon, 2018. English. NNT : 2018LYSE1261 . tel-02060540

**HAL Id: tel-02060540**

**<https://theses.hal.science/tel-02060540>**

Submitted on 7 Mar 2019

**HAL** is a multi-disciplinary open access archive for the deposit and dissemination of scientific research documents, whether they are published or not. The documents may come from teaching and research institutions in France or abroad, or from public or private research centers.

L'archive ouverte pluridisciplinaire **HAL**, est destinée au dépôt et à la diffusion de documents scientifiques de niveau recherche, publiés ou non, émanant des établissements d'enseignement et de recherche français ou étrangers, des laboratoires publics ou privés.



N°d'ordre NNT : 2018LYSE1261

**THESE de DOCTORAT DE L'UNIVERSITE DE LYON**

opérée au sein de  
**l'Université Claude Bernard Lyon 1**

**Ecole Doctorale N° ED 340**

**Biologie Moléculaire, Intégrative et Cellulaire (BMIC)**

**Spécialité de doctorat: Biochemistry**

**Discipline: Immunology**

Soutenue publiquement le 04/12/2018, par:

**Éva SIVADÓ**

---

**New bacterial transglutaminase Q-tag  
substrate for the development of site-specific  
Antibody Drug Conjugates**

---

**Devant le jury composé de:**

JOUBERT, Nicolas	MCU HDR	Université de Tours	Rapporteur
POUL, Marie-Alix	PU HDR	IRC Montpellier	Rapporteuse
BERNET, Agnès	PU HDR	CRCL Lyon	Examinatrice
CHARDÈS, Thierry	DR CNRS HDR	IRC Montpellier	Examinateur
VALSESIA-WITTMANN, Sandrine	Cadre Bio2 HDR	CLB	Directrice de thèse
EL ALAOUI, Saïd	CEO	Covalab	Co-directeur de thèse
MARTINEAU, Pierre	DR INSERM HDR	IRC Montpellier	Invité

# ACKNOWLEDGEMENT

---

First of all, I would like to thank Said El Alaoui, who established this project, for his confidence and for giving me the opportunity to learn a lot through working on such an interesting, innovative and challenging project. I would like to express my gratitude also for his valuable guidance as a co-supervisor of my thesis. This work has not been made possible by the contribution and support of my academic supervisor, Sandrine Valsesia-Wittmann, to whom I am really grateful not only for the scientific but also for her personal advises, for the “free-coaching” and sharing of “20-years of experiences”. I have really enjoyed working in her team, where I had chance to pick up some knowledge also in immunology and oncology. Working under their supervision not only allowed to progress but also encouraged me to continue working in research.

I would like to thank to all my colleagues at Covalab and CLB, especially to Sabrina, Tala, Anne-Cath and Meddy. I am grateful to Sabrina not only for the monoclonal antibody production but also the nice time we spent together inside and outside the lab. Thank you Tala for sharing “your mum” with me, your encouraging support and the nice time we spent together. I feel happy to find such a good friends as both of you.

Many thanks to all who contributed to my work, especially to IONTAS for big batch mAb production, to the team of Charles Dumontet for *in vivo* mice experiments, to Christophe Vanbelle for microscopy analysis, to Jean Guy Delcros for accepting the participation in my thesis committee and for Biacore measurement, to Pierre Martineau for accepting the participation in my thesis dissertation and committee and for supplying the scFv construct, to Guillaume Brachet-Schaeffer for the HIC analysis, to Camille Martin and Francesca Bryden for the MS analysis.

In addition I would like to thank to my examiners Dr. Nicolas Joubert and Dr Marie-Alix Poul for reviewing my thesis manuscript and to Prof Agnès Bernet, Dr Thierry Chardès and Dr Pierre Martineau for serving as my dissertation committee.

Last but not least, my heartfelt thanks go to my family, Béci and friends who have supported me a lot during the last years. I felt you very close despite the physical distance.

This work was supported by CLARA foundation and CIFRE.

# TABLE OF CONTENTS

---

<b>CONTENT OF TABLES AND FIGURES</b> .....	<b>5</b>
<b>SUMMARY</b> .....	<b>7</b>
<b>RÉSUMÉ</b> .....	<b>8</b>
<b>ABBREVIATIONS</b> .....	<b>9</b>
<b>1 INTRODUCTION</b> .....	<b>13</b>
1.1 TARGETED CANCER THERAPY .....	13
1.1.1 <i>Antibodies as therapeutic agents:</i> .....	13
1.1.2 <i>Antibody fragments:</i> .....	15
1.2 ANTIBODY-DRUG CONJUGATES.....	17
1.2.1 <i>Target and antibody:</i> .....	18
1.2.2 <i>Linker technology:</i> .....	19
1.2.3 <i>Cytotoxic payload:</i> .....	23
1.3 ADC DESIGN – TOWARDS HOMOGENEITY .....	27
1.3.1 <i>First generation:</i> .....	28
1.3.2 <i>Second generation:</i> .....	28
1.3.3 <i>Third generation:</i> .....	30
1.4 ANTIBODY-DRUG CONJUGATES IN THE CLINICS.....	35
1.4.1 <i>Gemtuzumab ozogamicin:</i> .....	38
1.4.2 <i>Inotuzumab ozogamicin:</i> .....	39
1.4.3 <i>Brentuximab vedotin:</i> .....	40
1.4.4 <i>Trastuzumab emtansine:</i> .....	41
1.5 TRANSGLUTAMINASES.....	46
1.5.1 <i>Mammalian transglutaminases:</i> .....	46
1.5.2 <i>General features of microbial transglutaminase:</i> .....	48
1.5.3 <i>Hypothetical catalytic mechanism of mTG:</i> .....	48
1.5.4 <i>Structure and substrate specificity of mTG:</i> .....	50
1.5.5 <i>mTG mediated conjugation of antibodies:</i> .....	52
<b>2 AIM OF THE THESIS</b> .....	<b>55</b>
<b>3 NEW BACTERIAL TRANSGLUTAMINASE Q-TAG SUBSTRATE FOR THE DEVELOPMENT OF SITE SPECIFIC ANTIBODY DRUG CONJUGATES</b> .....	<b>57</b>
AIM .....	57
ABSTRACT .....	59
3.1 INTRODUCTION.....	60
3.2 MATERIALS AND METHODS .....	62
3.2.1 <i>Construction of recombinant antibodies with glutamine tag</i> .....	62
3.2.2 <i>Expression and purification of recombinant antibodies</i> .....	64
3.2.3 <i>Enzymatic conjugation</i> .....	64
3.2.4 <i>MS analysis</i> .....	65

3.2.5	<i>Immunoreactivity analysis (Surface Plasmon Resonance)</i>	66
3.2.6	<i>Internalisation assay</i>	66
3.2.7	<i>In vitro cytotoxicity assay</i>	67
3.2.8	<i>Biodistribution</i>	67
3.2.9	<i>Tumor homing study</i>	68
3.2.10	<i>In vivo anti-tumor activity assay</i>	68
3.2.11	<i>Ethics statement</i>	69
3.3	RESULTS AND DISCUSSION	70
3.3.1	<i>Generation of site-specific immunoconjugates</i>	70
3.3.2	<i>Immunoreactivity and internalisation of the conjugates</i>	72
3.3.3	<i>In vitro cytotoxicity</i>	73
3.3.4	<i>In vivo biodistribution and tumor homing</i>	76
3.3.5	<i>In vivo anti-tumor activity</i>	77
3.4	CONCLUSION	79
3.5	REFERENCES	80
<b>4</b>	<b>GENERATION OF DIFFERENT ANTIBODY FORMATS FOR SITE-SPECIFIC CONJUGATION...</b>	<b>82</b>
	AIM	82
4.1	MATERIALS AND METHODS	83
4.1.1	<i>Construction of Fab and scFv antibodies fragments with Q-tag</i>	83
4.1.2	<i>Expression and purification of recombinant Fab</i>	84
4.1.3	<i>Expression and purification of recombinant scFv</i>	85
4.1.4	<i>Enzymatic conjugation</i>	86
4.1.5	<i>Immunofluorescent staining</i>	86
4.1.6	<i>Fluorescent activated cell sorting</i>	87
4.2	RESULTS AND DISCUSSION	88
4.2.1	<i>Enzymatic conjugation</i>	88
4.2.2	<i>Immunoreactivity analysis</i>	89
<b>5</b>	<b>OPTIMISED METHODS (SDS-PAGE AND LC-MS) REVEAL DEAMIDATION IN ANY TRANSGLUTAMINASES-MEDIATED REACTIONS</b>	<b>91</b>
	AIM	91
<b>6</b>	<b>CONCLUSION &amp; PERSPECTIVES</b>	<b>103</b>
<b>7</b>	<b>REFERENCES</b>	<b>108</b>
<b>8</b>	<b>PUBLICATIONS</b>	<b>118</b>

# CONTENT OF TABLES AND FIGURES

---

## INTRODUCTION

Table 1 ..... 25

Table 2 ..... 31

Table 3 ..... 34

Table 4 ..... 46

Figure 1 ..... 13

Figure 2 ..... 15

Figure 3 ..... 16

Figure 4 ..... 19

Figure 5 ..... 21

Figure 6 ..... 22

Figure 7 ..... 23

Figure 8 ..... 24

Figure 9 ..... 26

Figure 10 ..... 28

Figure 11 ..... 37

Figure 12 ..... 38

Figure 13 ..... 39

Figure 14 ..... 41

Figure 15 ..... 42

Figure 16 ..... 45

Figure 17 ..... 48

Figure 18 ..... 49

Figure 19 ..... 52

## **NEW BACTERIAL TRANSGLUTAMINASE Q-TAG SUBSTRATE FOR THE DEVELOPMENT OF SITE SPECIFIC ANTIBODY DRUG CONJUGATES**

Table 1 .....	62
Figure 1 .....	57
Figure 2 .....	63
Figure 3 .....	70
Figure 4 .....	72
Figure 5 .....	73
Figure 6 .....	75
Figure 7 .....	77

## **GENERATION OF DIFFERENT ANTIBODY FORMATS FOR SITE-SPECIFIC CONJUGATION**

Table 1 .....	83
Figure 1 .....	81
Figure 2 .....	87
Figure 3 .....	89

# SUMMARY

---

Antibody-drug conjugates (ADCs) are a powerful class of therapeutic agents, demonstrating success in the treatment of several malignancies. The currently approved ADCs are produced by chemical conjugations and exist as heterogeneous mixtures that negatively influence the pharmacokinetics and *in vivo* performance. Recently many of site-specific conjugation technologies have been developed to reduce heterogeneity and batch-to batch variability. Microbial transglutaminase (mTG) has been demonstrated as efficient tool for site-specific conjugation.

In this thesis we report the development CovIsoLink™ (Covalently Isopeptide Crosslinking) technology for the generation of homogenous immunoconjugates using a novel glutamine donor peptides (Q-tag) with improved affinity compared to the known peptides (ZQG, LLQG). As a proof of concept, the peptides sequences were engineered into the heavy chain C-terminal of Trastuzumab antibody. We demonstrated the reproducible and homogeneous conjugation of Q-tagged Trastuzumab with different payloads, without any unconjugated species. The ADCs were evaluated in series of *in vitro* and *in vivo* assays. We confirmed that the immunoreactivity and internalisation are not altered by the conjugation. Furthermore similar *in vitro* and *in vivo* tumor cell killing potency was demonstrated in comparison to Ado-Trastuzumab emtansine (Kadcyla®), which is already used in the clinic. Moreover we extend our site-specific conjugation technology to antibody fragments (Fab and scFv), evaluating their functionality by conjugation with AlexaFluor488-cadaverine and in antigen binding assays.

Thus, using novel glutamine donor peptides, our technology provides an alternative enzymatic conjugation strategy for the engraftment of different payloads resulting in homogeneous batches, without unconjugated species.

# RÉSUMÉ

---

Les ADCs (Antibody-Drug Conjugates) correspondent à une nouvelle stratégie thérapeutique anti-tumorale particulièrement prometteuse. Néanmoins, les ADCs actuellement utilisés en clinique sont obtenus par conjugaisons chimiques, résultant en des mixtures hétérogènes impactant négativement leurs pharmacocinétiques et leurs performances *in vivo*.

Récemment, différentes stratégies de couplage site-spécifique ont été développées afin de réduire cette hétérogénéité. Dans cette thèse, nous rapportons le développement d'une nouvelle technologie CovIsoLink™ (Covalently Isopeptide Crosslinking) permettant la génération d'ADCs par utilisation de nouveaux peptides glutamine Q-Tag présentant des affinités optimisées par rapport à des peptides disponibles (ZQG, LLQG) pour une enzyme bactérienne la transglutaminase (mTG).

La preuve de concept de cette technologie a été réalisée par insertion de ces peptides Q-Tag en C-ter de la région codant pour la chaîne lourde des anticorps anti-HER2 (Trastuzumab). Nous avons ainsi pu démontrer la conjugaison homogène et reproductible de différentes drogues sans contamination par des chaînes d'anticorps non conjuguées. Nous avons pu montrer que l'immunoréactivité et la capacité d'internalisation de ces ADCs n'étaient pas altérées par la conjugaison et qu'ils présentaient *in vitro* et *in vivo*, des propriétés de lyse de cellules tumorales similaires au Ado-Trastuzumab emtansine (Kadcyla®), actuellement en clinique. Par ailleurs, afin de généraliser notre technologie à différents formats d'anticorps nous avons générés des fragments Fab et scFv et évalué leur fonctionnalité.

Ainsi, nous avons pu prouver que l'utilisation de nouveaux peptides optimisés Q-Tag substrat de la transglutaminase permettait une stratégie de couplage alternative plus homogène par couplage de différentes molécules sans espèce contaminante non couplée.

# ABBREVIATIONS

---

AcBut	4-(4-acetylphenoxy)butanoic acid
ADC	Antibody-drug conjugates
ADCC	Antibody-dependent cellular cytotoxicity
Ala/A	Alanine
ALCL	Anaplastic large cell lymphoma
AML	Acute myeloid leukemia
Arg/R	Arginine
Asn/N	Asparagine
Asp/D	Aspartic acid
B-ALL	B-cell acute lymphoblastic leukemia
BMC	Metastatic breast cancer
BsAb	Bispecific antibody
CDC	Complement-dependent cytotoxicity
CDR	Complementarity determining region
CH	Constant heavy chain
CL	Constant light chain
CovADC-DM1	Trastuzumab-Qtag <sub>2</sub> -PEG <sub>4</sub> -SMCC-PAB-DM1
CovADC-MMAE	Trastuzumab-Qtag <sub>2</sub> -PEG <sub>4</sub> -VC-PAB-MMAE
CovIsoLink™	Covalently Isopeptide Crosslinking
Cys/C	Cysteine
DAPI	4',6-diamidino-2-phenylindole
DAR	Drug-to antibody ratio
DM1	N <sup>2'</sup> -Deacetyl-N <sup>2'</sup> -(3-mercapto-1-oxopropyl)maytansine

DM4	N <sup>2'</sup> -Deacetyl-N <sup>2'</sup> -(4-mercapto-4-methyl-1oxopentyl)maytansine
DMEM	Dulbecco's modification of Eagle medium
DMSO	Dimethyl sulfoxide
dNTP	Deoxynucleotide
EGFR	Epidermal growth factor receptor
Fab	Antigen-binding fragments
FACS	Fluorescent activated cell sorting
Fc	Fragment crystallisable
FcR	Fcy receptors
FcRn	Neonatal Fc receptor
FDA	US Food and Drug-Administration
Gln/Q	Glutamine
Glu/E	Glutamic acid
Gly/G	Glycine
HAS	Human serum albumin
HER2	Human epidermal growth factor receptor 2
His/H	Histidine
HL	Hodgkin's lymphoma
IC <sub>50</sub>	Half maximal inhibitory concentration
IgG	Immunoglobulin G
Ile/I	Isoleucine
K <sub>D</sub>	Equilibrium dissociation constant
K <sub>M</sub>	Michaelis constant
LC/MS	Liquid chromatography/mass spectrometry
Leu/L	Leucine
Lys/K	Lysin

mAb	Monoclonal antibody
MAPK	Mitogen-activated protein kinase
MDR	Multiple drug resistance
MMAE	Monomethyl auristatin-E
MMAF	Monomethyl auristatin-F
mTG	Microbial transglutaminase
NHL	Non-Hodgkin lymphomas
NHL	Non-Hodking lymphoma
NK	Natural killer cells
O/N	Overnight
OS	Overall survival
PBD	Pyrrlobenzodiazepine
PBS	Phosphate buffered saline
PCR	Polymerase chain reaction
PEG	Polyethylene glycol
PFS	Progression-free survival
Phe/F	Phenylalanine
PK	Pharmacokinetic
Q-tag	Glutamine donor peptide tag
rAb	Recombinant antibody
rh	Recombinant human
RT	Room temperature
scFv	Single chain variable fragments
SDS-PAGE	Sodium Dodecyl Sulfate polyacrylamide gel electrophoresis
SMCC	Succinimidyl-4-(N-maleimidomethyl)cyclohexane-1-carboxylate
SPDB	N-succinimidyl-4-(2-pyridyldithio)butanoate

SPR	Surface plasmon resonance
SRB	Sulforhodamine B
T-DM1	Ado-Trastuzumab emtansine /Kadcyla®
TG	Transglutaminase
TNF	Tumor necrosis factor family
Trp/W	Tryptophan
Tyr/Y	Tyrosine
Val/V	Valine
VC	Valine-citrulline
VH	Variable heavy chain
VHH	Single variable domain or nanobody
VL	Variable light chain
Wt	wild type

# 1 INTRODUCTION

---

---

## 1.1 TARGETED CANCER THERAPY

### 1.1.1 Antibodies as therapeutic agents:

In the recent years, antibody based therapies have achieved considerable success, particularly in oncology, chronic inflammatory and autoimmunity diseases. In this thesis, we focus on targeted therapy in cancer. The basis of tumor targeting mAbs relies on the difference in the target expression between the malignant and healthy tissues. Thanks to the high specificity of mAbs, targeted therapies can increase the efficacy and decrease the toxicity, leading to potentially improved clinical benefits<sup>1</sup>. Since the approval of the first therapeutic antibody, Rituximab (Rituxan; Genentech/Biogen Idec) by the US Food and Drug-Administration (FDA) in 1997 to treat patients with non-Hodking lymphoma (NHL)<sup>2</sup>, mAb-based medicines have become a major approach.

Antibodies can mediate their activity by different mode of actions. They can compete with other interaction partners in the antigen binding thus interfering with the function of the target signalling molecules or inducing apoptosis. In addition, once bound to their target, antibodies can exhibit several immunomodulatory effects through their fragment crystallizable (Fc) region. The Fc part of human IgG1 isotype can interact with Fcγ receptors (FcR) on immune effector cells, including macrophages, neutrophils, dendritic cells and natural killer (NK) cells, to trigger the elimination of tumor cells by phagocytosis, lysis or antibody-dependent cellular cytotoxicity (ADCC). It has been demonstrated that among them, ADCC plays the major role in the *in vivo* action of mAbs. Furthermore the targeted cells can be killed by complement-dependent cytotoxicity (CDC) through the interaction with the complement component C1q<sup>3</sup>.

However, the therapeutic activity of the naked mAb is limited mostly by the insufficient pharmacokinetics (PK), tissue penetration and interaction with the immune system. Thanks to the advanced developments in molecular biology, antibody engineering allows to modulate biological properties such as affinity, avidity, half-life and biodistribution as well as to generate different formats. Fc- and glycoengineering allow to optimise the effector functions and plasma-half life<sup>4</sup>. Beside the application of unconjugated antibodies for cancer therapy, mAb can be armed with highly potent cytotoxic drugs, cytokines or radionuclides to further enhance their clinical performance. In addition to the direct conjugation, cancer cells can be targeted by indirect arming approaches like liposome-encapsulated formats (immunoliposomes).

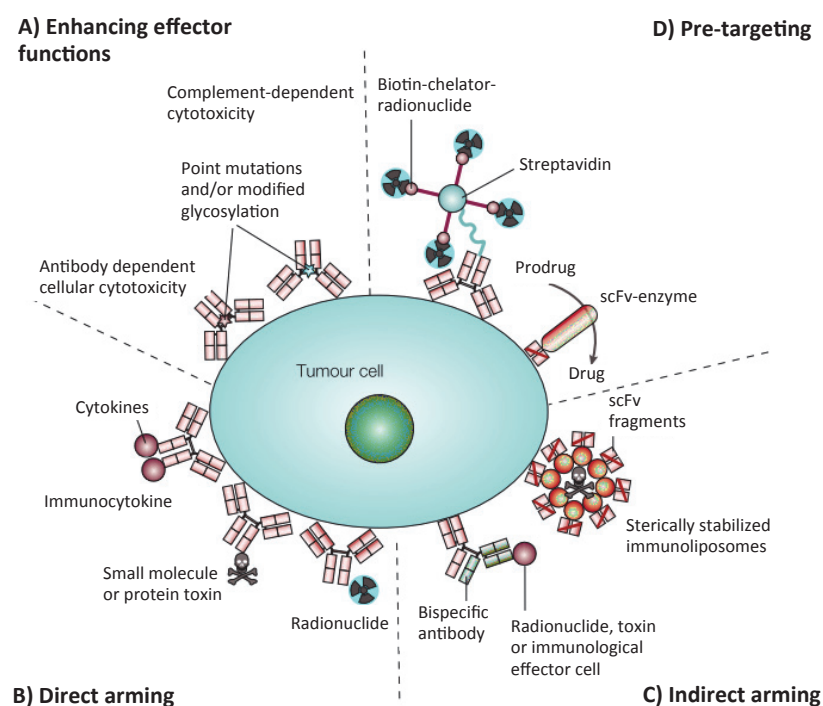


**Figure 1. Strategies for enhancing the potency of antitumour antibodies.** A) Enhancing antibody-dependent cellular cytotoxicity or complement-dependent effector functions by site-directed mutations and glycoengineering. B) Direct arming approaches involve conjugation of the antibodies to, cytokines, cytotoxic drugs/protein toxins and radionuclides. C) Indirect arming of antibodies can be generated by attaching engineered antibody fragments to the surface of liposomes loaded with cytotoxic compounds. D) Pre-targeting strategies are based on the prior administration of non-radioactive tumor antigen targeting antibody-constructs followed by the subsequent application of a radioactive labelled or low molecular weight substances (Figure taken from Carter *et al.*<sup>5</sup>).

On the other hand, bispecific antibodies (BsAbs) can be used either by indirect arming or direct arming or by bridging tumor cells to immune effector cells, since BsAbs have two different antigen binding sites. Pre-targeting strategies are based on the prior administration of non-radioactive tumor antigen targeting antibody-constructs followed by the subsequent application of a radioactive labelled or low molecular weight substances or the enzymatic activation of the prodrug on the tumor site. (**Figure 1**)<sup>5</sup>. The FDA approved antibodies as a single agents display modest activity against tumors, therefore they are often combined with conventional chemotherapy.

### 1.1.2 Antibody fragments:

Immunoglobulin G (IgG) is predominantly used format in current antibody drugs, but a few antibody fragment conjugates have been already approved<sup>4</sup>. This field is rapidly expanding, “the new age” is for the engineered multivalent antibodies in different formats and with modified structure.

IgG antibodies exhibit prolonged residence in the blood circulation, but on the other hand they have several limitations in cancer therapy including insufficient penetration into solid tumors due to their size or Fc $\gamma$ -mediated bystander activation of the immune system. The antigen-binding fragments can potentially overcome these limitations; because of their reduced size they can diffuse into the tumor mass more rapidly and efficiently. This benefit is counterbalanced with a shorter plasma-half life, due to the absence of the FcRn-mediated recycling<sup>6</sup>. Attempts are ongoing to optimize their pharmacokinetic properties. Some strategies have been developed to increase the *in vivo* half-life of the antibody fragments, by the chemical addition of polyethylene glycol (PEG)<sup>7</sup> or by the fusion to human serum albumin (HSA)<sup>8</sup>. However the long plasma half-life is not necessary for certain applications, where the risk of toxicity can be increased by prolonged exposure for example in radioimmunotherapy or imaging<sup>3</sup>.

Antigen-binding fragments (Fab), single chain variable fragments (scFv) and the “third generation” single variable domain (VHH or nanobody) represent the main types in antibody fragment technologies (**Figure 2**). **Fabs** are heterodimers, containing one

constant and one variable domain of heavy and light chains. Their *in vivo* performance has been well characterized and several of them have been already approved by FDA and introduced to the clinical treatment<sup>9</sup>.

**scFv** contains a single polypeptide chains, in which the variable region sequences of light and heavy immunoglobulin chains are fused together by flexible polypeptide linker. They retain the binding activity of the parental IgG molecule, although the avidity is different. Their serum half-life is very short (~2h), therefore many variants are generated to optimize avidity and stability<sup>9</sup>.

**Nanobodies** are a promising class of antibody fragments. They are expressed by camelids, consisting of a single monomeric variable antibody domain. They display high affinity against a large scale of antigens and very high stability, in addition they show considerable sequence homology with the human VHIII gene family. Furthermore they can be efficiently engineered as a part of more complex molecular scaffolds<sup>3</sup>.

These antibody fragment molecules opened up new perspectives for cancer therapy, making the antibody based drugs more efficient. Thus numerous companies are involved in their development and clinical evaluation.

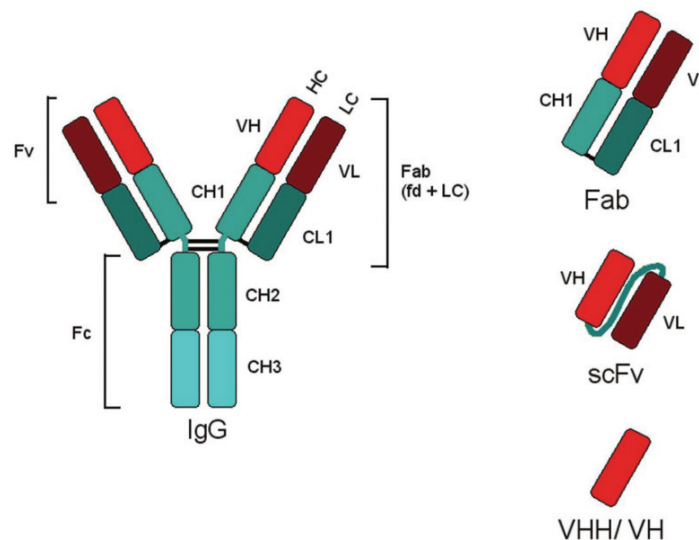


**Figure 2. Schematic representation of IgG molecule antibody fragment types.** CH, constant heavy chain; CL, constant light chain; IgG, immunoglobulin; Fab, antigen binding fragment; scFv, single chain variable fragment, VH, variable heavy chain; VL, variable light chain. (Figure taken and adapted from Nelson<sup>9</sup>)

## 1.2 ANTIBODY-DRUG CONJUGATES

Currently, cancer patients are mainly treated with surgery, chemotherapy, radiation, immunotherapy, targeted therapy or any of the combinations. Since chemotherapeutics agents are not specific for tumor cells, they have a systemic toxicity that limits the range of dosage between minimum effective dose and the maximum tolerated dose that can have an effective therapeutic response without significant adverse effects, called as therapeutic window. On the other hand, antibody therapies lack the full potential to kill tumor cells by their own, leading to acquired resistance during therapy or relapse after the treatment. Therefore, mAbs therapies are life-long, which is very expensive and not fully bearable. Antibody-drug conjugates (ADC) are an emerging class of anticancer agents; they designed to combine the advantages of mAbs and cytotoxic compounds: referred as the idea of the “magic bullet” concept postulated by Paul Ehrlich in 1900<sup>10</sup>. In ADCs, the drug is covalently conjugated to a tumor-antigen specific mAb *via* a synthetic linker. Upon binding to the respective antigen, the ADC-antigen complex becomes internalized through receptor-mediated endocytosis, from the endosomal vesicles they are transported to the lysosomes, where the ADC is degraded and the free cytotoxic agent is released inside

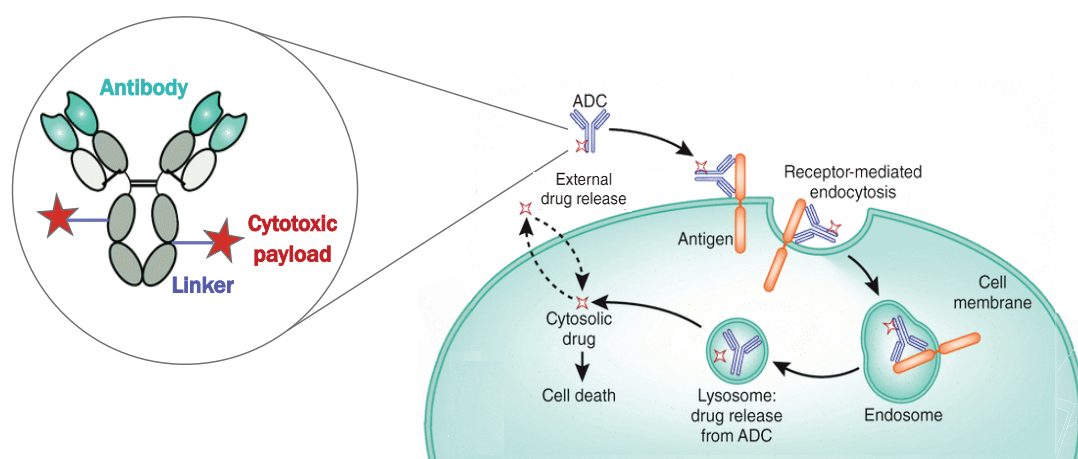


**Figure 3. General structure of antibody-drug conjugates and mechanism of action.** Upon ADC binding the antigen-ADC complex becomes internalized through receptor-mediated endocytosis. Following the degradation in the endosomal-lysosomal system the drug releases resulting in cancer cell death. (Picture taken and adapted from Senter & Sievers<sup>11</sup>).

the target cell, resulting in cell death. The drug may be released into the tumor environment and the neighbouring cells can be also killed due to the bystander effect (**Figure 3**). Thanks to the high selectivity, stability and PK profile of the mAbs, even 1000-fold more potent small-molecule toxins than the conventional chemotherapeutic drugs can be delivered inside the tumor cells in targeted manner. Thus, the percent of tumor reaching drugs are higher, the off-target side effects are lower that can improve the therapeutic window. In addition ADCs can overcome resistance against the unmodified antibodies<sup>12</sup>.

However the concept of ADC is simple, over the past 30 years, so far only four ADCs have reached to the clinic. This reveals the challenges and difficulties in the optimisation of the key parameters, since their structure are complex and each unit has different specific properties. The success of ADC depends on many factors, including the choice of the target tumor antigen, antibody, linker, cytotoxic agent and conjugation methods, which will be discussed below.

### **1.2.1 Target and antibody:**

The identification and validation of the proper target is the first major step in ADC development. The target should be localised on the cell-surface and homogeneously overexpressed on tumor cells compared to the normal tissues (low or normal expression level) to reduce off-target toxicity<sup>13</sup>. The problem of the heterogeneous antigen expression in solid tumors can be overcome by the conjugation of membrane-permeable drugs that can trigger cell death on the neighbouring cells following their cleavage and release so called “bystander effect”. However this bystander effect can increase the systemic toxicity in particular by release of drugs in negative normal cells.

The high specificity and affinity ( $K_D < 10$  nM) of the antibody are essential for the efficient uptake into the target cells<sup>14</sup>. However the  $K_D$  can affect not only the uptake but also the penetration in the tumor site and the internalisation of the antibodies inside the cell. The antibodies with lower  $K_D$  can enter better inside the tumor, while the antibodies with too strong binding can be retained in the perivascular

spaces<sup>15</sup>. On the other hand, the high affinity can increase the internalisation rate in the cell<sup>16</sup>. The uptake and the release of the drug depend both on the efficacy of the internalisation and the rate of the recycling. These parameters can be modified by affinity-based selection and/or Fc-engineering of the antibodies since IgG-FcRn (neonatal Fc receptor) interaction can significantly enhance their half-life by the increased intracellular lysosomal recycling<sup>17</sup>. However, it has been reported that non-internalizing ADCs can also exhibit potent activity in some cases and that ADCs often induce a strong bystander effect<sup>18</sup>. Therefore, considering the level of expression of the target, the rate of its internalisation, the affinity for the antibody combined with FcRn interactions, routes and efficacy of ADC might be altered.

The success of therapy is determined by the shedding of the antigens as well. The membrane-associated antigens may be released from the tumors into the blood stream and the ADCs can bind to these circulating antigens as well. Thus, the antigen shedding should be reduced to improve trafficking to solid tumors<sup>19,20</sup>.

The antibodies should also not be or minimally immunogenic. The problem of the early murine antibody generation based ADCs has been solved, thanks to the currently humanisation technology. Today, fully human antibodies are used for ADC application. The most common format is IgG isotype, especially IgG1 because this can trigger immune-mediated effector functions, such as ADCC and CDC<sup>21</sup>. These independent functions of the antibody can provide supplementary clinical benefits, but can also contribute to increased toxicity and reduced tumor localisation<sup>22</sup>. The optimal PK property of the antibody (slower clearance in plasma and longer half life) is important contributory factor as well.

Thus, during the selection of the target and the antibody, all these parameters should be considered for the effective delivery of the cytotoxic compounds.

### **1.2.2 Linker technology:**

One of the main challenges in ADC development is the design and selection of the linker. The functional balance of the linker is a key factor. It should be very stable in the circulation to avoid systemic toxicity through premature release of the drug but

upon delivery into the target cells, it should allow the rapid and efficient release of the active free cytotoxic payload. The bystander effect, which can increase the therapeutic potency in certain cases such as heterogeneous solid tumors, can be modified by the choice of the linker. Charged linker-drug metabolites do not cause bystander effect, since they cannot cross the plasma membrane, while bystander effect can be achieved by the release of neutral linker-drug metabolites that can diffuse across the membrane<sup>23</sup>. Polar linkers can be valuable tools to improve the solubility of ADC. It has been demonstrated that reducing the hydrophobicity of ADCs improves the PK properties and therapeutic index<sup>24</sup>. In addition, polar linkers can reduce multiple drug resistance (MDR), which is often induced by the upregulation of MDR1 protein. Since hydrophobic metabolites are better substrates for MDR1 transporter than hydrophilic compounds, charged or polar metabolites (for example sulfo-SPDB and Mal-PEG4-NHS) can enhance the potency of ADC therapy against MDR1<sup>+</sup> cells<sup>25</sup> (**Figure 4**).

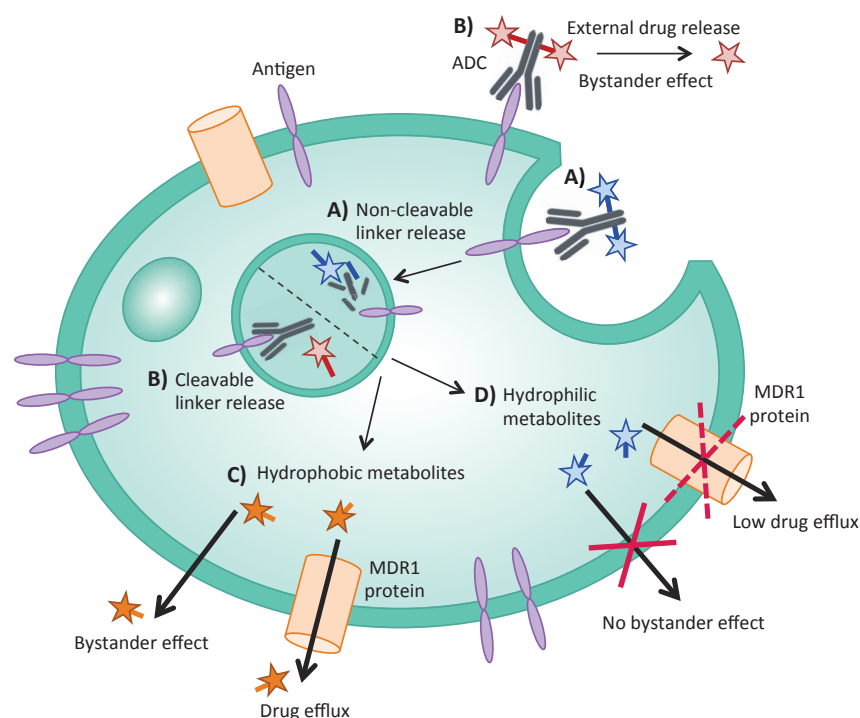


**Figure 4. Schematic representation of linkers based on their release mechanisms and chemical properties.** A) Non-cleavable linkers release their payloads by lysosomal proteolytic degradation following internalisation. B) Cleavable linkers release the cytotoxic drug in cytosolic compartments by different mechanisms. Depending on the linker stability, external drug release may happen by non-specific way. C) Hydrophobic metabolites can diffuse across the membrane causing bystander effect and MDR1 displays more reactivity towards them than D) hydrophilic compounds, which cannot cross the plasma membrane. ADC, antibody drug conjugate; MDR1, multiple drug resistance 1 protein.

Based on the release mechanism they can be divided into cleavable and non-cleavable linkers and each of them have different advantages and disadvantages. For the selection of the proper linker all the other components of the ADCs (target, antibody, drug) should be considered and it should be individually evaluated based on the toxicity and efficacy of the ADC construct.

### ***Cleavable linkers:***

Cleavable linkers use different mechanism to release the cytotoxic drug in specific compartment (**Figure 5**). Acid sensitive **hydrazone linkers** are designed to remain intact in the blood circulation (neutral environment, pH 7.3-7.5) and release the free drug in the acidic environment of the endosomes (pH 5-6.5) and lysosomes (pH 4.5-5) upon internalisation into the targeted cells<sup>26</sup>. However, different clinical studies showed a non-specific release of the drug in the circulation due to the unspecific linker cleavage by blood protease. The stability of the hydrazone linkage and thereby the *in vivo* half-life of the ADC can be improved by chemical modifications<sup>27</sup>. Hydrazone linker technology has been used in the development of Gemtuzumab ozogamicin and Inotuzumab ozogamicin.

**Disulfide linkers** are chemically labile linkers. Their selective delivery is based on the difference in the glutathione concentration between the extracellular milieu (2-20  $\mu\text{mol/L}$  in plasma) and the cytoplasm (0.5-10  $\text{mmol/L}$ )<sup>28</sup>. The glutathione concentration is especially high in hypoxic tumor cells due to the enhanced activity of reductive enzymes<sup>29</sup>. The drug is released inside the reducing environment following internalisation. Additionally, the intracellular protein disulfide isomerase is also capable to reduce disulfide bounds<sup>30</sup>. Disulfide linkers are used in many maytansinoid conjugates.

Lysosomal **protease sensitive peptide linkers** may provide a better control of drug release compared to the chemically cleavable linkers. Peptide bound containing linkers exhibit good serum stability with an average 7-10 days half-life, since the proteases are inactivated in the plasma due to the higher pH and the presence of protease inhibitors. Upon receptor mediated endocytosis and subsequential trafficking, the drug is released inside the cells by the cleavage of lysosomal enzymes,

such as cathepsins and plasmin<sup>31</sup>. Several ADCs have been developed using peptide linkers, such as Brentuximab vedotin approved by FDA, in which the payload was conjugated *via* a cathepsin-B cleavable valine-citrulline (VC) linker to the antibody. However, by CRISPR-Cas9 experiments *in vitro*, it was shown that cathepsin B is dispensable for the cleavage of VC cleavable linker<sup>32</sup>. This recent observations suggest alternative mechanisms for ADC efficacy independent of linker cleavage by proteases.

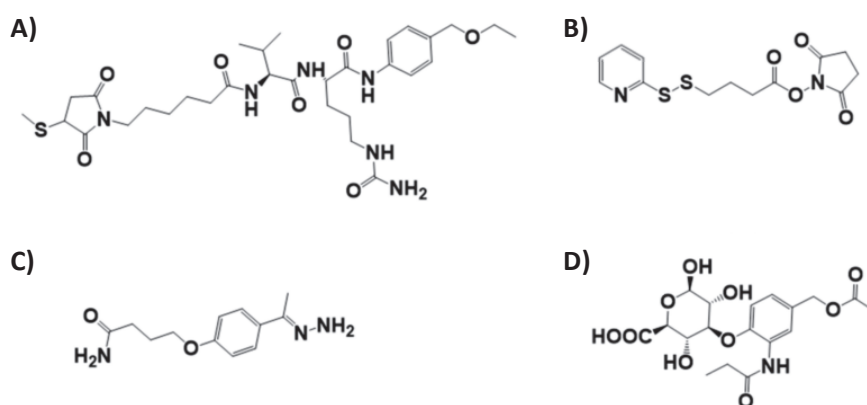


**Figure 5. Chemical structure of key cleavable linkers used for ADC development.** A) Lysosomal protease selective Val-Cit dipeptide linker; B) Glutathione sensitive SPDB linker; C) Acid sensitive AcBut linker; D)  $\beta$ -glucuronidase sensitive linker.

**$\beta$ -glucuronide linkers** release the cytotoxic compound through the cleavage of the  $\beta$ -glucuronide glycosidic bond by  $\beta$ -glucuronidase that is abundantly present in the lysosomes and overexpressed in the necrotic tumor areas. Tumor-infiltrating neutrophils and macrophages also produce proteolytic enzymes, such as  $\beta$ -glucuronidase to promote angiogenesis and tumor progression. The enzymatic catalysis is hypoxia and pH dependent, so the enzyme is active at acidic pH while it is inactive outside the cells at physiological pH<sup>33</sup>. This provides high stability in the circulation. In addition the highly hydrophilic nature of the  $\beta$ -glucuronide linker can improve the solubility of the hydrophobic drugs and thus decrease ADC aggregation<sup>34</sup>. This type of cleavable linker can find suitable application in case of necrotic, hypoxic, myeloid infiltrated solid tumors to trigger microenvironment targeting.

### **Non-cleavable linkers:**

In case of the non-cleavable linkers, there is no mechanism for the extracellular cleavage. From one hand, they provide higher stability in the blood circulation than the cleavable linkers limiting the non-specific drug release thus potentially improve the therapeutic index<sup>11</sup>. On other hand, they are more dependent on the biology of the target cell. So that, good internalization and lysosomal delivery are required for the complete degradation leading to a potential disadvantage. Following the proteolytic degradation of the ADC the free drug is released and at least one amino acid residue attached to it<sup>35</sup>. The drug-amino acid metabolites are more hydrophilic and less membrane permeable, that restricts bystander effect. The most commonly used non-cleavable linkers are the **succinimide-thioether bonds**, which are formed by the reaction of maleimides with thiols, such as in Ado-Trastuzumab emtansine approved by FDA (**Figure 6**).

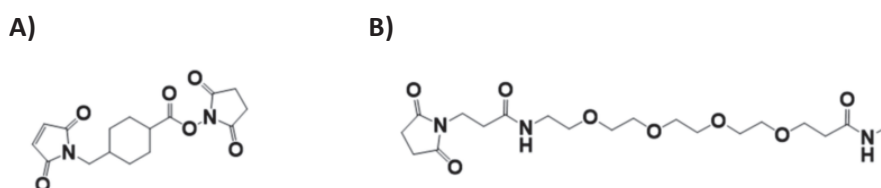


**Figure 6. Chemical structure of key non-cleavable linkers used for ADC development.** A) SMCC linker; B) PEG4Mal linker.

### **1.2.3 Cytotoxic payload:**

The success of ADC substantially depends also on the selection of the optimal drug. The early ADCs were developed with the conjugation of chemotherapeutic compounds such as doxorubicin, methotrexate and flurouracil, but these products failed in the clinical studies. It has been demonstrated that only 0.0003-0.08 % of an *in vivo* injected antibody dose is present per gram of tumor, therefore the cytotoxic potency of the payloads should be very high (with an IC<sub>50</sub> range approximately 10<sup>-10</sup>—10<sup>-12</sup> M) for successful therapy<sup>36</sup>. The drug should have acceptable water solubility to limit ADC aggregation, rapid clearance and immunogenicity<sup>25</sup>. In addition it should be

stable in the blood circulation. The cytotoxic drugs currently being used in ADC construction can be divided in two categories based on the mechanism of action: microtubule inhibitors and DNA-damaging agents. Furthermore a potential new drug  $\alpha$ -amanitin, an RNA polymerase II inhibitor is recently under investigation<sup>14</sup>.

### **Microtubule inhibitors:**

Antimitotic agents are the commonly used warheads for ADC development. The majority of the ADCs that are undergoing in clinical trials are conjugated with these types of payloads. Tubulin polymerisation inhibitors (**Figure 7**) bind to the microtubule and block tubulin assembly, causing G2/M phase cell cycle arrest that leads to cell death. Rapidly dividing cancer cells are more sensitive for the antimitotic drugs than the healthy cells.

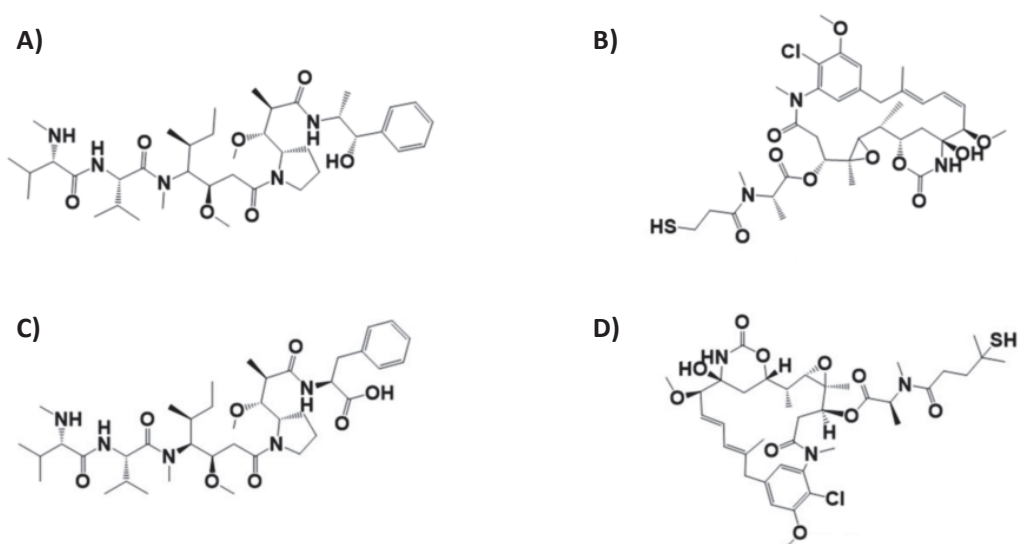


**Figure 7. Chemical structure of key tubulin polymerization inhibitors payloads used of ADC development.** A) monomethyl auristatin-E (MMAE); B) Mertansine (DM1); C) Monomethyl auristatin-F (MMAF); D) Ravtansine (DM4).

**Auristatin derivatives** are water soluble and highly potent (average  $IC_{50}$  is in sub nanomolar range) synthetic analogues of dolastatin 10, isolated from the sea hare *Dolabella auricularia*. Among them, monomethyl auristatin-E (MMAE) and MMAF are currently being used for ADC generation and other analogues are also being

investigated. The main difference between them relies in the fact that MMAE can penetrate the cell membrane and trigger bystander effect, whereas MMAF is impermeable due to the presence of a charged phenylalanine residue at the C-terminus<sup>35</sup>.

**Maytansinoids** are another class of tubulin inhibitors represented by N<sup>2</sup>-Deacetyl-N<sup>2</sup>-(3-mercapto-1-oxopropyl)-maytansine (DM1) and N<sup>2</sup>-deacetyl-N<sup>2</sup>-(4-mercapto-4-methyl-1-oxopentyl)-maytansine (DM4), derivatives of maytansine, extracted from the bark of African shrub *Maytenus ovatus*. Similar to auristatin derivatives, they also exhibit good stability and acceptable aqueous solubility<sup>37</sup>.

**Tubulysins** are promising new class of antimitotic agents. Tubulysins are originally isolated from myxobacteria and ADCs conjugated with their analogues have been entered in clinical trials currently<sup>37</sup>.

### **DNA damaging agents:**

DNA damaging payloads includes **calicheamicins**, **duocarmycins**, **anthracyclines** and **pyrrolobenzodiazepines** (PBDs) (**Figure 8**). They exhibit potent cytotoxic activity ( $IC_{50} < 10^{-9}$  M) by binding at the minor groove of the DNA and causing DNA strand scission, alkylation or crosslinking. Two FDA approved ADCs, Gemtuzumab ozogamicin and Inotuzumab ozogamicin are conjugated with the derivative of calicheamicins. Nowadays, PBDs are considered as attractive payloads, since they are extremely potent ( $IC_{50}$  in the pM concentration range) and can cause bystander-killing effect as well. Several PBD conjugates are recently in early stage of clinical studies<sup>35</sup>.

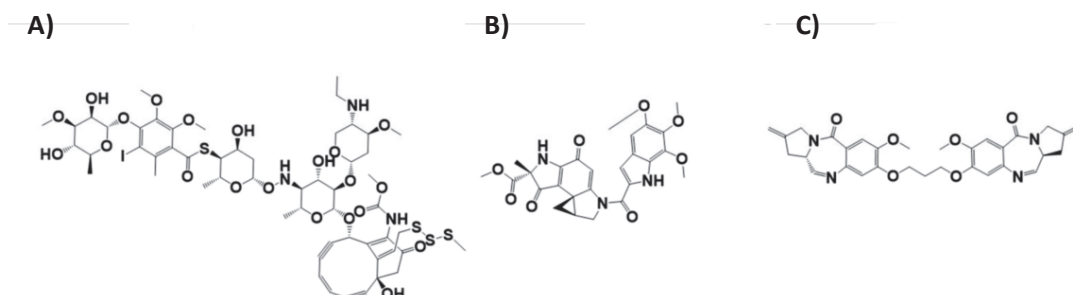


**Figure 8. Chemical structure of key DNA damaging payloads used of ADC development.** A) Calicheamicin  $\gamma$ 1; B) Duocarmycins A; C) SJG-136 PBD dimer.

For the construction of ADCs, these linkers and payloads can be used in different combination. **Table 1** is a brief, non-exhausting summary of the possible drug-linker compositions that are presented above.

Payload	Linker	Active metabolite	Chemical property	Bystander effect	IC50
<b>Microtubule inhibitors</b>					
<b>DM1</b>	SPP (Cleavable)	DM1	Hydrophobic	Yes	Picomolar
	SMCC (Non-cleavable)	Lys-SMCC-DM1	Hydrophilic	No	
	MC (Non-cleavable)	Cys-MC-DM1	Hydrophilic	No	
<b>DM4</b>	SPDB (Cleavable)	DM4,	Hydrophilic	No	
	Sulfo-SPDB (Cleavable)	DM4	Hydrophilic	No	
<b>MMAE</b>	VC (Cleavable)	MMAE	Hydrophobic	Yes	Subnano-molar
	VA (Cleavable)	MMAE	Hydrophobic	Yes	
<b>MMAF</b>	VC (Cleavable)	MMAF	Hydrophilic	No	Subnano-molar
	VA (Cleavable)	MMAF	Hydrophilic	No	
	MC (Non-cleavable)	Cys-MC-MMAF	Hydrophilic	No	
<b>Tubulysin</b>	VC (Cleavable)	Tubulysin	Hydrophobic	Yes	Subnano-molar
<b>DNA damaging agents</b>					
<b>Calicheamicin</b>	Acetyl butyrate (Cleavable)	Calicheamicin	Hydrophobic	Yes	Nanomolar
<b>Duocarmycin</b>	VC (Cleavable)	Duocarmycin			Nanomolar
<b>PDB</b>	VC (Cleavable)	PDB	Hydrophobic	Yes	Picomolar
	VA (Cleavable)	PDB	Hydrophobic	Yes	

**Table 1. Antibody-drug conjugate linker payload combinations.** SPP, N-succinimidyl 4-(2-pyridyldithio) pentanoate; SMCC, succinimidyl 4-(N-maleimidomethyl) cyclohexane-1-carboxylate; SPDB, N-succinimidyl 4-(2-pyridyldithio)pentanoate; MMAF, monomethyl auristatin F; MC, maleimidocaproyl; MMAE, monomethyl auristatin E; VC, valine-citrulline; PDB, pyrrolobenzodiazepine.

## 1.3 ADC DESIGN – TOWARDS HOMOGENEITY

Although, ADCs were designed to extend the range of the optimised dosage of drugs that can treat the patients effectively without causing toxicity or having significant adverse effect, the therapeutic window remained still quite narrow for many of the ADCs that are currently used in the clinical treatment or undergoing in clinical trials (**Figure 9**). Further attempts are ongoing in order that ADCs can deliver their full potential and simplify the manufacturing challenges. Besides the selection of the optimal target, antibody, linker and payloads; the conjugation chemistry and optimal drug loading play also a very important role to improve the safety, efficacy and toxicity profiles.

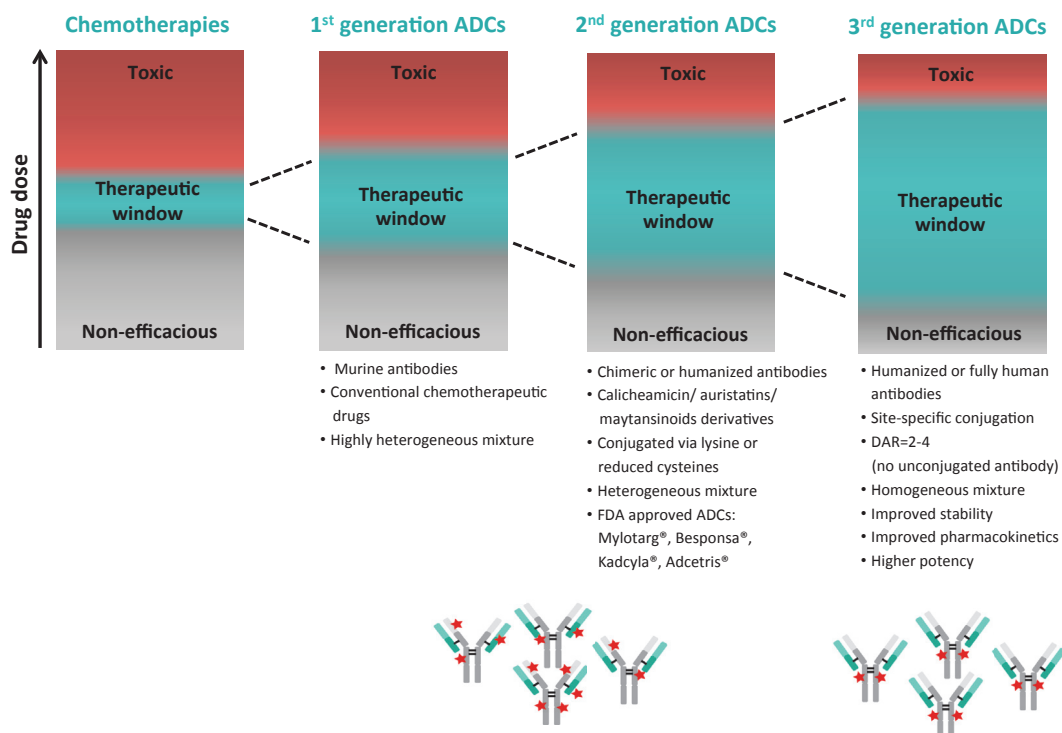


**Figure 9. ADCs are designed to improve the therapeutic window.** ADCs can increase efficacy and decrease toxicity in comparison to conventional chemotherapeutic treatment. The targeted delivery of drugs to the malignant cells increase the percentage of tumor reaching toxin molecules, thus lowering the minimum effective dose and increasing the maximum tolerated dose. Nevertheless, in case of the first -and second generation ADCs the therapeutic window remained rather narrow. The optimization of antibody, linker, payload and conjugation technologies are important to improve the therapeutic index of the third generation ADCs. (Figure adapted from Beck *et al.*<sup>37</sup>)

### 1.3.1 First generation:

The first generation ADCs were developed in the early 1990s by the conjugation of conventional chemotherapeutic compounds, such as KS1/4-methotrexate targeting EpCam molecule or -desacetylvinblastine and BR96-doxorubicin targeting Lewis-Y protein immunoconjugates. KS1/4 murine monoclonal antibody was conjugated with methotrexate through amide bond or with desacetylvinblastine by hydrazone or hemisuccinate linkers targeting non-small lung carcinoma<sup>38,39</sup>. BR96-doxorubicin was generated for the treatment of metastatic breast cancer, in which doxorubicin was attached to the chimeric BR96 antibody *via* hydrazone-based bond<sup>40</sup>. When clinical trials were undertaken to investigate their efficacy, they exhibited modest therapeutic activity. The reason for the failure of these first generation ADCs was probably related to several parameters: the poor potency of the payloads, the instability of the linker, the high heterogeneity of the ADC population or faster clearance due to the immunogenicity of the antibody. This demonstrated the need for improvement of PK properties for better ADC efficacies.

### 1.3.2 Second generation:

The second generation ADCs were developed using more potent (100-1000 fold) cytotoxic payloads such as DNA-targeting calicheamicins or the tubulin targeting auristatins and maytansinoids derivatives engrafted on humanised antibodies. Thanks to the enhanced potency of the conjugated compounds and the improved linker stability, these ADCs demonstrated potent antitumor activity allowing approval by FDA and introduction to clinic for four of them. The therapeutic index was improved but it remained moderate due to the heterogeneity of the ADC mixture. Various numbers of drugs are attached at different positions and considerable percent of the final product is not conjugated resulting in species with distinct PK properties. These immunoconjugates are prepared by conventional, non site-specific chemical conjugation methods; the payloads are attached to the solvent-exposed lysine (*via* succinimide ester derivatization) or interchain cysteine residues (maleimide chemistry)

of the antibody<sup>41</sup>. In this manner the batch-to batch variability is rather high, thus the ADC production can require different manufacturing processes.

It has been demonstrated by Wang *et al.*, that lysine conjugation may involve 40 different sites out of 86 lysine residues located both in the light and heavy chain regions. In average 6 drugs were attached to the antibodies (**Figure 10A**). Thus the ADCs exhibit high level of heterogeneity (>10<sup>6</sup> species) with broad range of stoichiometry and several iso-stoichiometric species. In addition complementarity determining regions (CDR) can be also modified affecting the antigen binding ability<sup>42</sup>.

Conjugation through cysteine residues results in reduced subpopulations of ADCs compared to the coupling *via* lysine residues. IgG1 scaffold contains four interchain and twelve intrachain disulfide bounds<sup>43</sup>. The interchain disulfides (two between the hinge region and two between each heavy and light chains) are more susceptible to reduction than the intrachain bounds, providing eight possible conjugation sites. Thus the drug loading can varied from 0 to 8 per antibody that offers potentially >100 species<sup>44</sup> (**Figure 10B**).

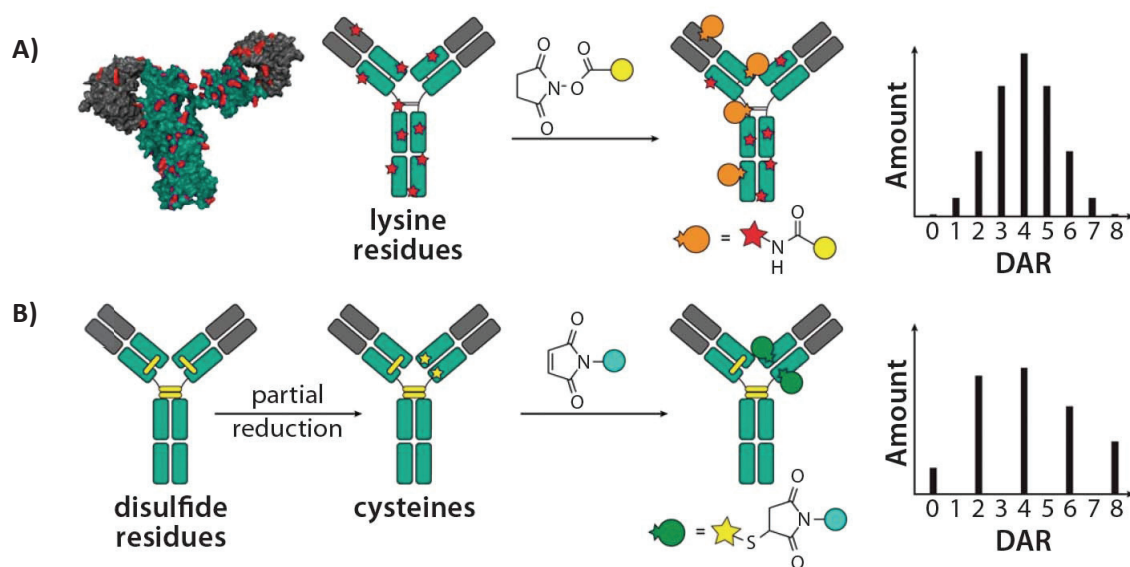


**Figure 10. Schematic representation of A) lysine and B) cysteine conjugates and their expected drug to antibody ratio profile (DAR).** (Picture taken and adapted from Bath *et al*<sup>16</sup>).

The clinical efficacy of these heterogeneous ADCs is negatively influenced by the variable drug-to antibody ratio (DAR) and site of conjugation due to the nonselective conjugation technologies. The importance of DAR loading and its effect on PK properties has been investigated in several studies. Hamblett *et al.* compared the therapeutic potential of cAC10-MMAE conjugates loading different number of drugs (DAR 2, 4 and 8). They found that low DAR decreased the antitumor potency while the higher conjugation level impaired the antigen binding activity and increased the aggregation of the ADC leading to high plasma clearance and toxicity<sup>45</sup>. Thus, the optimal DAR is a key factor for the improvement of the therapeutic window and the clinical success. However, these conjugates existed as heterogeneous mixtures. Pillow *et al.* have reported that in addition to the favourable DAR, the homogeneity of the ADC has also a significant benefit for the *in vivo* performance<sup>46</sup>. In this study the clinically approved nonselectively conjugated Ado-Trastuzumab emtansine was compared to the site-specific ThioTmab-MPEO-DM1, constructed by THIOMAB technology where cysteine residues were engineered into the antibody at specific sites to allow only site specific conjugation. The results showed that the homogeneous THIOMAB ADC displayed improved preclinical therapeutic index over heterogeneous Trastuzumab emtansine<sup>44,46</sup>.

### **1.3.3 Third generation:**

Since the development and approval of the second generations ADCs, significant improvements have occurred to overcome therapeutical challenges. One of the main challenges remained, to optimize manufacturing processes in order to obtain homogeneous conjugates with well-defined and uniform drug stoichiometry. In case of homogeneous ADCs, the tolerability and efficacy profile can be more predictable helping to better understand the factors contributing to the therapeutic success. Thus the clinical outcome of the patients can be potentially advanced<sup>47</sup>.

Recently, many of site-specific conjugation technologies were developed in order to control the DAR, reduce heterogeneity and batch-to batch variability as well as to further increase therapeutic window<sup>44</sup>. In the site-specific conjugates, controlled

number of drugs are attached to defined positions that allows to investigate the effect of the DAR, the location and the linker properties on the biodistribution, PK and therapeutic activity of the resulting immunoconjugates. Recent studies demonstrated the role of the conjugation site in the stability and activity of the ADCs *in vivo*. Shen *et al.* constructed three ADCs variants, conjugated at different structural and chemical environments using THIOMAB technology. The three ADCs displayed different *in vivo* potency, due to the linker stability determined by the structural and chemical environments around the coupling site<sup>48</sup>. In another comparison study the different site-specific conjugates were generated by enzymatic conjugation, using microbial transglutaminase. Indeed, Strop *et al.* demonstrated that the alternations in stability and pharmacokinetics of ADCs can be directly attributed to the site of the conjugation rather than the instability of the linker as it was absorbed with maleimide conjugation<sup>49</sup>. A better understanding of these parameters could help to design more efficient ADCs.

Numerous site-specific methods are currently under investigation, which are summarized in **Table 2**<sup>37</sup>. Based on the antibody scaffold we can distinguish two main strategies. One of them uses the native antibody and the selective conjugation is achieved by novel linker chemistry. The second one requires molecular engineering to introduce the coupling site into the antibody sequence such as mutations of cysteine residues, glycoengineering or insertion of unnatural amino acids or peptide sequences for enzymatic approaches<sup>50</sup>. Among them the microbial transglutaminase based conjugations are described in detail in the section 1.5.5.

Presumably, the future ADC design should trend towards the selection of the optimal site-specific conjugation methods depending on the individual ADC considering the antibody and linker. The present ADC medications are quite expensive. Thus the production cost-effective is also an important point that should be taken into account during the development of novel technologies.

Engineering technology	Conjugation chemistry	Technology nar	Owner (collaborators)
<b>Engineered cysteine and selenocysteine*</b>			
Engineered cysteine (HC-A114C and LC-V2015C)	Thiol plus maleimide	THIOMABs	Genentech
Engineered cysteine (HC-S239C)	Thiol plus self-hydrolyzing maleimide ‡	Engineered cystei mAbs	Seattle Genetics
Engineered cysteine	Thiol plus maleimide	NA	Pfizer
Engineered cysteine (HC-S239C and S442C)	Thiol plus maleimide	NA	MedImmune/ AstraZeneca
Engineered cysteine (hinge cysteine t serine mutation)	Thiol plus maleimide	ThiofleximAbs	MedImmune/ AstraZeneca
Engineered cysteine (LC-Q124C)	Thiol plus maleimide	Actibody	Kyowa Kirin
Engineered cysteine	Thiol plus maleimide	SAP	Novartis
Engineered cysteine and selenocyste	Thiol plus phenyloxadiazole sulfone	Selenomabs and Thioselenomabs	Scripps Research Institute
<b>Unnatural amino acid engineering*</b>			
Engineered pAcPhe (HC-A114)	Oxime ligation, alkoxyamine-keto-group reaction	EuCODE	Ambrx
Engineered pAMF	SPAAC, copper-free click chemistry	Xpress CF+	Sutro Biopharma
Engineered N6 -((2-azidoethoxy)carbonyl)-l-lysine	SPAAC, copper-free click chemistry	AzAbs	Allozyne
<b>Enzyme-assisted ligation (formylglycine-generating enzyme, transglutaminase and sortase)</b>			
Engineered L-C-X-P-X-R tag (various positions) plus FGE treatment	Cysteine oxidized to formylglycine, HIPS ligation	SMARTag	Catalent/ Redwood
Engineered glutamine (L-L-Q-G) tag (various positions) plus BTG treatment	Ligation of $\gamma$ -carboxamide group from glutamine residues plus primary amines	BTG	Pfizer
HC-Q295 and/or HC-N297Q plus PGNase F and plus BTG treatment	Ligation of $\gamma$ -carboxamide group from glutamine residues plus primary amines	TG-ADC	ETH Zurich/ Innate Pharma
L-P-E-T-G tag (C termini of HC and LC) plus SrtA treatment	Ligation LPETG plus primary amine of polyglycine motif	SMAC	NBE Therapeutics

Engineering technology	Conjugation chemistry	Technology name	Owner (collaborators)
<b>Glycan remodelling: metabolic engineering, chemical oxidation and glycoengineering</b>			
Glycan metabolic engineering (fucose in glycans linked to N297) and incorporation of 6-thiofucose peracetate plus fucosyltransferase VIII treatment	Maleimide plus 6-thiofucose	NA	Seattle Genetics
Fucose periodate oxidation (fucose in glycans linked to N297)	Fucose-specific conjugation of hydrazide	NA	Philogen
Glycan engineering (sialic acids in glycans linked to N297), and galactosyl- and sialyltransferase treatments	Periodate oxidation (aldehyde) plus amino-oxypayload, oxime ligation	NA	Genzyme/Sanofi
Glycan engineering (azido-modified sialic acids in glycans linked to N297), and galactosyl- and sialyltransferase treatments	Strain-promoted alkyne-azide cycloaddition, copper-free click chemistry	NA	University of Georgia
Galactosyltransferase treatment plus UDP-keto-galactose incorporation	C2-keto-gal oximation	NA	US National Cancer Institute
Glycan engineering (GlcNAc in glycans linked to N297), and endoglycosidase and glycosyltransferase treatment and azide tagging	Strain-promoted alkyne-azide cycloaddition, copper-free click chemistry	GlycoConnect, HydraSpace	Synaffix
<b>Amino-terminal engineered serine</b>			
Engineered serine (N-terminal LC)	Site selective aldehyde oxidation plus oxime ligation	NA	MedImmune/AstraZeneca
Engineered serine (N-terminal HC or LC)	Site selective aldehyde oxidation, oxime ligation	SeriMabs	ImmunoGen
<b>Cysteine rebridging<sup>§</sup></b>			
Cysteine chemical rebridging (native hinge interchain crosslinking)	Thiol plus bis-sulfone	ThiBridge	Abzena/PolyTherics
Cysteine chemical rebridging (native hinge interchain crosslinking)	Thiol plus dibromomaleimide	NGM	University College London/ThioLogics
Cysteine chemical rebridging (native hinge interchain crosslinking)	Thiol plus dibromomaleimide	SNAP	Igenica Biotherapeutics
<b>Avoiding or limiting retro-Michael drug deconjugation</b>			
Basic pH-driven succinimide ring-opening (native or engineered cysteine)	Thiol plus maleimide followed by pH 9.2 treatment (45 °C, 48 hours)	Succinimide ring hydrolysis	Pfizer
Basic amino group adjacent to the maleimide (native or engineered cysteine)	Thiol plus maleimide	Self-hydrolysing maleimides	Seattle Genetics

Engineering technology	Conjugation chemistry	Technology name	Owner (collaborators)
<b>Avoiding or limiting retro-Michael drug deconjugation</b>			
Ring-opened linker and N-substituted succinimide thioethers (native or engineered cysteine)	Thiol plus maleimide	NA	ProLynx
Ring-opened linker (native or engineered cysteine)	Thiol plus maleimide	NA	MedImmune/ AstraZeneca
Ring opening by anion exchange chromatography (engineered cysteine, LC-Q124C)	Thiol plus maleimide	Actibody, AEX	Kyowa Kirin
Maleimide replacement (native or engineered cysteine)	Thiol plus arylpropionitrile	CBTF	Syndivia
Self-hydrolysable hydrophilic maleimidomethyl dioxane-based linker (native or engineered cysteine)	Thiol plus maleimide	MTDF	Syndivia

**Table 2. Selected site-specific conjugation technologies and associated stabilization chemistries.** A, alanine; AzAbs, azide antibodies; BTG, bacterial transglutaminase; C, cysteine; CBTF, sodium 4-((4-(cyanoethynyl)benzoyl)oxy)-2,3,5,6-tetrafluorobenzenesulfonate; E, glutamate; EWM, electron-withdrawing maleimides; FGE, formylglycine-generating enzyme; G, glycine; GlcNAc, N-acetylglucosamine; HC, heavy chain; HIPS, hydrazino-iso-Pictet–Spengler; L, lysine; LC, light chain; MDTF, sodium 4-(maleimidomethyl)-1,3-dioxane-5-carboxyloxy-2,3,5,6-tetrafluorobenzenesulfonate; N, asparagine; NA, not available; NAM, N-aryl maleimides; NGM, next-generation maleimide; P, proline; pAcPhe, p-acetylphenylalanine; pAMF, para-azidomethyl-l-phenylalanine; PGNase F, peptide:N-glycosidase F; R, arginine; Q, glutamine; S, serine; SAP, spatial aggregation propensity; SMAC, sortase- enzyme mediated antibody conjugation; SPAAC, strain-promoted azide–alkyne cycloaddition; SrtA, sortase A; T, threonine; THIOMABs, thio-engineered monoclonal antibodies; UDP, uridine diphosphate.; V, valine; \*Vector engineering. ‡ Promotes slower deconjugation. § No need for antibody or cell engineering (Table taken from Beck *et al.*<sup>37</sup>).

## 1.4 ANTIBODY-DRUG CONJUGATES IN THE CLINICS

In the recent years the number of ADCs entering to clinical trial are rapidly increasing, showing rapid progress and success in this field. The improvements in the next generation conjugation technologies and payload stability are contributing to this dynamic development. **Table 3** summarise the landscape of ADCs in the clinic.

ADC	Payload	Target	Lead identification	Phase
Gemtuzumab ozogamicin	Calicheamicin	CD33	AML	FDA-approved
Inotuzumab ozogamicin	Calicheamicin	CD22	ALL	FDA-approved
Brentuximab vedotin	MMAE	CD30	HL/ALCL	FDA-approved
Trastuzumab emtansine	DM1	HER2	Breast cancer	FDA-approved
Vadastuximab talirine	PBD	CD33	AML	3
Rovalpituzumab tesirine	PBD	DLL3	SCLC	3
Mirvetuximab soravtansine	DM4	FOLR1	Ovarian cancer	3
Sacituzumab govitecan	SN-38	TROP-2	mTNBC	3
HuMax-AXL-ADC	MMAE	AXL	Solid tumors	2
SAR566658	DM4	CA6	Solid tumors	2
Coltuximab ravtansine	DM4	CD19	B-cell malign	2
Denintuzumab mafodotin	MMAF	CD19	B-cell malign	2
Pinatuzumab vedotin	MMAE	CD22	B-cell malign	2
IMGN529	DM4	CD37	B-cell malign	2
Lorvotuzumab mertansine	DM1	CD56	SCLC	2
Milatumzumab doxorubicin	Doxorubicin	CD74	Multiple myeloma	2
Polatuzumab vedotin	MMAE	CD79b	B-cell malign	2
Indatuximab ravtansine	DM4	CD138	Multiple myeloma	2
SAR408701	DM4	CEA	Solid tumors	2
Labetuzumab govitecan	SN-38	CEA	mCRC	2
ABT-414	MMAF	EGFR	Glioblastoma	2
AGS-16C3F	MMAF	ENPP3	mRCC	2
Glembatumumab vedotin	MMAE	GPNMB	Breast cancer, melanoma	2
MLN0264	MMAE	GUCY2C	Pancreatic cancer	2
MM-302	Liposomal doxorubicin	HER2	Breast cancer	2
RC48-ADC	MMAF	HER2	Solid Tumors	2
MEDI-4276	Tubulysin	HER2	Breast and gastric cancer	2
U3-1402	DXd	HER3	NSCLC	2
IMGN388	DM4	Integrin alpha	Solid tumors	2
SGN-15	Doxorubicin	Lewis Y	Prostatic Neoplasms	2

ADC	Payload	Target	Lead identification	Phase
Anetumab ravtansine	DM4	MSLN	Neoplasms	2
BMS-986148	Not disclosed	MSLN	Solid tumors	2
Cantuzumab ravtansinea	DM4	MUC1	Multiple myeloma	2
Lifastuzumab vedotin	MMA	NaPi2b	Ovarian cancer, NSCLS	2
MLN2704	DM1	PSMA	Prostate cancer	2
PSMA ADC 1301	MMAE	PSMA	Prostate cancer	2
Tisotumab vedotin	MMAE	TF	Cervical Cancer	2
PF-06263507	MMAF	5T4	Solid tumors	1
GSK2857916	MMAF	BCMA	Multiple myeloma	1
BAY1129980	Auristatin W derivative	C4.4a	Neoplasms	1
BAY79-4620	MMAE	CA9	Neoplasms	1
HKT288	Maytansine	Cadherin-6	Ovarian cancer, RCC	1
ADCT-402	PBD	CD19	B-cell malign	1
SGN-CD19B	PBD	CD19	NHL, DLBCL, FL3	1
ADCT-301	PBD	CD25	HL, NHL	1
AMG 172	DM1	CD27L	ccRCC	1
AVE9633	DM4	CD33	AML	1
AGS67E	MMAE	CD37	Lymphoid Malignancy	1
Bivatuzumab mertansine	DM1	CD44v6	SCC	1
MDX-1203	Duocarmycin	CD70	NHL, RCC	1
Vorsetuzumab mafodotin	MMAE	CD70	NHL, RCC,	1
SGN-CD70A	MMAF	CD70	RCC, DLB, FL	1
SGN-CD123A	PBD	CD123	AML	1
LOP628	Maytansine	cKit	Solid tumor, AML	1
BIIB015	DM4	Cripto protein	Solid tumors	1
ABBV-838	MMAE	CS1	Multiple Myeloma	1
SC-002	Not disclosed	DLL3	SCLC	1
DEDN6526A	MMAE	EDNRB	Malignant melanoma	1
PF-06647263	Calicheamicin	EFNA4	mTNBC	1
IMGN289	DM1	EGFR	Solid tumors	1
AMG 595	DM1	EGFRvIII	Glyomas	1
MEDI-547	MMAF	EPHA2	Solid tumor, AML	1
BAY1187982	Auristatin W derivative	FGFR2	Solid tumors	1
LY3076226	DM4	FGFR3	Advanced or metastatic cancer	1
AGS62P1	Not disclosed	FLT3	AML	1
XMT-1522	Auristatin	HER2	Breast and cancer, NCLC	1
SYD-985	Duocarmycin	HER2	Breast cancer	1
DS-8201A	DXd	HER2	Neoplasms	1
RC48-ADC	MMAF	HER2	Solid tumors	1
SAR428926	DM4	LAMP-1	Neoplasms	1
SGN-LIV1A	MMAE	LIV-1	Breast cancer	1
ABBV-085	MMAE	LRRC15	Solid tumors	1
DMOT4039A	MMAE	MSLN	Ovarian cancer	1
Cantuzumab mertansine	DM1	MUC1	Colorectal cancer	1
Sofituzumab vedotin	MMAE	MUC16	Ovarian cancer	1
Enfortumab vedotin	MMAE	Nectin-4	Urothelial carcinoma	1
PF-06650808	Auristatin	NOTCH3	Solid tumors	1
PCA-062	Not disclosed	p-CAD	TNBC, head, neck cancer and esophageal cancer	1

ADC	Payload	Target	Lead identification	Phase
PF-06647020	Auristatin	PTK7	Neoplasms	1
ASG-5ME	MMAE	SLC44A4	Neoplasms	1
ASG-15ME	MMAE	SLITRK6	Urothelial Cancer	1
Vandortuzumab vedotin	MMAE	STEAP1	Prostate cancer	1
CDX-014	MMAE	TIM-1	RCC, ovarian cancer	1
DFRF4539A	MMAE	Not disclosed	Multiple Myeloma	1
AbGn-107	Not disclosed	Not disclosed	Gastric, colorectal, and pancreatic adenocarcinoma	1
SC-003	Not disclosed	Not disclosed	Ovarian cancer	1

**Table 3. Overview of registered ADCs and ADCs in clinical trial for cancer treatment.** ALCL, anaplastic large-cell lymphoma; ALL, acute lymphoblastic leukemia; AML, acute myeloid leukemia; AXL, AXL receptor tyrosine kinase; BCMA, B-cell maturation antigen; CA6, carbonic anhydrase 6; CA9, carbonic anhydrase 9; ccRCC, clear cell renal cell carcinoma; CD, cluster of differentiation; CEA, carcinoembryonic antigen; CLL, chronic lymphocytic leukaemia; DLBCL, diffuse large B-cell lymphoma; DLL3, delta-like canonical Notch ligand 3; DMC, data monitoring committee; EDNRB, endothelin receptor type B; EFNA4, ephrin A4; EGFR, epidermal growth factor receptor; ENPP3, ectonucleotide pyrophosphatase/ phosphodiesterase 3; EPHA2, EPH receptor A2; FGFR2, fibroblast growth factor receptor 2; FGFR3, fibroblast growth factor receptor 3; FL3, grade 3 follicular lymphoma; FMS-like tyrosine kinase 3; FOLR1, folate receptor 1; GPNMB, glycoprotein non-metastatic B; GUCY2C, guanylate cyclase 2 C; HER2, human epidermal growth factor receptor 2; HER3, human epidermal growth factor receptor 3; HL, Hodgkin Lymphoma; LAMP-1, lysosomal-associated membrane protein 1; LRR15, leucine rich repeat containing 15; mCRC, metastatic renal cell carcinoma; MMAE, monomethyl auristatin E; MMAF, monomethyl auristatin F; MSLN, mesothelin; mRCC, metastatic renal cell carcinoma; MUC1, mucin 1; MUC16, mucin 16; mTNBC, metastatic triple-negative breast cancer; NaPi2b, sodium-dependent phosphate transport protein 2B; NHL, non-Hodgkin lymphoma; NOTCH3, notch 3; NSCLC, non-small-cell lung cancer; p-CAD, p-cadherin; PBD, pyrrolobenzodiazepine; PSMA, prostate-specific membrane antigen; PTK7, protein tyrosine kinase 7; RCC, renal cell carcinoma; SCC, squamous cell carcinoma; SLC44A4, solute carrier family 44 member 4; SCLC, small-cell lung cancer; SLITRK6, SLIT like family member 6; STEAP1, STEAP family member 1; TF, tissue factor; TIM-1, T cell immunoglobulin and mucin protein-1; TNBC, triple-negative breast cancer TROP-2, trophoblast cell-surface antigen (Adapted from Moek *et al.*<sup>51</sup>).

Among all the ADCs currently in clinic, the majority of FDA approved ADCs are targeting hematopoietic malignancies.

### 1.4.1 Gemtuzumab ozogamicin:

Gemtuzumab ozogamicin (CMA-676, Mylotarg<sup>®</sup>, Pfizer) is a combination of the cytotoxic agent calicheamicin, attached to a monoclonal antibody targeting CD33 *via* a hydrazone linker (**Figure 11**). Its improved clinical benefit was demonstrated compared to standard chemotherapy and in 2000 it was the first approved by FDA approved for the treatment of elderly patients with acute myeloid leukemia (AML). However post-approval clinical studies showed not considerable benefit and poor safety profile, thus in 2010 Pfizer withdrew it from the market. AML19 (ClinicalTrials.gov, identifier NCT00091234) and ALFA0701 (ClinicalTrials.gov, identifier NCT00927498) trials demonstrated that combination of induction therapy plus low dose of Mylotarg<sup>®</sup> improved the clinical outcome and decreased toxicity. In 2017 it was re-approved by FDA, administrating in lower recommended dose and different schedules<sup>52</sup>.

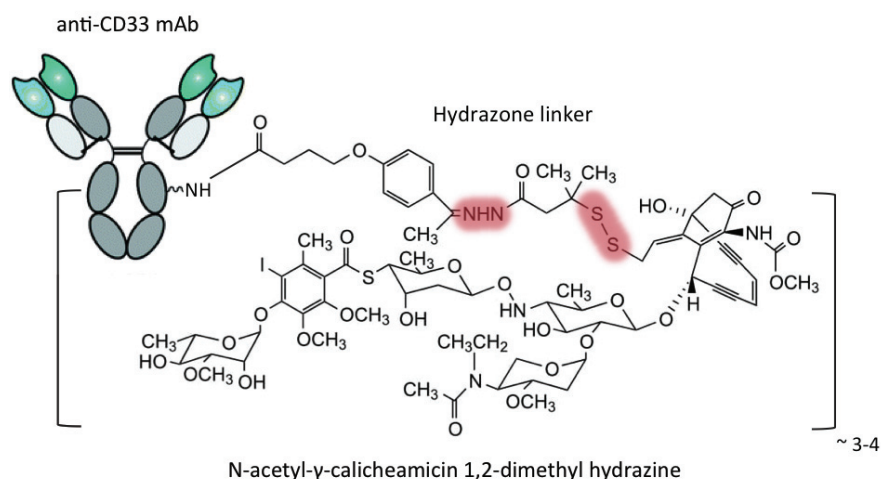


**Figure 11. Structure of Gemtuzumab ozogamicin (Mylotarg<sup>®</sup>).** The possible sites of cleavage in the linker, the hydrazone group and the disulphide bond, are shown in red. (Picture modified from Akkapeddi *et al.*<sup>53</sup>).

CD33 is a transmembrane protein, expressed on the surface of myeloblasts in up to 90 percent of AML patient, but also on normal hematopoietic progenitor cells. However, CD33 has relatively low expression level and slow internalisation rate that results in lower drug delivery. Therefore the selection of a highly potent drug is crucial to compensate this limitation. N-acetyl-γ-calicheamicin 1,2-dimethyl hydrazine, a semisynthetic derivative of calicheamicin is covalently conjugated to the lysine

residues of the humanised Gemtuzumab (hP67.6) antibody *via* a bifunctional (4-(4-acetylphenoxy)butanoic acid) with an average DAR of 3-4 and approximately 50% of unconjugated antibody. The resulted cleavable acid-labile hydrazine linker enables the drug release in the lysosomes following the internalisation of the ADC-antigen complex. Then, calicheamicin is transported into the nucleus where it binds to the minor groove of DNA inducing double strand DNA brakes that lead to the inhibition of DNA synthesis and cancer cell death *via* apoptosis<sup>54</sup>. Since Gemtuzumab is IgG4 isotype, Mylotarg® does not mediate any effector functions but has a long circulating half-life.

### 1.4.2 Inotuzumab ozogamicin:

Inotuzumab ozogamicin (CMC-544, Besponsa®) is CD22 targeted ADC consisting a humanised IgG4 Inotuzumab monoclonal antibody (G544) linked to N-acetyl  $\gamma$  -calicheamicin 1, 2-dimethyl hydrazine dichloride *via* hydrazone linker (**Figure 12**). The ADC exists as a heterogeneous mixture with an average DAR of 6<sup>54</sup>. CD22 is a transmembrane glycoprotein expressed on the surface of B cells. It is expressed in

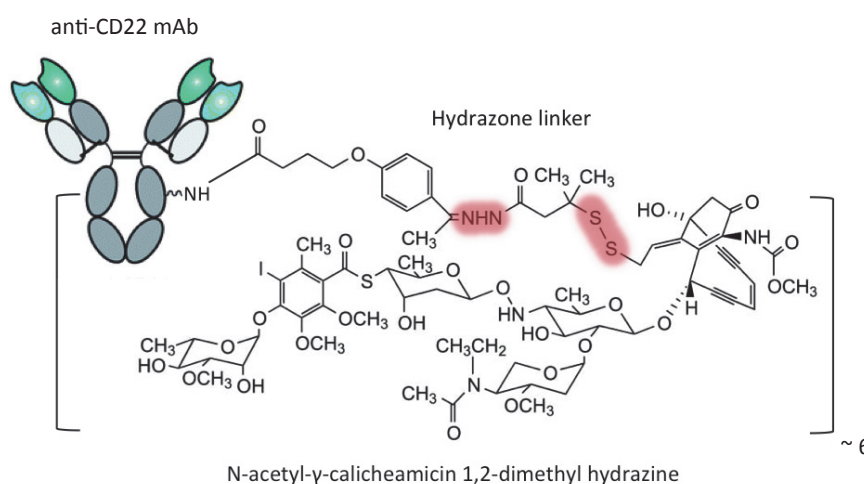


**Figure 12. Structure of Inotuzumab ozogamicin (Besponsa®).** The possible sites of cleavage in the linker, the hydrazone group and the disulphide bond, are shown in red. (Picture modified from Akkapeddi *et al.* <sup>53</sup>).

most of (>90%) the non-Hodgkin lymphomas (NHL) and all in mature B-cell acute lymphoblastic leukemias (B-ALL)<sup>55</sup>. The conjugation method and the mechanism of ADC action are the same as in case of Gemtuzumab ozogamicin (1.2.3).

In clinical trials it was demonstrated that CMC-544 improved the overall survival to 56%, but in NHL there was a lack of improvement. In 2017 it was approved by the US FDA for the treatment of adults with relapsed or refractory B-ALL alone or in combination with chemotherapy. Further clinical evaluations are currently ongoing (ClinicalTrials.gov, CMC-544).

### 1.4.3 Brentuximab vedotin:

Brentuximab vedotin (SGN-35, Adcetris<sup>®</sup>) is an ADC consisting of monomethyl auristatin E (MMAE, vedotin) attached to the cysteine residues of cAC10 antibody *via* stable, cleavable VC dipeptide linker<sup>56</sup> (**Figure 13**). Maleimide chemistry is used for the conjugation that results in an average of four drugs per antibody. cAC10 (SGN-30) is a chimeric monoclonal IgG1 antibody against CD30, a transmembrane cytokine receptor belonging to the tumor necrosis factor family (TNF). This protein is appropriate to be targeted since it has limited expression on the surface of Hodgkin's lymphomas (HL) cells, Reed-Sternberg cells, anaplastic large cell lymphomas (ALCL) and other lymphoid and non-lymphoid tumor cells<sup>57</sup>. The naked cAC10 antibody entered to clinical program, but the trial was discontinued because its moderated activity<sup>58</sup>.

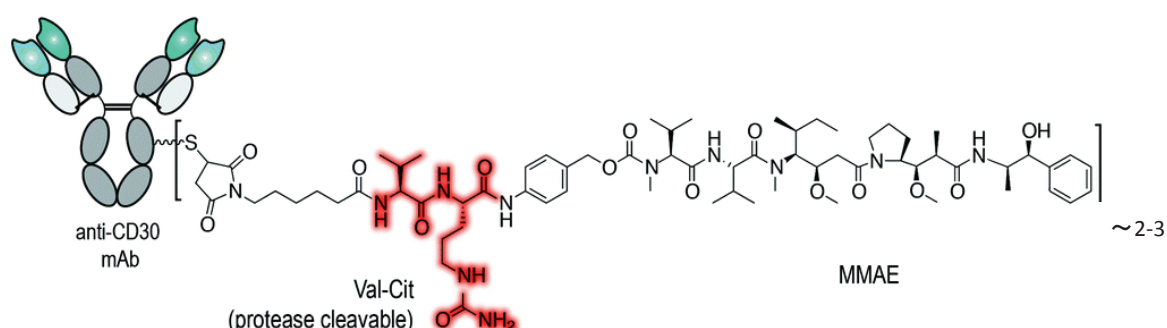


**Figure 13. Structure of Brentuximab vedotin (Adcetris<sup>®</sup>).** Val-Cit, valine-citrulline linker; MMAE, monomethyl auristatin E (Picture taken from Akkapeddi *et al.*<sup>53</sup>).

Then it was further developed in ADC format by Seattle Genetics and approved by FDA in 2011 for the treatment of ALCL patients who had relapsed following stem cell transplantation or combined chemotherapy treatment. The main anti-tumor mechanism is due to targeted delivery of MMAE inside the tumor cells, that is released by proteolytic cleavage in the endosomes following internalisation of the ADC-CD30 complex. MMAE is a potent anti-mitotic agent, a synthetic analogue of dolastatin 10 that induces apoptotic cell death by cell cycle arrest following its binding to tubulin. In addition immunogenic cell death, antibody-dependent cellular phagocytosis and the bystander effect can also contribute to the clinical activity<sup>59</sup>.

Brentuximab vedotin is administered at 1.8 mg/kg dose every three weeks, that has been demonstrated to improve the prognosis and the OS of patients with a good tolerability and safety. Currently other phase III clinical trials are ongoing for the further evaluation (ClinicalTrials.gov, SGN-35).

#### 1.4.4 Trastuzumab emtansine:

Ado-trastuzumab emtansine (T-DM1, Kadcyla<sup>®</sup>) was developed by ImmunoGene and approved in 2013 by FDA for the treatment of patients of HER2 positive metastatic breast cancer (MBC). T-DM1 is a combination of Trastuzumab (Herceptin<sup>®</sup>) and maytansinoid derivative DM1 attached *via* a non-cleavable thioether linker (N-succinimidyl 4-(N-maleimidomethyl) cyclohexane-1-carboxylate, SMCC), with an average DAR of 3.5 (**Figure 14**).

HER2 (also known as ErbB2) transmembrane glycoprotein is the member of the epidermal growth factor receptor (EGFR) family. They can be divided into three main structural units: a large N-terminal extracellular ligand binding domain, a transmembrane domain, an intracellular kinase domain and a C-terminal region with tyrosine autophosphorylation sites<sup>60</sup> (**Figure 15**). HER2 is known as an orphan receptor, since unlike of the other EGFR receptors (HER1, HER3, HER4), its extracellular domain binding ligand has not been identified yet. HER2 constitutively exists in an active conformation, and preferentially forms heterodimers with any of the ligand-bound EGFR members<sup>60</sup>. However cancer studies revealed that HER2/HER3

combination is most common and the most mitogenic dimer, promoting tumorigenesis<sup>61,62</sup>. Receptor dimerisation results in the transphosphorylation of tyrosine residues within the cytoplasmic domain, initiating cell proliferation and survival through both mitogen-activated protein kinase (MAPK) and PI3K/Akt intracellular signaling pathways<sup>62</sup>.

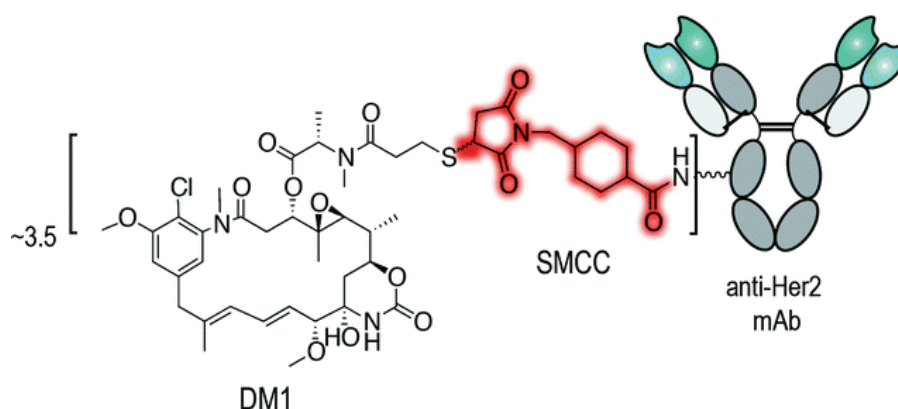


**Figure 14. Structure of ado-trastuzumab emtansine (T-DM1, Kadcyła®).** SMCC, succinimidyl-4-[N-maleimidomethyl]-cyclohexane-1-carboxylate; DM1, thiol-containing maytansinoid. (Picture taken from Akkapeddi *et al.*<sup>53</sup>).

Amplification of HER2 receptors occurs in 20-25% of breast carcinomas<sup>63</sup>, 10–30% of gastric/gastroesophageal cancers<sup>64</sup> and correlates with aggressive tumor growth and poor prognosis. The genetic amplification of HER2 can be detected in more than 90% of HER2-positive breast cancer cases<sup>65</sup>. Mutations in the transmembrane domain can result in spontaneous homodimerisation<sup>66</sup> and constitutive autoactivation<sup>67</sup>. Furthermore, HER2 overexpression has been also reported in ovary<sup>68</sup>, endometrium<sup>69</sup>, bladder<sup>70</sup>, lung<sup>71</sup> cancers. Thanks to the accessibility of the extracellular domain, HER2 serves as a target for antibody therapies. The humanised anti-HER2 monoclonal antibody (clone4D5) Trastuzumab (Herceptin®) significantly increased the survival rates of patients with HER2-positive breast and gastric/gastroesophageal cancers. However, many of these patients relapsed or developed resistance during the treatment<sup>72,73</sup>. To improve the targeted therapy and overcome resistance, Trastuzumab was further developed in an ADC format and approved for the treatment of patient with HER2 positive MBC who have been previously received Trastuzumab and taxane therapy.

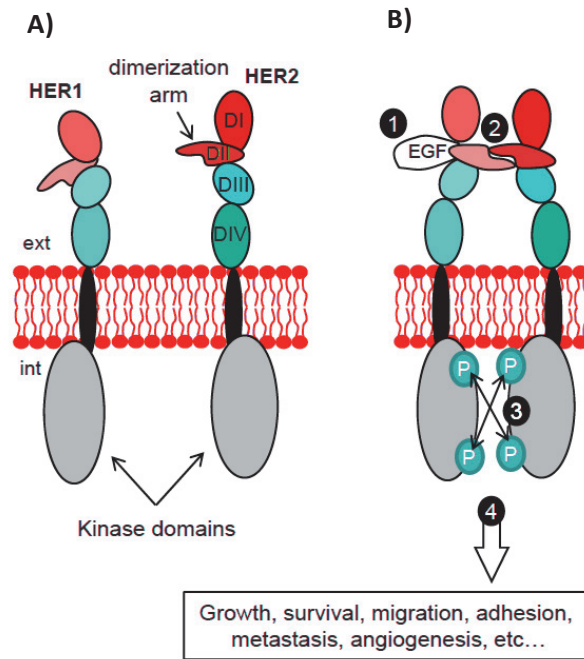


**Figure 15. Mechanism of EGFR receptors.** (A) EGFR receptors composed of an extracellular (divided into DI-DIV subunits), a transmembrane and an intracellular kinase domain. In the absence of the ligand they exhibit in monomer format. HER2 is a unique ligand-independent member of the family and its dimerization arm constitutively exists in open-conformation. (B) The binding of the ligand (1) mediates dimerization (2) that triggers the transphosphorylation of the catalytic domains (3) leading to the activation of several proliferative signalling pathways (4). (Picture taken from Luo *et al.*<sup>74</sup>)

DM1 is a derivative of a cytotoxic agent maytansine, isolated from the Ethiopian shrub *Maytenus serrata*. They inhibit microtubule polymerization by binding to tubulins at the *Vinca* site that leads to apoptotic cell death by cell cycle arrest at G2/M checkpoint<sup>75</sup>. Their cytotoxicity was demonstrated on several tumor cell lines, but due to the high nonselective systemic toxicity, it failed in clinical trials when administered systematically. DM1 (mertansine or emtansine) is a functional proper format of maytansine for ADC application, containing a thiol-group (-SH). SMCC, a non-cleavable and bifunctional (succinimide ester and maleimide functional groups) crosslinking agent is used in T-DM1. It reacts with thiol-group in DM1 and the lysine residues in Trastuzumab allowing the conjugation *via* a nonreducible thioether bound.

The conjugation does not alter the functional properties of the naked antibody, thus T-DM1 combines the mechanism of both Trastuzumab and DM1 and mediates antitumoral effects through several mechanisms. Binding of the antibody to the IV

extracellular domain of HER2 disturbs the dimerization and suppresses proliferative signal transduction<sup>76</sup>. Fc region can trigger ADCC through the recognition by macrophages or natural killer cells<sup>77</sup>. The binding to HER2 furthermore facilitates receptor-mediated internalization of the HER2-ADC complex into the endosomal-lysosomal compartments. Since T-DM1 contains a non-cleavable linker, the complete proteolytic degradation of the antibody is required for the release of lysine-MCC-DM1<sup>23</sup>. Due to the charge of the lysine, the active metabolite cannot pass through the plasma membrane, therefore the bystander effect is prevented limiting toxic effect.

In preclinical studies, T-DM1 demonstrated potent inhibition of cell proliferation in Trastuzumab-resistant breast cancer *cells in vitro*<sup>78</sup> and tumor growth inhibition in Trastuzumab and Lapatinib resistant mice models *in vivo*<sup>77</sup>. Tolerability and safety was evaluated in Phase I studies applying two different administration schedules (once-weekly or once every 3 weeks) including HER2-positive MBC patients who already received Trastuzumab treatment. Both schedules demonstrated that T-DM1 has considerable clinical benefit. It was concluded that weekly dosing of 2.4 mg/kg had antitumor activity and was adequately tolerated. In Phase II studies 3.6 mg/kg dose was administered in every 3 weeks. T-DM1 efficacy was examined in three groups of patients: 1) previously treated with Trastuzumab and chemotherapy; 2) previously treated with anthracycline, taxane, capecitabine and lapatinib, trastuzumab; 3) combination therapy with T-DM1 and Pertuzumab. Pharmacokinetic (PK) parameters revealed that the terminal half-life of T-DM1 is around 3-4.5 days and 9-11 days for total Trastuzumab; furthermore accumulation of T-DM1 was not reported. The safety profile was confirmed and significant improvement of progression-free survival (PFS) was demonstrated<sup>79</sup>. Three Phase III studies have been completed, verifying the clinical potency of T-DM1 treatment. EMILIA (ClinicalTrials.gov, identifier NCT00829166) was a randomized study to evaluate the efficacy of T-DM1 in comparison to Lapatinib plus Capecitabine. In MARIANNE (ClinicalTrials.gov, identifier NCT01120184) trial T-DM1 was examined in combination with Pertuzumab or Pertuzumab-placebo versus in the combination of Trastuzumab plus taxane. Furthermore T-DM1 evaluated in TH3RESA (ClinicalTrials.gov, identifier NCT01419197) compared to treatment of physician's choice. T-DM1 treatment

showed an improved median overall survival (OS) and PFS in patients with advanced MBC who have been treated with HER2-directed therapy or taxane.

Although many HER2-positive patient can benefit from T-DM1 treatment, resistance could unfortunately be developed. The molecular mechanisms behind the resistance have been not completely discovered yet. Considering the mechanism of T-DM1 action, it can be related to the loss of HER2 expression or disruptions in internalization processes; incomplete lysosome degradation; alternations in the Vinca site of tubulin; increased efflux of lysine-MCC-DM1 by drug-transporters<sup>80</sup>.

## 1.5 TRANSGLUTAMINASES

### 1.5.1 Mammalian transglutaminases:

Transglutaminases (TGs; EC 2.3.2.13) are a family of structurally and functionally related enzymes that catalyze calcium dependent posttranslational modifications of proteins (**Figure 16.**). They are known as nature's biological glue, their transamidase activity consists of protein crosslinking *via* isopeptide bonds between a glutamine and lysine residue and also of the incorporation of low molecular weight amines or site-specific deamidation<sup>81</sup>.

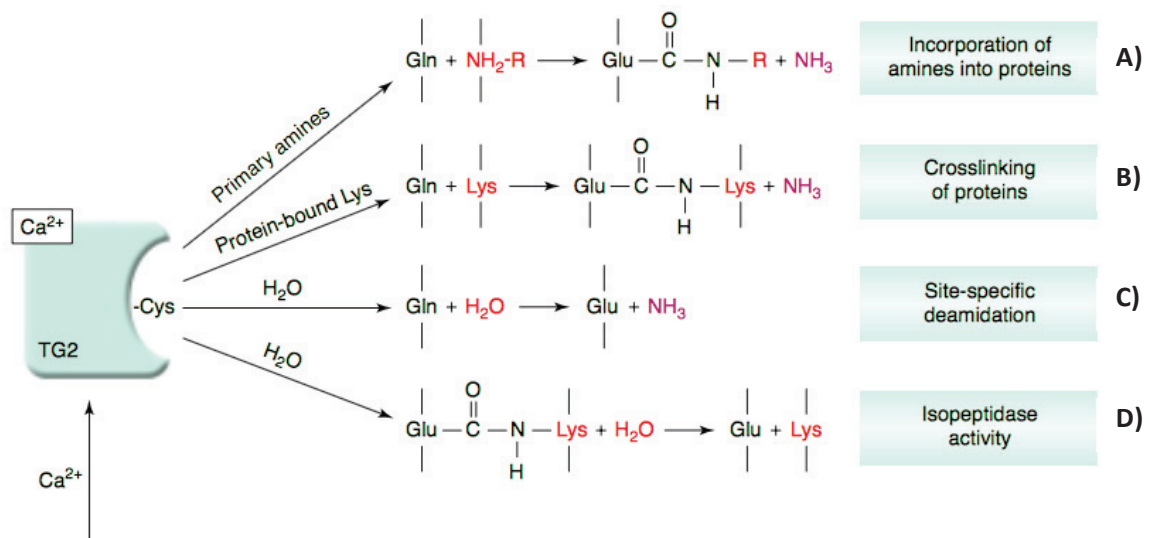


**Figure 16. Biochemical reactions catalysed by TGs.** (A) Transglutaminases catalyse Ca<sup>2+</sup>-dependent acyl-transfer reaction between the side chains of peptide-bound glutamine and lysine residue. (B) Low molecular mass amines can replace lysines in transamidating reactions. (C) In the absence of suitable amines, water can act as a nucleophile resulting in deamidation of glutamine residues<sup>81</sup>. (D) TG2 similar to FXIIIa has isopeptidase activity and can hydrolyse  $\gamma$ : $\epsilon$  isopeptides *in vitro*.<sup>82</sup> (Picture modified from Fesus L and Piacentini M<sup>83</sup>).

In the first step, the active site cysteine reacts with the  $\gamma$ -glutaminyll group of the proteins or peptides leading to the formation of a thioester intermediate and the release of ammonia. In the second step, the acyl group is transferred to nucleophilic group, either an  $\epsilon$ -amino group of a distinct protein-bound lysine or free amine

resulting in the formation of isopeptide bond<sup>84</sup>. In the absence of amine donors or at lower pH when they are not accessible due to the protonation, water can act as a nucleophile and the enzyme catalyses the deamidation of glutamine residue<sup>85</sup>. Moreover TG2 and FXIIIa display isopeptidase activity, the hydrolysis of  $\gamma:\epsilon$  isopeptides has been demonstrated upon test tube conditions<sup>82</sup>.

They are widely distributed enzymes and have been identified from unicellular organisms to mammals and plants. In mammals, nine distinct TG members have been described: keratinocyte (TG1), tissue (TG2), epidermal (TG3), prostate (TG4), type 5 (TG5), neuronal (TG6), type 7 (TG7), blood coagulation factor XIII-A subunit (FXIII-A), and the catalytically inactive erythrocyte band 4.2 protein<sup>86</sup>. **Table 4** summarises the main features of TGs<sup>87</sup>. However, the overall primary structure of TG enzymes is different, they all contain the same amino acid sequence at the active site<sup>88</sup>.

Protein	Distribution	Biological function
<b>TG1</b>	Membrane-bound in keratinocytes	Cell envelope formation in keratinocytes differentiation
<b>TG2</b>	Widely distributed in many tissues; cytosolic, nuclear, membrane, extracellular	Programmed cell death, differentiation, cytoskeletal functions, cell motility and adhesion, signal transduction
<b>TG3</b>	Hair follicle, epidermis, brain	Terminal differentiation of keratinocyte, hair follicle
<b>TG4</b>	Prostate	Reproduction and fertility in rodents
<b>TG5</b>	Foreskin keratinocytes, epithelial barrier lining, skeletal muscular striatum	Epidermal differentiation
<b>TG6</b>	Testis and lung	Responsible for the later stages of cell envelope formation in the epidermis and the hair follicle
<b>TG7</b>	Ubiquitous but predominantly testis and lung	Not characterized
<b>FXIIIa</b>	Platelets, placenta, synovial fluid, chondrocytes, astrocytes, macrophages	Blood coagulation and wound healing
<b>Band 4.2</b>	Erythrocyte membranes, bone, marrow, spleen	Membrane functions

**Table 4. Important features of TG proteins.** (Table modified from Metha K<sup>87</sup>).

### 1.5.2 General features of microbial transglutaminase:

TGs and their homologous have been also identified in lower organism, including different bacterial species<sup>89-91</sup>. Among them, firstly microbial transglutaminase (mTG) from the culture of *Streptoverticillium sp.* S8112 was isolated by Ando *et al.* in 1989<sup>92</sup> and identified as a variant *Streptomyces mobaraensis*. So far it has been the best characterized and widely used in the areas of biomedicine<sup>93</sup> and industrial applications such as food processing to modulate and improve the physical and textural properties of protein-rich products<sup>94</sup> and for the production of protein based materials, for example films/polymers<sup>95</sup>.

This enzyme is produced in a zymogen form and activated by proteases. During the conversation to the mature form, a 45 amino acid peptide is released from the N-terminus and the active site becomes accessible<sup>96</sup>. The crystal structure of mTG shows no similarity to the mammalian counterparts and the molecular size is smaller (37.8 kDa)<sup>97</sup>. Unlike other TGs, enzymatic activity of mTG is Ca<sup>2+</sup> independent, and it extends a wider thermo (42-55 °C) and pH stability (pH 5-9)<sup>92,98</sup>. These characteristics and the ability of the mass-production by conventional fermentation at low cost are advantageous for the industrial applications of mTG.

### 1.5.3 Hypothetical catalytic mechanism of mTG:

The active site of TGs shows similarity to papain-like cysteine proteases, containing a Cys-His-Asp catalytic triad (where Cys is cysteine, His is histidine and Asp is aspartic acid)<sup>99</sup>. mTG also contains a Cys residue which is essential for the acyl transfer reaction. However the amino acid sequence has no significant homology to the mammalian TGs, the hydrophobic environment around the active site Cys residue is similar to those of the other TGs<sup>100</sup>. Thus the hypothetical catalytic mechanism of mTG is very similar as well (**Figure 17**)<sup>97</sup>. The catalytic triad of mTG is formed by Cys<sup>64</sup>, Asp<sup>255</sup>, His<sup>274</sup> residues; in the proposed mechanism the Cys<sup>64</sup> and Asp<sup>255</sup> residues are principally involved in the acyl transfer reaction. The first step, is a nucleophile attack of thiolate ion of Cys<sup>64</sup> to react with the acyl donor ( $\gamma$ -carboxiamide of a glutamine)

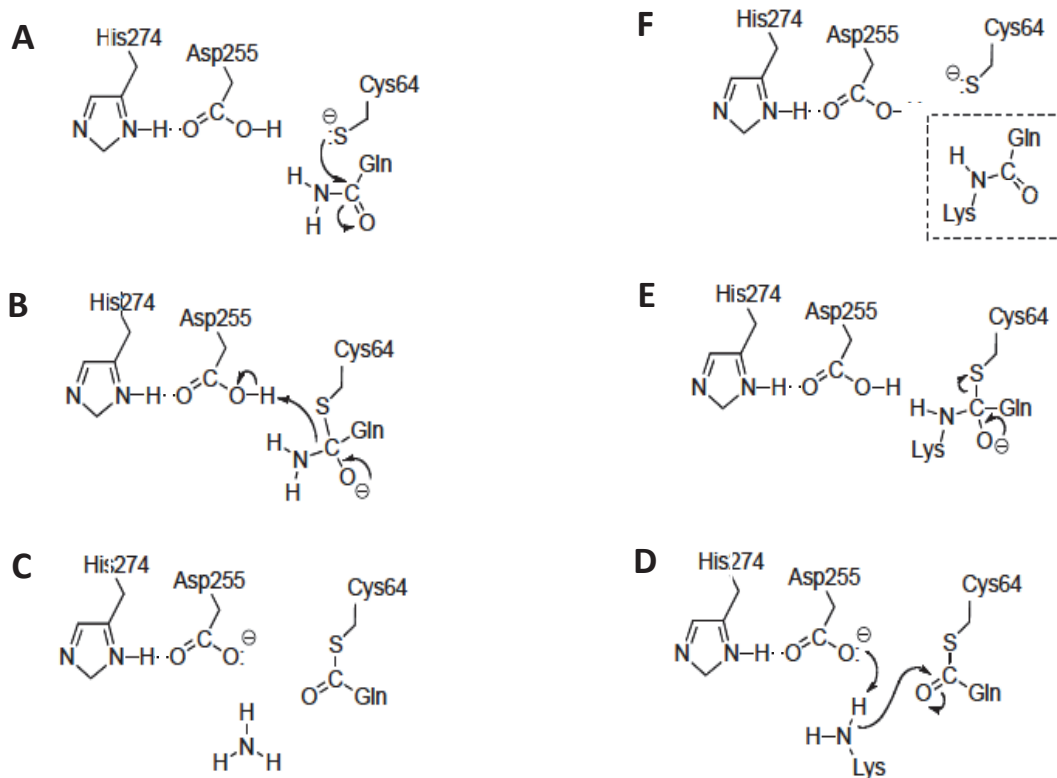


**Figure 17. Hypothetical catalytic mechanism of mTG.** **A)** In the first step the active site cysteine reacts with the  $\gamma$ -glutamyl group of the proteins or peptides leading to a thioester intermediate that is followed by the formation of **B)** acyl-enzyme intermediate and **C)** the release of ammonia. **D)** The transfer of the acyl group to an amine substrate results in the formation of the isopeptide bound. As a final steps, **E)** the product is released and **F)** the enzyme is regenerated. (Figure taken from Kashiwagi T *et al.*<sup>97</sup>).

forming a thioester intermediate (**Figure 17A**). In the next step Asp<sup>255</sup> donates a proton to the acyl-enzyme intermediates (**Figure 17B**) and ammonia is released (**Figure 17C**). Then, the primary amine (side chain of lysine of proteins or other aliphatic amine) reacts with the active site and the negatively charged side chain of Asp<sup>255</sup> residue subtracts a proton from the acyl acceptor (**Figure 17D**) resulting in a NE ( $\gamma$ -glutamyl)lysine isopeptide or ( $\gamma$ -glutamyl)amine bound. Finally the product is released and the active side of the enzyme is regenerated (**Figure 17E and F**). This isopeptide bound is very stable: it cannot be hydrolysed by any of the known eukaryotic enzymes and it is highly resistant to temperature, detergents, reducing and chaotropic agents.

In the absence of the suitable primary amines or at low pH when their availability is limited due to the protonated ionization state<sup>101</sup>, water can serve as a nucleophilic acyl acceptor substrate and the enzyme catalyses the deamidation of

glutamine to glutamate<sup>85,102</sup> (**Figure 16C**). The conversion of an uncharged amino acid to a negatively charged residue can introduce alteration in the protein's conformation and modulate the physicochemical properties. However, the hydrolysis of glutamine donor substrate can be avoided by applying higher molar excess of the amine donor substrate<sup>102,103</sup>. It has been reported that mTG displays lower deamidation rate than other TGs<sup>104,105</sup>, that may be explained by the essential role of negatively charged Asp<sup>255</sup>, while a positively charged His residue is required for the catalytic activity of other TGs. Thus positively charged amino acids are rather attracted by the electrostatic interaction with Asp<sup>255</sup> residue than neutral ones such as water molecule<sup>97</sup>.

#### 1.5.4 Structure and substrate specificity of mTG:

However the difference in the overall crystal structure, the catalytic triad (Cys<sup>64</sup>, Asp<sup>255</sup>, His<sup>274</sup>) is located in  $\beta$ -turn containing  $\alpha$ -helix and  $\beta$ -sheets secondary structure that shows similarity to other TGs<sup>97,100</sup> (**Figure 18.**). The catalytic activity is mainly based on a Cys-Asp diad, where Asp<sup>255</sup> is essential for the enzymatic reaction and play the role of the His residue in FXIII-like TGs and cysteine proteases<sup>97</sup>. It has been reported that mTG displays border substrate specificity for the glutamine donor substrate and higher reaction rate than the mammalian TGs<sup>106</sup>; that may be explained

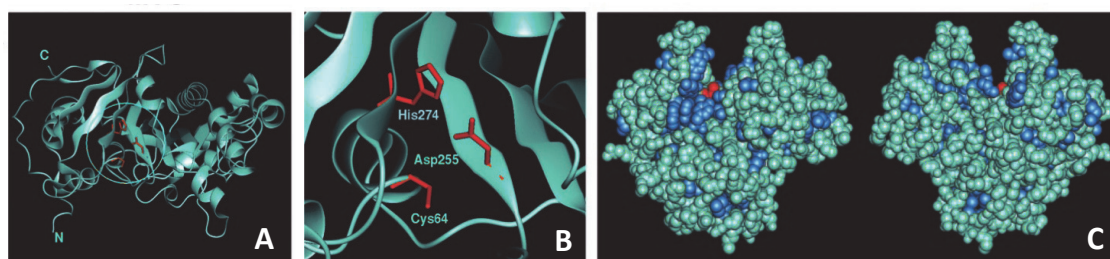


**Figure 18. Structure of microbial transglutaminase from *Streptomyces mobaraensis*.** (A) Overall crystal structure as a ribbon model. (B) Structure of the active site: the catalytic triad (Cys<sup>64</sup>, Asp<sup>255</sup>, His<sup>274</sup>) are represented by the red wire model. (C) Van der Waal model, the front and the rear views are shown on the left and right, respectively. Aromatic and hydrophobic residues: blue, Cys64: red, other residues: green. (Picture modified from Kashiwagi T et al<sup>97</sup>).

by these structural dissimilarities. A cleft becomes exposed in the active form of mTG, located in the upper site of the enzyme. Tagami *et al.* reported that this region plays a role in substrate binding, moreover the hydrophobic and aromatic residues along the active site are important for the interaction. Docking and nuclear magnetic resonance based studies revealed, that small molecular weight CBZ-Gln-Gly (where Gln is glutamine, and Gly is Glycine) is stretched across the cleft whereas the recognition of larger molecular weight substrates such as ovalbumin may expanded on the external surface area of the cleft<sup>107</sup>.

The physiological role of mTG is poorly understood and there is only few data available about its the natural substrates<sup>108-111</sup>. Since mTG is widely used in the industry, information regarding the substrate specificity and sequence preference is important to improve its application. TGs are generally less selective towards the amine donor residue while the specificity of the enzymatic reaction is mainly determined by the glutamine donor substrate<sup>112</sup>. Recently the acceptance of mTG towards several different proteins was investigated and the reactive glutamine residues were identified. In addition the preferred substrate sequences for the enzyme were suggested by peptides library screening studies.

The analysis of granulocyte colony stimulating factor, human growth factor hormone, apomyoglobin<sup>109</sup>, type I collagen<sup>110</sup>,  $\alpha$ -lactalbumin and thermolysine<sup>113</sup> revealed some general structural features required for the enzyme-substrate interaction. The glutamine residues attacked by mTG were located in disordered regions, indicating that the chain flexibility is favourable for the binding<sup>107,109</sup>. Similarly to other TGs, the globular proteins become more accessible substrates after partial unfolding, such as heat denaturation<sup>113</sup>.

Leu-Leu-Gln-Gly (LLQG) sequence was firstly identified as a natural peptide substrate of the enzyme and used for protein modification<sup>104,114</sup>. Some studies have been carried out to determine the effect of neighbouring amino acids around the glutamine as well as the preferred substrate sequences. Using a heptapeptide containing six of Gly and one of Gln residues Ohtsuka *et al.* observed that N-terminal substitution of glutamine with hydrophobic amino acids such as valine (Val) or leucine (Leu) increased the reactivity for mTG<sup>115</sup>. The location matter of the Leu in -1 position (N-terminal side) was verified also by Sugimura *et al.* and in addition the importance of

certain amino acids in desired positions was explored. They demonstrated a tendency for the aromatic amino acids (tryptophan, Trp; phenylalanine, Phe or tyrosine, Tyr) at -3 to -5, arginine (Arg) and hydrophobic amino acids at +1 and +2 (C-terminal side) as well as at -1 or -2, furthermore aromatic residues at +3 orientation to the reactive glutamine. These preferred N-terminal sequences can confirm the crucial role of hydrophobic residues in the cleft region in the recognition of the substrate. Besides, the positive charged Arg in C-terminal direction can be favourable for the interaction with the negatively charged Asp<sup>255</sup> catalytic residue<sup>116</sup>. A further study also confirmed the positive influence of hydrophobic and basic amino acids, especially Arg, Tyr, and Leu for the enzymatic reaction<sup>117</sup>.

Similarly to other TGs, it has been demonstrated that mTG can accept a board range of the amine donor substrate in native proteins or non-natural derivatives<sup>111,118,119</sup>.

Overall it can be concluded that mTG is promiscuous for the amine donor substrate, however in case of the glutamine donor substrate the primary structure, the neighbouring amino acids and the conformational factors are important.

### **1.5.5 mTG mediated conjugation of antibodies:**

Microbial transglutaminase is widely used for protein modification. Recently it has been discovered that it can be an efficient tool for the production of homogeneous ADCs<sup>49,120–122</sup>. Since the enzyme catalyses the crosslinking reaction between two substrates, in principle the conjugation can be carried out in two ways: the glutamine donor can be localised in the antibody sequence and the payload molecule contains the amine donor residue or vice versa. The coupling can be achieved by reactive groups in the native IgG sequence as well as by engineered small peptide substrates.

Despite human IgG1 contains approximately 60 glutamine residues, mTG does not recognize any of them in the native antibody structure. It has been reported that after deglycosylation of the antibody, a glutamine at 295 position (Q295) in the heavy chain can become a conjugation site for the enzyme, resulting in a DAR2. The substitution of an asparagine at 297 position to glutamine (N297Q) can lead to

DAR4<sup>120–122</sup> (**Figure 19A**). This mutation, leading to DAR4 was originally generated to achieve more rapid blood clearance of radiolabeled Immunoconjugates<sup>123</sup>. Nevertheless, this technology was demonstrated to be a potential ADC conjugation method, but because of the absence of the N-glycosylation, the reduced plasma-half life and potential alterations in their stability and aggregation rate should be considered.

The mTG-based approach was further developed by engineered peptide sequences. Strop *et al.* inserted the sequence of LLQG peptide at 90 different positions in the antibody sequence to investigate the effect of the location site of the drug *in vivo* on the linker stability and PK properties (**Figure 19B**). They demonstrated that the

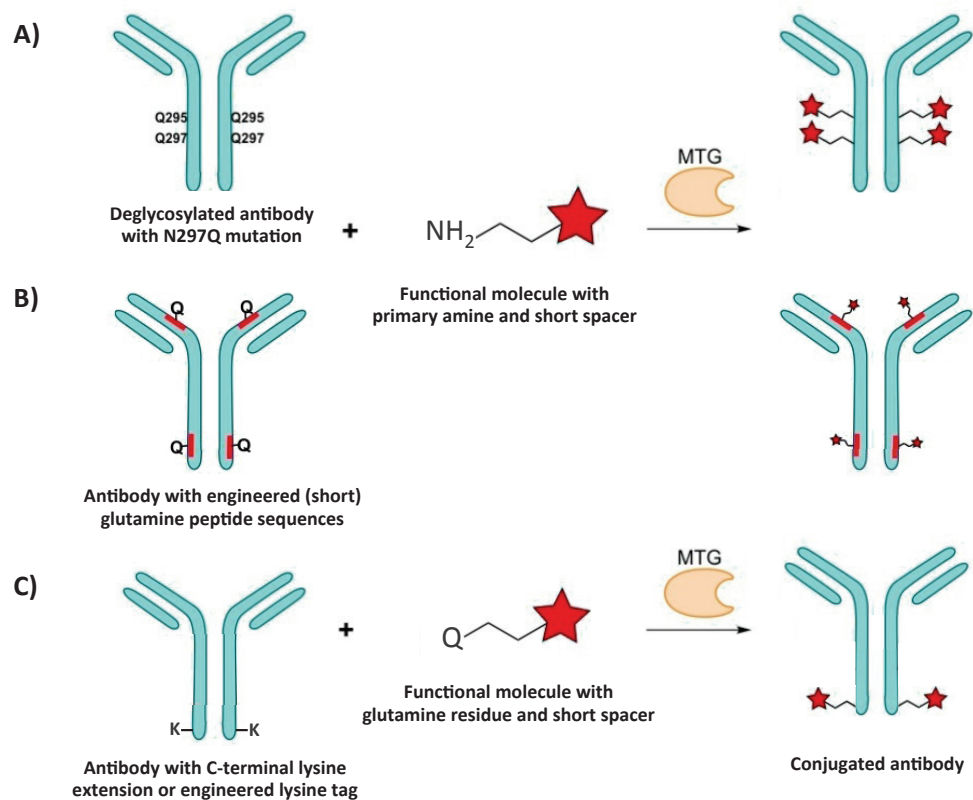


**Figure 19. Microbial transglutaminase mediated conjugation of antibodies.** A) Deglycosylated antibody with N297Q point mutation. B) Antibody with engineered glutamine peptide sequence. C) Antibody with engineered lysine tag or extension with C-terminal lysine residue. MTG, microbial transglutaminase; N, asparagine; Q, glutamine. (Figure adapted from [http://zedira.com/by/Roger\\_Schibli](http://zedira.com/by/Roger_Schibli)).

C-terminal position in the heavy and light chains is the best allowing the development of suitable ADCs<sup>49</sup>. Another attempt has been reported to optimize the conjugation reactions by the modification of substrate tag. The authors took the general rule that the tertiary structure can be more important for the protein-protein interactions than the amino acid sequence as a basis. A conformationally locked recognition motif was designed and introduced to the C-terminal heavy chain sequence. The conjugation efficiency was approximately 85-86% in case of fluorescently labelled cadaverine<sup>124</sup>.

There are some studies about mTG mediated modification of the antibodies also *via* lysine residues. Since the transamidation of the wild type antibody with glutamine donor payloads cannot be observed, the conjugation can be achieved by analogue approaches as described above. Either a short lysine tag<sup>120</sup> or a single amino acid mutation can be introduced into the antibody sequence (**Figure 19C**). Lysine substitution in flexible structure environments or by blocking the cleavage of heavy chain C-terminal lysine residue during the *in vitro* production can result in acyl acceptor sites for the enzymatic modification. Furthermore the extension of the C-terminal with any nonacidic, nonproline amino acids could increase the reaction efficacy<sup>125</sup>.

## 2 AIM OF THE THESIS

---

ADCs have shown promising clinical results and over the last 30 years several important developments have been achieved to advance their potency. Thanks to the targeted delivery, they can improve the therapeutic window in comparison with the conventional chemotherapeutic treatment. The current ADCs approved by U.S. Food and Drug Administration (FDA) are generated by traditional chemical conjugations (*via* lysine or cysteine residues of the antibodies) and exist as heterogeneous mixtures. Recent studies have revealed that the heterogeneity of ADCs negatively influences their *in vivo* performance. In order that ADCs can deliver their full potential, the development of efficient site-specific conjugation methods is essential. Currently several site-specific technologies have been established and undergoing clinical investigations in order to reduce heterogeneity and batch-to batch variability. The increasing number of new conjugation strategies demonstrates the interest and importance of this approach. Among them, enzymatic methods (sortase A, formylglycine generating enzyme, mTG) are based on the insertion of short peptide sequences into the antibody backbone that can be suitable for different antibody formats as well. mTG has several advantages properties, including its low cost production, formation of a highly stable isopeptide bond and mild reaction conditions, that is well represented by its numerous industrial and biotechnological applications.

Covalab has years of experiences in antibody customer services and transglutaminase research field, such as in the development of isoenzyme specific peptide-based activity assays or active site inhibitors. Considering the benefits and demonstrated success of mTG-technology, the development of site-specific homogeneous ADC was addressed. Strop *et al.* have reported that the insertion of LLQG tag is an efficient tool for the generation of site-specific ADCs<sup>1</sup>. This sequence was previously identified as a natural peptide substrate for the enzyme and it has been already used for protein modifications.

The aim of my thesis was to improve the mTG-based ADC approach. Since transglutaminases can accept wide range of amine donors and the selectivity of the

reaction is determined by the glutamine donor substrate, we addressed to increase the conjugation efficacy by using optimised glutamine donor peptides (Q-tag). Previously, Covalab has designed a synthetic peptide library<sup>2</sup> to enhance their reactivity in comparison with LLQG, and four potential peptides with low apparent  $K_M$  (Michaelis constant is the substrate concentration at which the reaction rate is half of the maximum) have been selected.

In the first part of the project the enzymatic conjugation method (CovIsoLink™) with the full-length antibody was developed and evaluated (Page 56). For ADC generation, as a proof of concept we selected the sequence of Trastuzumab targeting HER2 receptor. First, the conjugation technology was established: following the construction and production of the Q-tagged recombinant antibodies the reaction rate was examined, the most efficient Q-tagged antibody was selected and engrafted with different payloads. Then the functionality and the therapeutic value of CovADCs were studied in a series of *in vitro* and *in vivo* assays in comparison to T-DM1, currently the only FDA approved ADC for solid tumor.

In the second part of the project, we aimed to demonstrate that this technology can be generalised to different antibody formats, such as Fab and scFv, retaining their antigen binding. Due to the smaller size, these fragments shows increased tumor distribution but on the other hand, their plasma half life is reduced. The ability for deeper penetration into the tumor mass can be especially advantageous in case of solid tumors and the short half life can be beneficial for radiotherapy or diagnostic approaches. As a proof of concept, the conjugation of Q-tagged scFv and Fab constructs with fluorescent compound was carried out in order to evaluate the coupling efficiency and their immunoreactivity (Page 81).

In the third part of my thesis, a recently submitted (FEBS Open bio) article about an optimised method for rapid and easy detection and examination of transglutaminase mediated transamidation (cross-linking) and deamidation (depending of availability of the amine donor) reactions. As an outlook of the ADC project, the better understanding of the transglutaminase reactions is important, because for ADC production the reaction conditions should be optimised to avoid deamidation. Theses results will be presented in page 90.

### 3 NEW BACTERIAL TRANSGLUTAMINASE Q-TAG SUBSTRATE FOR THE DEVELOPMENT OF SITE SPECIFIC ANTIBODY DRUG CONJUGATES

---

#### AIM

Microbial transglutaminase has been demonstrated as an efficient tool for the generation of site-specific ADCs either by deglycosylation of the antibody or by introducing a peptide-substrate sequence (Q-tag) into the antibody backbone. The aim of my thesis is to improve the mTG-mediated conjugation by engineering of optimised glutamine donor peptides into the sequence of the antibody. Previously Covalab has designed a synthetic peptide library<sup>2</sup> and four potential peptides with lower apparent  $K_M$  over the already known sequences have been selected.

In the first part of the project, the enzymatic conjugation technology (CovIsoLink™) with the full-length antibody was developed and established (**Figure 1**). The Q-tag peptides were genetically engineered into the heavy chain C-terminal of the Trastuzumab antibody and the coupling efficacy was assessed using AlexaFluor488-cadaverine and SDS-PAGE analysis (Fluorescent detection). Since the conjugation reaction resulted in antibody dimers and polymers, we addressed to identify and delete the lysine in the antibody sequence that can serve as an amine donor substrate resulting in cross-linked antibodies. Subsequently, the Q-tagged mAb with the highest reactivity toward mTG was conjugated with potent tubulin inhibitor payloads (DM1 and MMAE) and analysed by mass spectrometry. In order to validate the therapeutic value of our technology in comparison with T-DM1 that is already used for the treatment of the patients with HER2 positive MBC, CovADCs were examined in series of *in vitro* and *in vivo* assay, including cytotoxicity, immunostaining, biodistribution and anti-tumor activity.

In the next part of my thesis these results are presented in a paper format that is going to be submitted soon in Biochemical Journal.

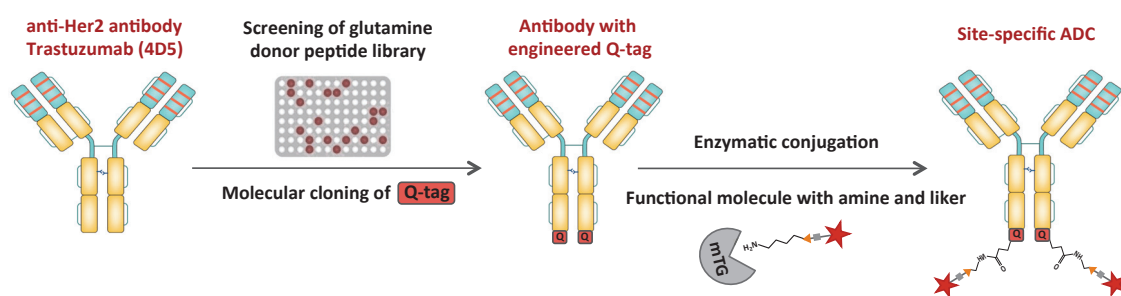


**Figure 1. CovIsoLink™ technology for mTG mediated site-specific antibody conjugation.** Q-tag, glutamine donor peptide-substrate; mTG, microbial transglutaminase. (Figure partially adapted from Beck *et al.*<sup>37</sup>).

# NEW BACTERIAL TRANSGLUTAMINASE Q-TAG SUBSTRATE FOR THE DEVELOPMENT OF SITE SPECIFIC ANTIBODY DRUG CONJUGATES

---

Eva Sivado<sup>1,2</sup>, Vincent Thomas<sup>1</sup>, Meddy El Alaoui<sup>1</sup>, Michael R. Dyson<sup>3</sup>, John McCafferty<sup>3</sup>, Charles Dumontet<sup>4</sup>, Said El Alaoui \*<sup>1</sup> and Sandrine Valsesia-Wittmann\*<sup>2</sup>

<sup>1</sup>Covalab, 11 Bd Einstein 69100 Villeurbanne, France, <sup>2</sup>Centre Léon Bérard, Innovations in Immunotherapy Platform, 28 rue Laennec 69008 LYON, France, <sup>3</sup>IONTAS Ltd, Babraham Research Campus, Babraham, Cambridge, CB22 3AT UK, <sup>4</sup>NSERM 1052/CNRS 5286/UCBL, Lyon, France.

## ABSTRACT

Antibody-drug conjugates (ADCs) are a powerful class of therapeutic agents, demonstrating success in the treatment of several malignancies. The currently approved ADCs are produced by chemical conjugations and exist as heterogeneous mixtures that negatively influence the pharmacokinetics and *in vivo* performance. Recently many site-specific conjugation technologies have been developed to reduce heterogeneity and batch-to batch variability. Microbial transglutaminase (mTG) has been demonstrated as efficient tool for site-specific conjugation. Here we describe CovIsoLink™ (Covalently Isopeptide Crosslinking) technology for the generation of homogenous immunoconjugates using a novel glutamine donor peptide (Q-tag) with improved affinity compared to the known peptides (ZQG, LLQG). We presented the reproducible and homogeneous conjugation of Q-tagged Trastuzumab with different payloads, without any unconjugated species. The ADCs were evaluated in series of *in vitro* and *in vivo* assays, demonstrating similar tumor cell killing potency as Ado-Trastuzumab emtansine (Kadcyla®) even with lower drug-to-antibody ratio (DAR).

## KEYWORDS

Site-specific antibody-drug-conjugates, Microbial transglutaminase, Homogeneous conjugates

---

## 3.1 INTRODUCTION

Antibody-Drug conjugates (ADCs) are a progressive class of anticancer agents. Adopting Paul Ehrlich's "magic bullet" idea, they were designed to selectively deliver highly potent cytotoxic payloads to the malignant cells<sup>3</sup>. They combine the advantages of therapeutic monoclonal antibodies (mAbs) and the chemotherapeutic compounds. In this manner, the target specificity of mAbs enables the potent acceleration of tumor reaching drugs while leaving the normal cells largely unaffected, thus decreasing the off-target toxicity and increasing the therapeutic window<sup>4</sup>. There is considerable progress and success in this field, the number of ADCs entering to clinical trials are rapidly increasing. Nevertheless, so far, only four ADCs have been approved by the U.S. Food and Drug Administration (FDA): CD30-targeted Adcetris® for the treatment of Hodgkin's lymphoma, HER2-targeted Kadcyla® (T-DM1) for breast cancer, CD33-targeting Mylotarg® for acute myeloid leukemia and CD22-targeted Besponsa® for B-cell acute lymphoblastic leukemia<sup>5</sup>. These Immunoconjugates are produced by conventional chemical conjugations of surface exposed lysine (*via* activated esters) or interchain cysteine (maleimide chemistry) residues, resulted in heterogeneous mixtures<sup>6</sup>. Thus, each subpopulation exhibits distinct pharmacokinetic (PK) properties.

The potential extension of the therapeutic index and the *in vivo* performance is limited by heterogeneity of ADCs<sup>7</sup>. Further attempts are ongoing in order that ADCs can deliver their full potential and simplify manufacturing challenges. Recently several site-specific conjugation technologies have been developed to control the drug-to antibody ratio (DAR), reduce heterogeneity and batch-to batch variability. Based on the antibody scaffold we can distinguish two main strategies: 1) the selective conjugation is achieved novel linker chemistry using the native mAb<sup>8</sup>. 2) Molecular engineering is required to introduce the coupling site into the mAb sequence such as mutation of cysteine residues<sup>7,9</sup>, glycoengineering<sup>10</sup> or insertion of unnatural amino acids<sup>11</sup> or peptide sequences for enzymatic approaches<sup>1,12-15</sup>.

Recent studies have demonstrated microbial transglutaminase (mTG) can be an efficient tool for the production of site-specific homogeneous ADCs. The enzyme catalyses the formation of a highly stable isopeptide bond between the  $\gamma$ -

carboxiamide group of glutamines and  $\epsilon$ -amino groups of lysine residues<sup>16</sup>. The conjugation can be achieved by deglycosylation of the antibody and introducing a single amino acid mutation (N297Q)<sup>13,14</sup> or by genetically engineered peptide sequence (LLQG)<sup>1</sup>. However it should be considered, that the absence of N-glycosylation can reduce the plasma-half life and alter the stability and aggregation rate of the ADCs. LLQG peptide was previously identified to be a natural substrate and have been used for protein modifications<sup>17</sup>.

In this study, we report the development CovIsoLink™ (Covalently Isopeptide Crosslinking) technology for the generation of homogeneous ADCs using novel and advanced mTG-substrate sequences engineered into the heavy chain C-terminal of Trastuzumab antibody. Since transglutaminases display broad amine donor substrate specificity, they are more selective towards the reactive glutamine donor residue<sup>18</sup>. We addressed to improve the mTG-mediated conjugation by the optimisation of glutamine-containing peptide substrates. Our group has previously designed a synthetic peptide library to enhance their reactivity in comparison with LLQG<sup>2</sup>. The ADCs were conjugated with several payloads and evaluated in series of *in vitro* and *in vivo* models. Even with lower DAR, they showed similar potency than Kadcyła® used in the clinic.

---

## 3.2 MATERIALS AND METHODS

### 3.2.1 Construction of recombinant antibodies with glutamine tag

The variable region sequence of Trastuzumab (clone 4D5) was cloned into TGEX-LC (human kappa) and TGEX-HC (human IgG1) mammalian expression vectors (Antibody Design Laboratories, USA) (**Figure 2**) by restriction cloning (LC: BspEI and BsaI, HC: BssHII and BsmBI, Thermo Fisher Scientific, France). The amino acid sequences of different glutamine-tag substrates (LLQG, Tag2, Tag3, Tag4, Tag5) specific for microbial transglutaminase were introduced into the C-terminal part of the heavy chain by overlap extension inverse polymerase chain reaction (PCR). The sequences of the peptide tags are not shown, since they are currently patented. Additionally the heavy chain C-terminal lysine453 was deleted by site directed mutagenesis.

The primers were designed with OligoAnalyzer 3.1 ([www.idtdna.com](http://www.idtdna.com)) and synthesized by Eurogentec (polyacrylamide gel electrophoresis (PAGE) purification), the sequences are listed in Table 1. 50 µl PCR reaction was composed of 0.5 µl template (5 ng), 2.5 µl of each primer (10 µM), 1µl dNTP mixture (10 mM) (Promega, France), 10 µl 5× Phusion HC buffer (New England Biolabs, France), 1.5 µl DMSO (New England Biolabs, France), 31.5 µl nuclease free H<sub>2</sub>O (B. Braun, France) and 0.5 µl Phusion high-fidelity DNA polymerase (2000 U/ml) (New England Biolabs, France). The PCR cycling parameters were 98°C 30 sec, (98°C 10sec, 72°C 1.5 min) × 30 cycles and 72°C 7 min.

Following the PCR reaction, 2 µl DpnI (10 U/µl) (Thermo Fisher Scientific, France) was added and the mixture was incubated at 37 °C for 4 h to degrade the original unmodified plasmid templates. After DpnI digestion, 5µl of the mixture was used to transfect low recombination NEB 5-alpha competent *E. coli* cells (New England Biolabs, France) according to the manufacturer's instructions. Plasmid DNA was isolated using PureYield Miniprep Kit (Promega, France) and sequenced.

Primers	Modifications	Sequences (5' to 3')
<b>For-ID1</b>	Insertion of LLQG	CTGCTCCAGGGATGAGCGGCCGAGATCCC
<b>Rev-ID1</b>	Insertion of LLQG	TCCCTGGAGCAGTTTACCCGGAGACAGGGA GAGGC
<b>For-ID2</b>	Insertion of Tag2	XXXXXX
<b>Rev-ID2</b>	Insertion of Tag2	XXXXXX
<b>For-ID3</b>	Insertion of Tag3	XXXXXX
<b>Rev-ID3</b>	Insertion of Tag3	XXXXXX
<b>For-ID4</b>	Insertion of Tag4	XXXXXX
<b>Rev-ID4</b>	Insertion of Tag4	XXXXXX
<b>For-ID5</b>	Insertion of Tag5	XXXXXX
<b>Rev-ID5</b>	Insertion of Tag5	XXXXXX
<b>For-ID6</b>	Deletion of lysine453	XXXXXX
<b>Rev-ID6</b>	Deletion of lysine453	XXXXXX

**Table 1. Primers used for insertion of glutamine tags and deletion of heavy chain C-terminal lysine.**

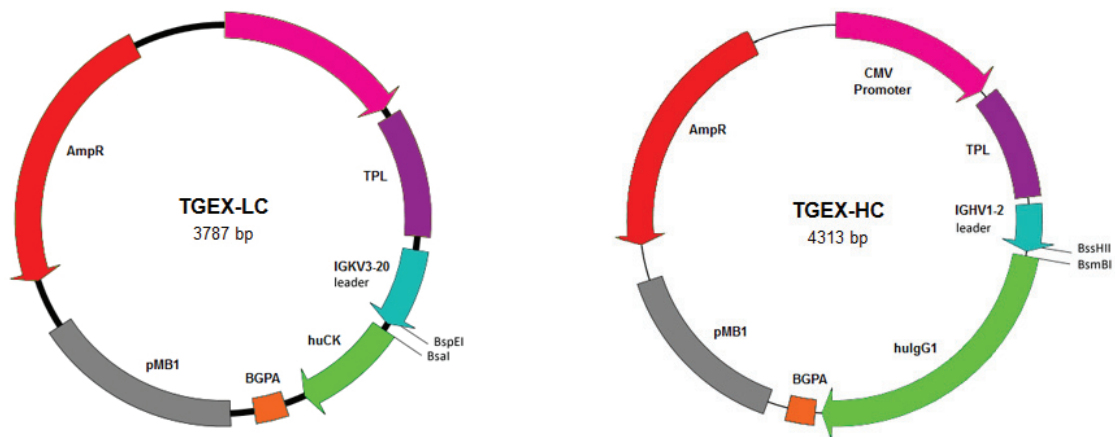


**Figure 2. Plasmid map of TGEX-LC and TGEX-HC cloning vectors (*Antibody Design Laboratories*).**

### 3.2.2 Expression and purification of recombinant antibodies

The recombinant antibodies (rAbs) were transiently expressed in HEK293AD cells (ATCC). Cotransfection of LC and HC plasmides were carried out with Lipofectamin 3000 (Thermo Fisher Scientific, France) in Opti-MEM reduced serum media (Thermo Fisher Scientific, France) according to the manufacturer's instructions.

Cell culture supernatants were purified by protein A-sepharose (GE Healthcare, France), washed with 1x PBS (140 mM NaCl, 2.7 mM KCl, 10 mM Na<sub>2</sub>HPO<sub>4</sub>, 1.8 mM KH<sub>2</sub>PO<sub>4</sub>), eluted with 0.1 M glycine pH3 and immediately neutralized with 1M Tris-HCl pH 8. The buffer was exchanged against 1x PBS with Zebaspin desalting column (MWCO 40 kDa, Thermo Fisher Scientific, France). The purity of the rAbs was assessed by Sodium Dodecyl Sulfate polyacrylamide gel electrophoresis (SDS-PAGE) and silver nitrate staining. The average yield of the purified mAbs was 10 mg/L.

### 3.2.3 Enzymatic conjugation

For conjugation of antimetabolic agents, amine-PEG4-VC-PAB-MMAE and amine-PEG4-SMCC-DM1 (reconstituted in DMSO; Sigma, France) were pre-incubated with 1mM triethylamine (Sigma, France) for 10 min at room temperature (RT) with gentle

shaking. The final antibody concentration was adjusted to 10 mg/ml and incubated with 30-fold (MMAE) or 10-fold (DM1) molar excess of the drugs in the presence of microbial transglutaminase (17 U/mg antibody; Zedira, Darmstadt, Germany) in PBS buffer. The reaction was performed overnight (O/N, 16 hours) at room temperature (RT) with gentle agitation. The excess of the payloads and the enzyme were removed by protein A purification (detailed in section 2.3.2) then the buffer was exchanged buffer against 1x PBS with Zebaspin desalting column (MWCO 40 kDa, Thermo Fisher Scientific, France). The products were analyzed by LC/MS.

The conjugation of fluorophores was carried out in PBS buffer, containing 0.25 mg/ml of antibody, 30 fold molar excess of AlexaFluor448-cadaverine or AlexaFluor647-cadaverine (Thermo Fisher Scientific, France) and 4 U/mg antibody of microbial transglutaminase. Following O/N incubation with gentle shaking at RT, the tagged antibodies were purified by proteinA (detailed in section 2.3.2). Fluorescent labeled conjugates were analyzed on 10% SDS-PAGE and visualized by UV-fluorescent detection and Silver-nitrate staining.

### **3.2.4 MS analysis**

Mass spectrometric analyses of ADCs were performed on a Bruker maXis mass spectrometer coupled to a Dionex Ultimate 3000 RSLC system. Prior to MS analysis, samples (ca. 5 µg) were desalted on a MassPREP desalting cartridge (2.1 x 10 mm, Waters) heated at 80 °C using 0.1% formic acid as solvent A and 0.1% formic acid in acetonitrile as solvent B at 500 µL/min. After 1 min, a linear gradient from 5 to 90% B in 1.5 min was applied; the first 1.5 min were diverted to waste. HRMS data were acquired in positive mode with ESI source over the m/z range from 900 up to 5000 at 1 Hz and processed using DataAnalysis 4.4 software (Bruker) and MaxEnt algorithm for spectral deconvolution.

### 3.2.5 Immunoreactivity analysis (Surface Plasmon Resonance)

Binding kinetics and affinity of wild type (Ab-Qtag) and heavy chain C-terminal lysine deleted rAb with engineered Tag2 (K453delAb-Qtag) or MMAE conjugated format (K453del-ADC-MMAE) to recombinant human Her2 protein (rh-Her2, Acro Biosystems, USA) was measured by Surface Plasmon Resonance method on Octect system (PALL FortéBio, France). Recombinant Abs were diluted in 1x kinetics buffer (PALL ForteBio, France) to achieve a final concentration of 5 µg/ml and were immobilized onto anti-human IgG Fc capture (AHC) biosensor (PALL ForteBio, France). Rh-Her2 was injected for 600 sec ranging from 2 nM to 20 nM (diluted in 1x kinetics buffer) and association/dissociation was monitored for 300 sec. Double-referenced binding curves were subtracted to prevent system artifacts and non-specific binding, then binding curves were fit to 1:1. The affinity constants ( $K_D$ ) were calculated from the ratio of the association and dissociation rate constants ( $k_{on}/k_{dis}$ ).

### 3.2.6 Internalisation assay

MDA-MB-231 cells and SKBR3 cells are plated in a 96 wells plate at 7500 cells per well. After 36 h, cells were washed with 100 µl of Fluorobright DMEM (Life technologies, France) to remove the phenol red. The lyso tracker dye was diluted 10 000 times, the cell mask dye was diluted 1000 times and were incubated together 30 min at 37°C. The nucleus staining was performed with 0.5 µg/ml of Hoechst 3342 (Life technologies, France) and then incubated 10 min at 37°C. The plate was washed again with 100µl of fluorobrite DMEM. The antibody was injected and the kinetic was immediately recorded at 37°C by an HCS Operetta microscope during 3 h. Control were performed on ice in order to block the cell metabolism. After 3h the plate was washed with PBS and the cells were fixed with 150 µL of paraformaldehyde at 4°C for 15 min. The plate was washed with 150 µl of PBS and imaged by confocal microscope (LSM 780 Confocal microscope, Zeiss, France).

### 3.2.7 *In vitro* cytotoxicity assay

*In vitro* cytotoxicity of CovADC-DM1 and CovADC-MMAE was compared to T-DM1 (Kadcyla, Roche, France) on BT-474 and SKBR3 Her2-positive breast cancer cell lines, MDA-MB-231 Her2-negative cell line was included in the assay to confirm target selectivity. All cell lines were obtained from ATCC and cultured in DMEM supplemented with 10% FBS, 100 U/ml penicillin/streptomycin and 2 mM L-glutamine (Life technologies, France). Cells were maintained at 37 °C with 5% CO<sub>2</sub> atmosphere. Optimal cell density of each cell lines was determined by IncuCyte S3 live-cell analysis system (Essence BioScience, UK). Cells were plated (SKBR3 and BT-474: 5,000 cell per well, MDA-MB-231: 1,250 cell per well) on 96 well plates. Following the incubation for 24 h, cell culture medium was removed and serial dilutions of ADCs and free unconjugated drugs were added in triplicates. After 3 days incubation cytotoxicity was evaluated by sulforhodamine B assay (SRB assay kit, Sigma, France) based on the measurement of cellular protein content according to the manufacturer's instructions. Briefly, cells were fixed with 50% (wt/vol) TriChloroacetic Acid (TCA) at 4 °C (30 µl/well, final concentration 11.5%) for 1 h. After washing with dH<sub>2</sub>O cells were stained with 100 µl of 0.04% (wt/vol) SRB solution for 30 minutes and subsequently washed with 1% (vol/vol) acetic acid to remove unbound stain. Cellular protein bound dye was solubilized in 200 µl of 10 mM Tris base solution (pH 10.5) and the absorption was measured at 510 nm (Microplate reader, Tecan, Switzerland). The raw data was processed using GraphPad Prism 7.0 (GraphPad Software, San Diego, USA). Error bars in graphs represent SEM of two measurements.

### 3.2.8 Biodistribution

Anti-Her2 CovADC-MMAE (2 mg/ml) was conjugated with DMSO dissolved Alexa Fluor 680-NHS ester (10 mg/ml) (Thermo Fisher Scientific, France) at a molar ratio of 1:44 in 0.1 M bicarbonate buffer pH 9 for 1 h at RT. Immunoconjugate was purified by protein A-sepharose (GE Healthcare, France) and the buffer was exchanged against 1x PBS as described in section 2.2.3. The degree of labeling was determined by spectrophotometry.

6 weeks-old NMRI Nude femal mice (n=11) were intravenously injected with 100 µg of CovADC-MMAE-alexa680 conjugate or vehicle control (PBS). *In vivo* 2D fluorescent images were acquired at the different time points (0, 1h, 2h, 3h, 5h (n=6) and 24h, 48, 72h (n=3) post injection) with Fluobeam700 (Fluotipcs, Optimal, Grenoble, France). Mice were sacrificed after 5h (n=3) and 72h (n=3) post injection, tissues of interest (heart, lungs, muscles, kidneys, brain, skin, adrenal, bladder, gut, spleen, stomach, ovary, pancreas, fat, liver) were removed and *ex vivo* 2D fluorescence was detected followed by the quantification of mean pixel values.

### **3.2.9 Tumor homing study**

$5 \times 10^6$  of human breast carcinoma derived BT-474 cells were implanted subcutaneously into 6 weeks-old femal SCID-CB17 mice (Charles River Laboratories, France). When the tumor reached an average volume of 100 mm<sup>3</sup>, mice were intraperitoneally injected with vehicle control (PBS) or 15 mg/kg of CovADC-DM1 (2 mice per group). Animals were sacrificed on day 1 and day 3 after administration of ADC and tumors were collected. Following the preparation of tumor sections, immunofluorescent staining was performed. Frozen samples were fixed in 70 % (v/v) ice cold ethanol for 30 minutes at -20 C min and then rehydrated in PBS for 30 minutes at RT. Staining with 0.5 µg of AlexaFluor488 labelled anti-DM1 mouse monoclonal antibody (Covalab, France) diluted in PBS was carried out at RT for 1h in a humid chamber and the slides were subsequently washed with PBS. Nuclei were visualised with DAPI (Vectashield Mounting medium with DAPI, Vector laboratories, CA, USA) diluted in fluorescence mounting medium (Vectashield Mounting medium, Vector laboratories, CA, USA). Tumor sections were imaged by confocal microscopy (LSM 780 Confocal microscope, Zeiss, France).

### **3.2.10 *In vivo* anti-tumor activity assay**

*In vivo* efficacy studies of ADCs were performed in Her2/Neu expressing ectopic xenograft mouse model. SCID-B17 mice (Charles River Laboratories, France) were

subcutaneously injected with  $5 \times 10^6$  of human breast carcinoma derived BT-474 cells, then 4-5 mm<sup>3</sup> of tumor fragment were subcutaneously implanted into 4 weeks old female SCID mice. Approximately 15 days after the tumor implantation, animals were randomized into groups with a mean tumor volume of 100-200 mm<sup>3</sup> (n=6 each). Tumor response was evaluated using a single intraperitoneal injection of 3 mg/kg ADCs or PBS as vehicle control. Tumor volume was measured in two dimension three times a week by caliper and calculated with the following formula: tumor volume =  $(4 * \pi * r^3)/3$ , where r median = average (length A/2; length B/2).

### **3.2.11 Ethics statement**

Animal experiments have been approved by the Ethics Committee for Animal Experimentation of the regional board CLB-ENS Lyon, France (Permit number: APAFiS# 11724 and DR2015-60).

---

## 3.3 RESULTS AND DISCUSSION

### 3.3.1 Generation of site-specific immunoconjugates

It has been demonstrated that mTG can be an efficient tool for the production of homogeneous ADC. Since transglutaminases are much selective toward the reactive glutamine than toward the lysine residue or primary amine, we aimed to improve the mTG technology by the optimisation of the glutamine donor sequence (Q-tag). To this aim, previously we have created and screened (by transglutaminase colorimetric activity assay)<sup>19</sup> a synthetic glutamine donor peptide library<sup>2</sup>. Among 90 different peptides analysed, four displayed higher reactive (low apparent  $K_M$  values) compared to LLQG which has been identified as a good substrate of the enzyme<sup>20</sup> and used by Strop *et al.* for the site-specific conjugation of engineered antibodies with Q-tag<sup>21</sup>. The 4 selected peptides were engineered into the C-terminal sequence coding for the heavy chains of the Trastuzumab targeting HER2/neu receptor. The conjugation efficacy was evaluated using AlexaFluor488-cadaverin as a payload, followed by SDS-PAGE analysis and fluorescent detection (**Figure 3B**). Based on the intensity of the fluorescent signal, the labelling level can be assessed: Tag2 (**lane 2**), Tag4 (**lane 4**) and Tag5 (**lane 5**) tagged antibodies showed higher signal intensity compared to LLQG (**lane 1**), suggesting better efficacy of coupling. For the further applications Q-tag<sub>2</sub> (Tag2, **lane 2**) was selected.

The conjugation of structurally different amine containing payloads required unique optimisation. The Immunoconjugates were analysed by mass spectrometry to determine the drug attachment in the antibody (**Figure 3C**). The coupling of AlexaFluor488-cadaverine resulted in the maximum yield in the expected DAR of 2 (**Figure 3D**). For different tubulin inhibitor drugs we obtained comparable conjugation efficacy. 75% of heavy chains were converted with PEG<sub>4</sub>-VC-PAB-MMAE (cleavable linker), the mixture of DAR1 and DAR2 was detected without any unconjugated antibodies (**Figure 3E**).

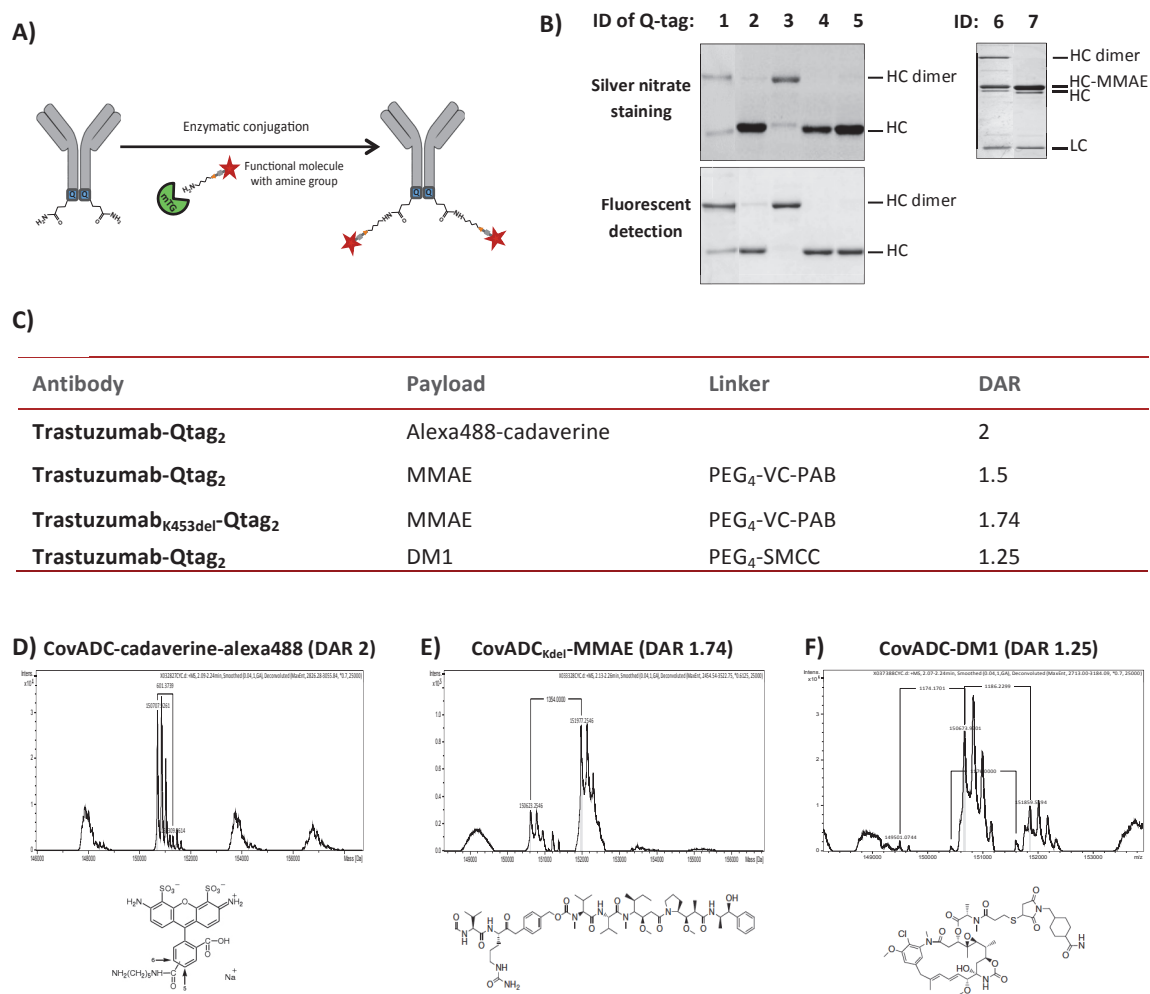


**Figure 3. Microbial transglutaminase mediated site-specific conjugation of antibody drug conjugates.** **A)** Schematic representation of antibody with engineered glutamine tag and microbial transglutaminase mediated conjugation. **B)** SDS-PAGE analysis of AlexaFluor488-cadaverine or MMAE conjugated engineered Trastuzumab-Qtag antibodies: 1-LLQG, 2-Tag2, 3-Tag3, 4-Tag4, 5-Tag5. ID 6: Trastuzumab-Qtag<sub>2</sub>-MMAE; ID 7: Trastuzumab<sub>K453del</sub>-Qtag<sub>2</sub>-MMAE. The reaction products were separated by 10% SDS-PAGE, then visualised by fluorescent detection and silver nitrate staining. LC, light chain; HC, heavy chain. **C)** Drug loading of Trastuzumab-Qtag1 antibodies determined by LC-MS (liquid chromatography/mass spectrometry) analysis. DAR, drug-to-antibody ratio; K453del, heavy chain C-terminal lysine453 deletion. LC-MS spectra of ADCs and structure of conjugated compounds: **D)** AlexaFluor488-cadaverine (640 Da), **E)** amine-PEG<sub>4</sub>-VC-PAB-MMAE (1370 Da) and **F)** amine-PEG<sub>4</sub>-SMCC-DM1 (1308 Da).

SDS-PAGE analysis revealed that the product contained aggregates, due to the covalent dimerization of the heavy chains (**Figure 1B, lane 6 and 7**). In silico analysis revealed the presence of lysine residues in the heavy chain C-terminal, known as amine donor substrate for mTG and can be responsible for interchains-crosslinking.

Deletion of lysine was performed to generate Trastuzumab<sub>K453del</sub>-Qtag<sub>2</sub> that was compared to wt (**Figure 1B, lane 6 and 7**) leading to monomer ADCs only with increased conjugation yield 1.74 drugs per antibody vs 1,5 (**Figure 1C**). The acceptance of mTG was lower toward PEG<sub>4</sub>-SMCC-DM1 (no cleavable linker), resulted in an average DAR of 1.25 upon the current reaction conditions (**Figure 3F**). These Immunoconjugates were used for the further experiments.

### 3.3.2 Immunoreactivity and internalisation of the conjugates

To verify that the conjugation has no adverse effect on the antigen binding, Biacore surface plasmon resonance (SPR) analysis was performed using rh-HER2 protein (**Figure 4A**). No significant difference could be detected in the kinetic parameters and the affinity constants of wild type, heavy chain C-terminal lysine deleted recombinant antibodies and the PEG<sub>4</sub>-VC-PAB-MMAE conjugated format.

Furthermore, the antigen binding ability of AlexaFluor647-cadaverine conjugated Trastuzumab-Qtag to HER2/neu receptor was examined by immunofluorescent staining on HER2/neu positive (SKBR3) (**Figure 4B**) and negative (MDA-MB-231) cell lines (**Figure 4C**). Specific recognition of HER2/neu receptor on the surface of HER2/neu expressing cells but not on target negative cells was performed by labelling at 4 °C. In addition, to examine the intracellular trafficking properties, the lysosomes were visualised by acidotropic green fluorescent probe (LysoTracker). Rapid internalisation of AlexaFluor647-cadaverine conjugated Trastuzumab-Qtag<sub>2</sub> (red colour) was observed at 37 °C after 10 min, followed by the transported to endosomes and lysosomes, leading to yellow merging co-localisation. This observation indicates that cellular processing of the antibody is not altered by the conjugation, thus, that the attached compound can be released.

Corresponding to our expectations these results prove that the site-specific conjugation preserve the functionality of the ADC, since the conjugation site is distant from the antigen-binding site.

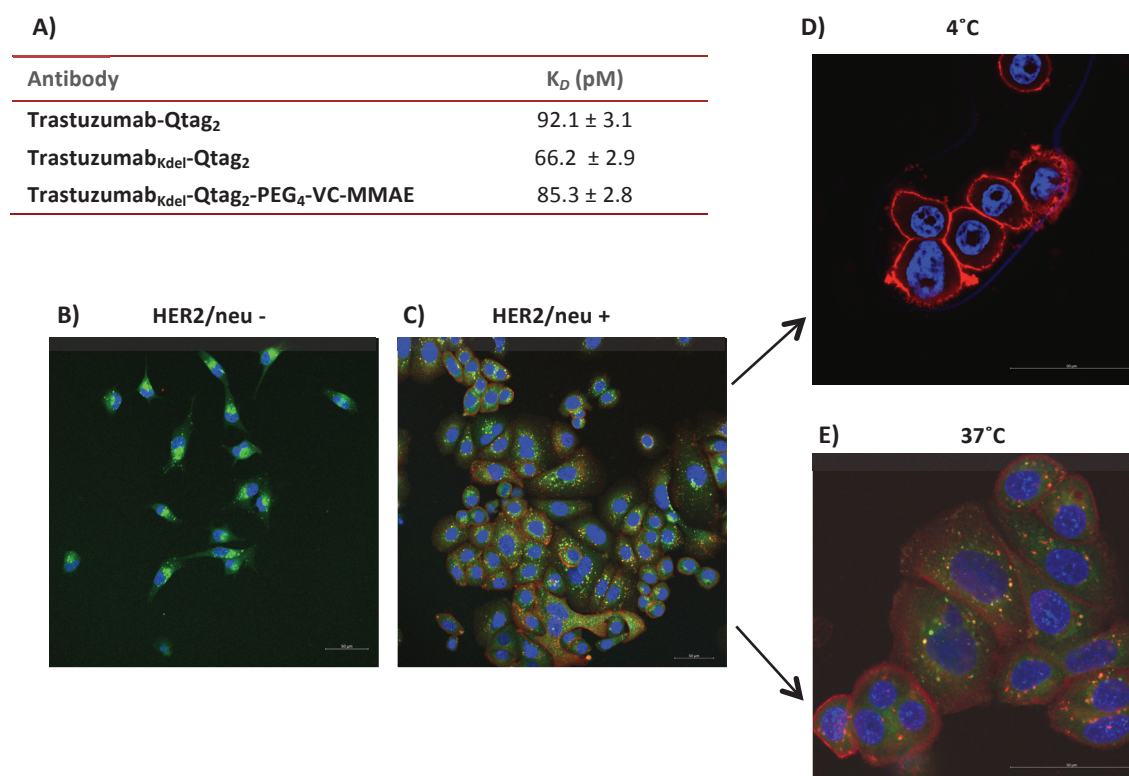
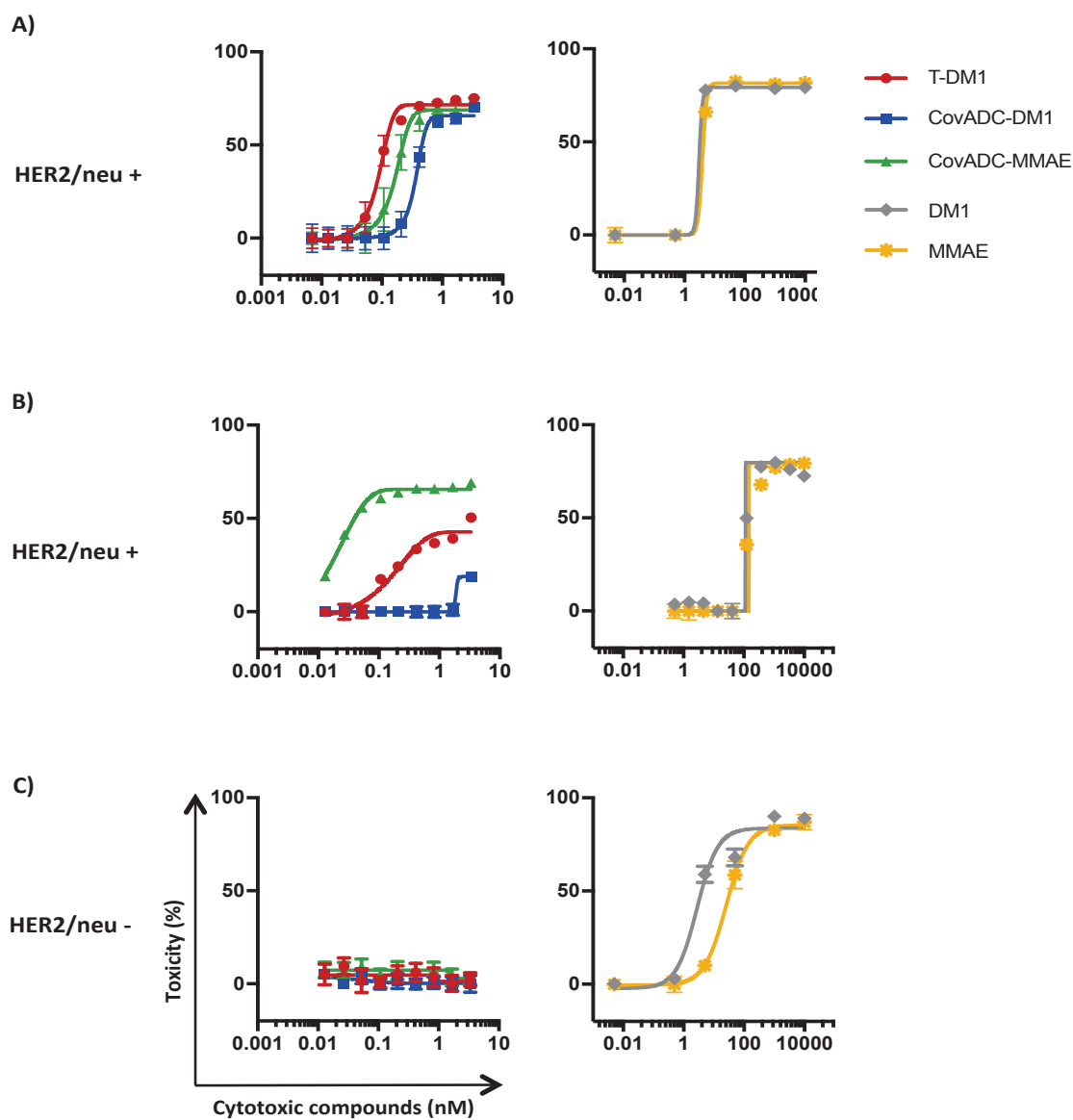


**Figure 4. Functional analysis of antigen binding properties.** A) Biacore surface plasmon resonance analysis of anti-human IgG FC captured (AHC biosensor) recombinant antibodies and conjugates with rhu-HER2 protein.  $K_D$ , affinity constant. Immunofluorescent staining of breast cancer cell lines: B) MDA-MB-231 (HER2/neu negative) and C) SKBR3 (HER2/neu positive). Evaluation of intracellular internalisation of AlexaFluor674 conjugated Trastuzumab-Qtag<sub>2</sub> in SKBR3 cells at D) 4 °C or E) 37 °C using fluorescent microscopy. Red, AlexaFluor674 signal; green, lysotracker; blue, DAPI (nucleus).

### 3.3.3 *In vitro* cytotoxicity

The functionality of ADCs were tested by the evaluation of their *in vitro* cytotoxicity and target selectivity on HER2/neu overexpressing (SKBR3, BT-474) and HER2/neu negative (MBA-MB-231) cell lines. Cell killing potency of our conjugates was compared to the commercially available T-DM1 (Kadcyla®). Cells were plated in 96 wells plate, a serial dilution of free drugs and ADC conjugated format was applied and incubated for 3 days. Toxicity was using Sulforhodamine B (SRB) colorimetric assay.



Cell lines / IC <sub>50</sub> (nM)	T-DM1	CovADC-DM1	CovADC-MMAE	DM1	MMAE
SKBR3 (HER2/neu+)	0.088 ± 0.01	0.363 ± 0.02	0.163 ± 0.07	3.039 ± 0.07	3.95 ± 0.66
BT-474 (HER2/neu+)	~0.02 ± 2.1	ND	~0.65 ± 10.21	112.9 ± 5.8	147.9 ± 6.25
MDA-MB-231 (HER2/neu-)	ND	ND	ND	2.78 ± 1.75	20.69 ± 7.75

**Figure 5. In vitro killing of ADCs.** A cytotoxicity assay was performed to evaluate inhibitory effect of free and conjugated drugs on cell proliferation. Two types of HER2/neu positive **A)** SKBR3, **B)** BT-474 and **C)** MDA-MB-231 a target negative cell line were used in the experiment. Three days after the addition of the drugs, cell death was quantified by sulforhodamine B assay. **D)** IC<sub>50</sub> values were determined by fitting of non-linear regression curves to the data using GraphPad Prism 7.0b (GraphPad Software Inc., San Diego, CA, USA) software. Data points represent the mean of two independent experiments and error bars represent SEM. T-DM1, Ado-Trastuzumab emtansine (Roche); CovADC-DM1, Trastuzumab-Qtag-PEG4-SMCC-PAB-DM1; CovADC-MMAE, Trastuzumab-Qtag-PEG4-VC-PAB-MMAE; ND, non-determined.

As presented in **Figure 5**, potent dose dependent cytotoxicity of ADCs was obtained on HER2/neu expressing cell lines (**Figure 5A and B**). No effect on target negative cell line was observed (**Figure 5C**). The unconjugated DM1 and MMAE both killed HER2/neu positive and negative cells with an  $IC_{50}$  between ~1-20 nM for SKBR3 (DM1:  $1.15 \pm 0.07$  nM, MMAE:  $1.93 \pm 0.07$  nM) and MBA-MB-231 (DM1:  $2.78 \pm 1.75$  nM, MMAE:  $20.69 \pm 7.75$  nM) cells, whereas they were approximately 100-fold less potent on BT-474 cells (DM1:  $118 \pm 1.5$  nM, MMAE:  $125 \pm 1.2$  nM). These results prove the specific toxicity of ADCs mediated through HER2/neu binding.

On SKBR3 cells, in agreement with the published data<sup>22</sup>, comparable  $IC_{50}$  values with the benchmark T-DM1 was obtained (T-DM1:  $0.078 \pm 0.01$  nM, CovADC-DM1:  $0.32 \pm 0.02$  nM, CovADC-MMAE:  $0.16 \pm 0.02$  nM) (**Figure 4A**). These values indicate a positive proportional correlation between drug loading and cell cytotoxicity *in vitro*.

Similarly to the free drugs, lower antiproliferative activity of ADCs on BT-474 cells was detected (**Figure 5A**). Interestingly, CovADC-MMAE exhibited higher toxicity than DM1 conjugates. Since there was no significant difference between DM1 and MMAE as an unconjugated format, we can hypothesize that the effect is due to the linker features, which act through the intracellular trafficking mechanism of HER2/neu receptor. Once more, CovADC-MMAE contains the protease-sensitive cleavable valine-citrulline (VC) dipeptide linker that is released by cathepsin B in the endosomes or lysosomes. In case of CovADC-DM1 and T-DM1 the complete lysosomal degradation of the antibody is required after internalization due to the non-cleavable SMCC linker. Thus efficacy of the cytotoxic compounds can be altered by the recycling properties of the receptor. In this recent study these properties were not further investigated.

### 3.3.4 *In vivo* biodistribution and tumor homing

To evaluate *in vivo* biodistribution of ADC in mice, CovADC-MMAE was labelled with 680 nm dye (AlexaFluor680) by NHS ester reaction. The protocol was optimized to yield in approximately 1.2 AlexaFluor 680 per ADC in order to minimize the effect (affinity and photophysical properties)<sup>23</sup> of the fluorophore conjugation. **Figure 6A** shows the 2D fluorescent images of mice at various time points after intravenously injection (0, 1, 2, 2, 5 24, 48, 78 hours). Rapid systemic dispersion was observed in one hour after injection. Then, it was eliminated by bladder, thus long-term retention of AlexaFluor680-ADC was not observed, indicating low toxic index. To confirm tissue distribution, mice were euthanized and the *ex-vivo* fluorescent signal of the organs was analysed at 5 and 72 hours post injection. As shown in **Figure 6A** and **B**, an

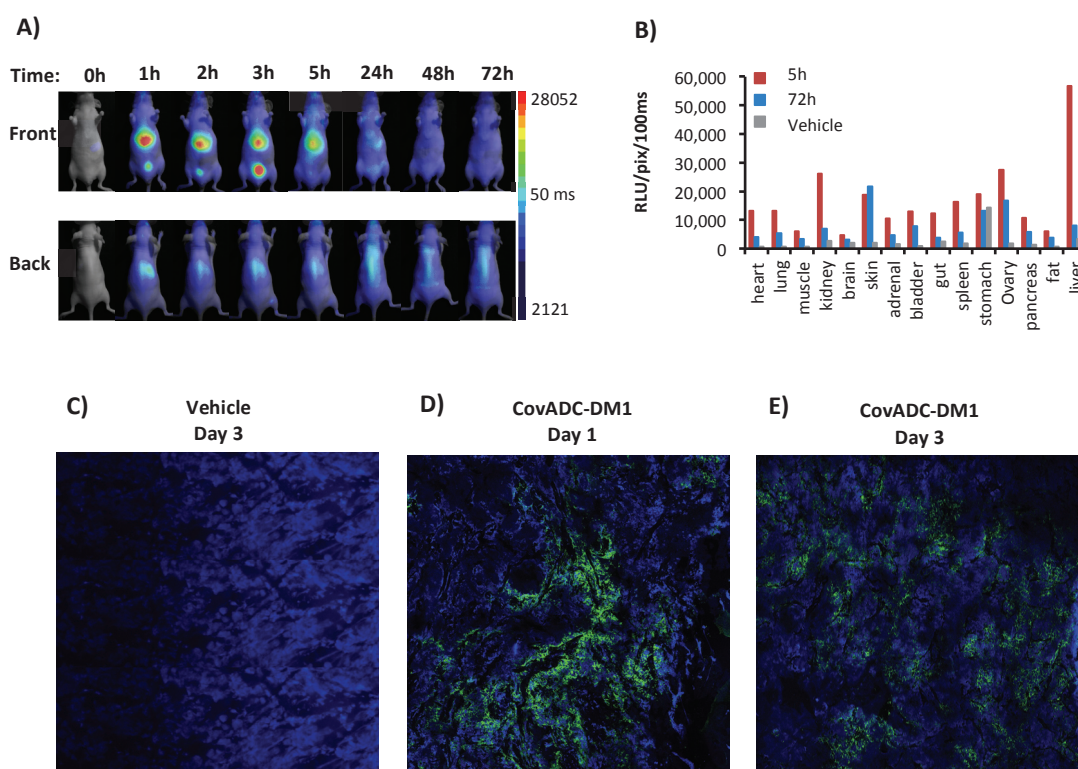


**Figure 6. Biodistribution of ADC.** **A)** 2D *in vivo* fluorescent images of NMRI Nudes mice and **B)** *ex vivo* fluorescent signal of organs after intravenous injection of AlexaFluor 680 labelled CovADC-MMAE. Immunofluorescent analysis of BT-474 tumor sections after intraperitoneal injection of **C)** vehicle control or CovADC-DM1 **D)** on day 1 and **E)** day 3. The green signal represent the homing of ADC using AlexaFluor488 labelled anti-DM1 mouse monoclonal antibody. Blue, DAPI (nucleus).

important uptake was observed during the first 5 hours post-injection in liver, kidney and bladder, whereas other organs showed minimal accumulation (**Figure 6B**). The persistent signal level in the skin might be correlated to the high microvascularization of this organ. The tissue distribution pattern profile is similar to the published data<sup>24</sup>.

Tumor homing of Trastuzumab-Qtag-PEG<sub>4</sub>-SMCC-PAB-DM1 was confirmed by immunofluorescent staining. HER2/neu positive tumor bearing Balbc/mice were intraperitoneally injected with the ADC (15mg/kg), and tumors were collected at day 1 and day 3 post injection. Confocal microscopy analysis of tumor cryosections with AlexaFluor488 labelled anti-DM1 mAb is shown in **Figure 6D**. Strong specific staining of Trastuzumab-Qtag-PEG<sub>4</sub>-SMCC-PAB-DM1 could be observed after 1 day, revealing the efficient homing of the ADC to the tumor. Whereas 3 days post injection the intensity of the fluorescent signal was weaker and the staining pattern was more distributed (**Figure 6E**). This result can indicate the perfusion of the ADC and the released cytotoxic compound in tumor site.

### 3.3.5 *In vivo* anti-tumor activity

The therapeutic activity of CovADC-DM1 and CovADC-MMAE was followed in HER2/neu overexpressing breast cancer mouse xenograft model and compared to commercially available T-DM1. SCID mice were implanted subcutaneous with BT-474 cell derived mammary tumors. 15-18 days after, the animals were randomized into groups with a mean tumor volume of 100-200 mm<sup>3</sup>. Tumor response was evaluated using a single administration of 3 mg/kg dose and tumor volumes were measured at different time intervals during three weeks. Compared to the vehicle control, the treatment led to inhibition of tumor growth for several days, then the tumours continued to grow (**Figure 7**). Even if T-DM1 has more drug molecules conjugated to the antibody (approximately 3-fold), both of ADCs exhibited very similar *in vivo* efficacy. This observation correlate with the previous studies, demonstrating that unlike *in vitro* cell cytotoxicity the higher DAR does not improve therapeutic activity<sup>25</sup>. CovADC-MMAE stabilized the tumor growth (cytotoxic effect) over a longer period as DM1 conjugates. Moreover we observed lower heterogeneity in the CovADC-MMAE

conjugate treated groups. In addition no significant difference (p value 0.068) between the wt and Kdel variant conjugated formats could be detected. These results show that our site-specific conjugates demonstrated comparable *in vivo* potency to the clinically used T-DM1.

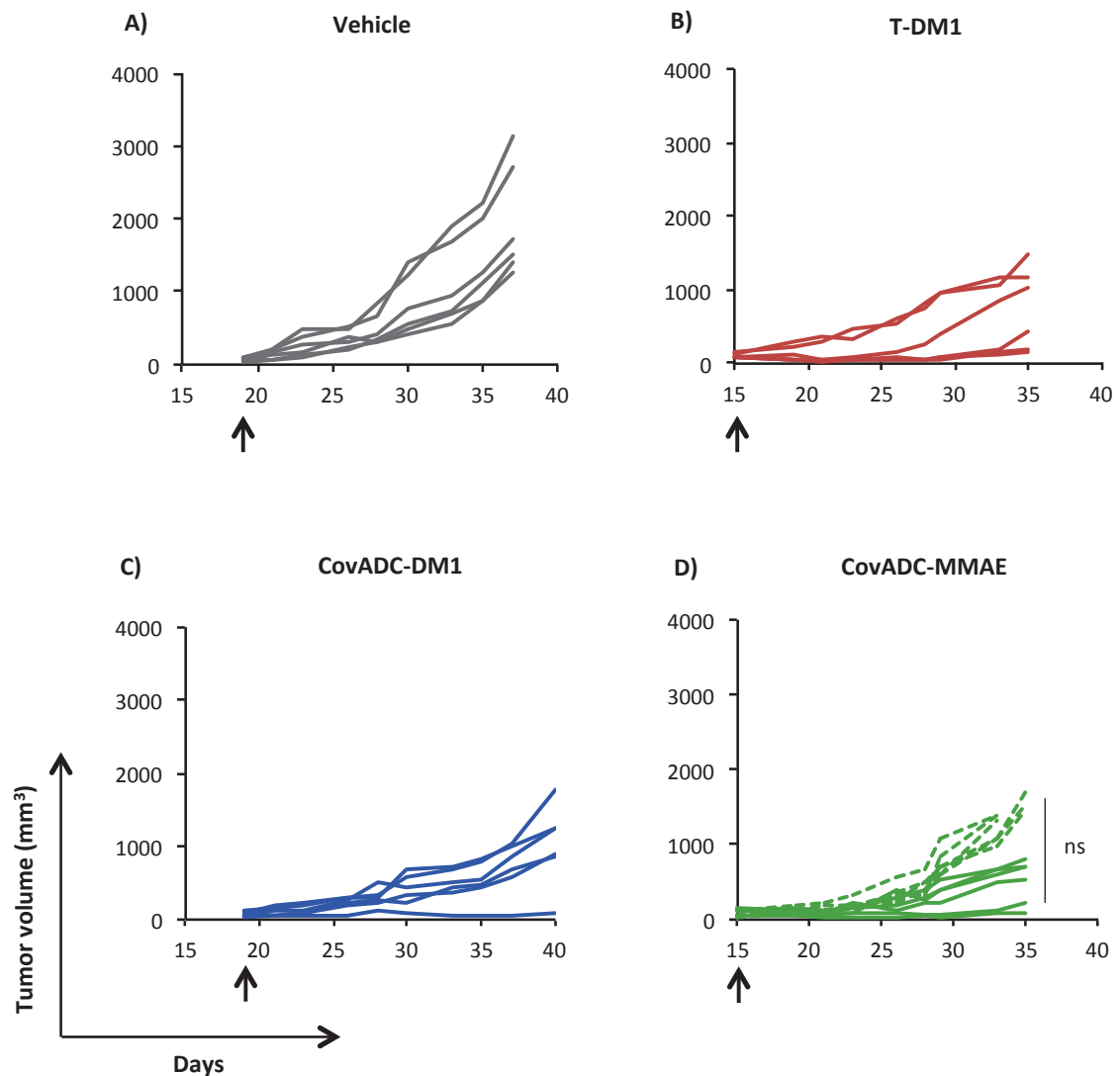


**Figure 7. *In vivo* evaluation of ADCs in a mouse ectopic xenograft model.** Immunodeficient SCID mice bearing subcutaneous BT-474 breast cancer cells derived tumors (n=6 mice per group) were treated intraperitoneally with **A)** vehicle control (PBS) as well as 3 mg/kg of **B)** T-DM1, **C)** CovADC-DM1 (Trastuzumab-Qtag-PEG4-SMCC-PAB-DM1) or **D)** CovADC-MMAE (Trastuzumab-Qtag-PEG4-VC-PAB-MMAE): wild type antibody (solid lines), C-terminal lysine deleted antibody (dashed lines) Statistical analysis between wild type and lysine deleted conjugates was calculated by unpaired one tailed t-test using GraphPad Prism 7.0b (GraphPad Software Inc., San Diego, CA, USA) software; ns=no significant (p value 0.068). Tumor size was followed over three weeks.

---

## 3.4 CONCLUSION

Using a novel glutamine peptide substrate, we developed CovIsoLink™ technology for the mTG mediated site-specific conjugation of antibodies. As a proof of concept the peptides were engineered into the sequence of Trastuzumab targeting HER2/neu receptor. We confirmed that the immunoreactivity and internalisation is not alerted by the conjugation. Moreover, no unconjugated species could be observed, confirming the optimized potential of this technology for larger GMP batch production requiring less purification processes. Furthermore compare to T-DM1, which is already used in clinic, similar *in vitro* and *in vivo* tumor cell killing potency was demonstrated, even with lower average DAR, suggesting lower risk of toxicity with similar efficacy. Thus, our technology provides the rationale for a suitable alternative enzymatic conjugation strategy of different payloads on optimized peptide for the production of homogeneous batches, without unconjugated species.

---

## 3.5 REFERENCES

1. Strop, P. *et al.* Location matters: Site of conjugation modulates stability and pharmacokinetics of antibody drug conjugates. *Chem. Biol.* **20**, 161–167 (2013).
2. PCT/EP2014/0792278.
3. Strebhardt, K. & Ullrich, A. Paul Ehrlich 's magic bullet concept : 100 years of progress. *Nat. Rev. cancer* **8**, 473–480 (2008).
4. Schrama, D., Reisfeld, R. A. & Becker, J. C. Antibody targeted drugs as cancer therapeutics. *Nat. Rev. Drug Discov.* **5**, 147–159 (2006).
5. Moek, K. L., de Groot, D. J. A., de Vries, E. G. E. & Fehrmann, R. S. N. The antibody-drug conjugate target landscape across a broad range of tumour types. *Ann. Oncol.* **28**, 3083–3091 (2017).
6. Alley, S. C., Okeley, N. M. & Senter, P. D. Antibody-drug conjugates: Targeted drug delivery for cancer. *Curr. Opin. Chem. Biol.* **14**, 529–537 (2010).
7. Junutula, J. R. *et al.* Site-specific conjugation of a cytotoxic drug to an antibody improves the therapeutic index. *Nat. Biotechnol.* **26**, 925–932 (2008).
8. Badescu, G. *et al.* Bridging disulfides for stable and defined antibody drug conjugates. *Bioconjug. Chem.* **25**, 1124–1136 (2014).
9. Li, X. *et al.* Site-Specific Dual Antibody Conjugation via Engineered Cysteine and Selenocysteine Residues. *Bioconjug. Chem.* **26**, 2243–2248 (2015).
10. Van Geel, R. *et al.* Chemoenzymatic Conjugation of Toxic Payloads to the Globally Conserved N-Glycan of Native mAbs Provides Homogeneous and Highly Efficacious Antibody-Drug Conjugates. *Bioconjug. Chem.* **26**, 2233–2242 (2015).
11. Axup, J. Y. *et al.* Synthesis of site-specific antibody-drug conjugates using unnatural amino acids. *Proc. Natl. Acad. Sci.* **109**, 16101–16106 (2012).
12. Beerli, R. R., Hell, T., Merkel, A. S. & Grawunder, U. Sortase enzyme-mediated generation of site-specifically conjugated antibody drug conjugates with high In Vitro and In Vivo potency. *PLoS One* **10**, 1–17 (2015).
13. Jeger, S. *et al.* Site-specific and stoichiometric modification of antibodies by bacterial transglutaminase. *Angew. Chemie - Int. Ed.* **49**, 9995–9997 (2010).
14. Dennler, P. *et al.* Transglutaminase-based chemo-enzymatic conjugation approach yields homogeneous antibody-drug conjugates. *Bioconjug. Chem.* **25**, 569–578 (2014).
15. Spidel, J. L. *et al.* Site-Specific Conjugation to Native and Engineered Lysines in Human Immunoglobulins by Microbial Transglutaminase. *Bioconjug. Chem.* **28**, 2471–2484 (2017).
16. Folk, J. & Finlayson, J. The epsilon-(gamma-glutamyl)lysine crosslink and the catalytic role of transglutaminases. *Adv Protein Chem* 1–133 (1977).

17. Ota, M., Sawa, A., Nio, N. & Ariyoshi, Y. Enzymatic ligation for synthesis of single-chain analogue of monellin by transglutaminase. *Biopolymers* **50**, 193–200 (1999).
18. Esposito, C. & Caputo, I. Mammalian transglutaminases: Identification of substrates as a key to physiological function and physiopathological relevance. *FEBS J.* **272**, 615–631 (2005).
19. Perez Alea, M. *et al.* Development of an isoenzyme-specific colorimetric assay for tissue transglutaminase 2 cross-linking activity. *Anal. Biochem.* **389**, 150–156 (2009).
20. Nonanaka, M., Matsuura, Y. & Motoki, M. Incorporation of Lysine-and Lysine Dipeptides into  $\alpha$ 1-Casein by  $\text{Ca}^{2+}$  -independent Microbial Transglutaminase. **60**, 131–133 (1996).
21. Strop, P. *et al.* Location matters: Site of conjugation modulates stability and pharmacokinetics of antibody drug conjugates. *Chem. Biol.* **20**, 161–167 (2013).
22. Phillips, G. D. L. *et al.* Dual targeting of HER2-positive cancer with trastuzumab emtansine and pertuzumab: Critical role for neuregulin blockade in antitumor response to combination therapy. *Clin. Cancer Res.* **20**, 456–468 (2014).
23. Szabó, Á. *et al.* The Effect of Fluorophore Conjugation on Antibody Affinity and the Photophysical Properties of Dyes. *Biophys. J.* **114**, 688–700 (2018).
24. Schneider, N. R. *et al.* Biodistribution of  $^{212}\text{Pb}$  conjugated trastuzumab in mice. *J. Radioanal. Nucl. Chem.* **296**, 75–81 (2013).
25. Hamblett, K. J. *et al.* Effects of Drug Loading on the Antitumor Activity of a Monoclonal Antibody Drug Conjugate Effects of Drug Loading on the Antitumor Activity of a Monoclonal Antibody Drug Conjugate. *Clin. Cancer Res.* **10**, 7063–7070 (2004).

## 4 GENERATION OF DIFFERENT ANTIBODY FORMATS FOR SITE-SPECIFIC CONJUGATION

### AIM

In order that ADCs can deliver the payload inside the tumor cells, their efficient tumor penetration is very important. Full-length antibodies have several advantageous PK properties; however because of their size the diffusion into solid tumors can be limited. Alternative antibody formats, including Fab and scFv display better tissue accessibility and in addition shorter plasma half-life. In certain application such as in radioimmunotherapy or imaging the rapid clearance is beneficial.

In the next part of the project, we aimed to extend our site-specific conjugation technology to antibody fragments (**Figure 1**). The glutamine donor peptide sequence, which proved to be the most efficient in case of the full-length mAb was engineered into Fab and scFv constructs encoding the variable region of Trastuzumab. As a proof of concept, their functionality was evaluated by the conjugation with AlexaFluor488-cadaverine and in antigen binding assays.

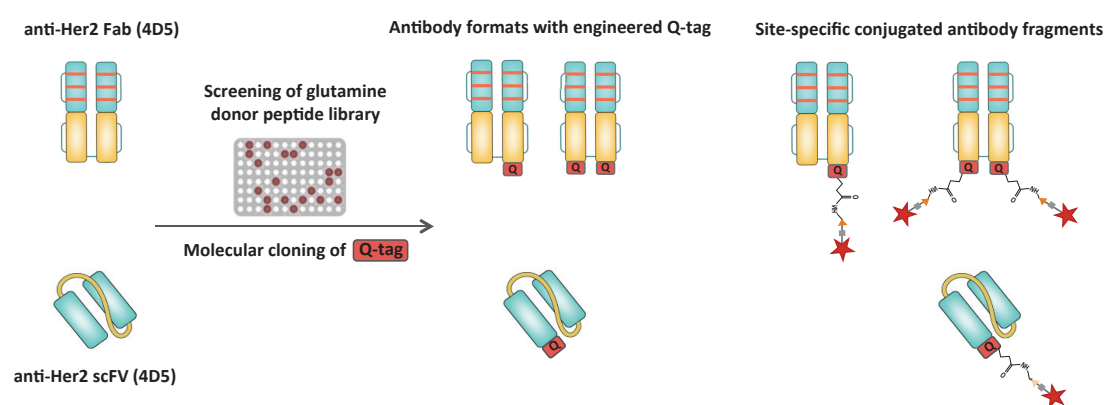


**Figure 1. CovisoLink™ technology for mTG mediated site-specific conjugation of antibody fragments.** Q-tag, glutamine donor peptide-substrate; mTG, microbial transglutaminase. (Figure partially adapted from Beck *et al.*<sup>37</sup>).

---

## 4.1 MATERIALS AND METHODS

### 4.1.1 Construction of Fab and scFv antibodies fragments with Q-tag

Antibody-binding fragment (Fab) fragment with C-terminal heavy chain glutamine tag was created from TGEX-VH<sub>4D5</sub>-HC-Qtag<sub>2</sub> (human IgG1) vector, encoding the variable region of Trastuzumab (clone 4D5) and the sequence of Tag2 peptide tag, by the deletion of CH2 and CH3 domains. For the construction of C-terminal light chain glutamine tagged Fab, overlap extension invers PCR was carried out with TGEX-VL<sub>4D5</sub>-LC (human kappa) vector. The cloning vector of single chain variable fragment (pET23NN-scFv<sub>4D5</sub>-LLQG tag) was kindly supplied by Pierre Martineau (Institut de Recherche en Cancérologie de Montpellier, France). LLQG tag was substituted to Tag2 tag by overlap extension invers PCR.

The primers were designed with OligoAnalyzer 3.1 ([www.idtdna.com](http://www.idtdna.com)) and synthesized by Eurogentec (polyacrylamide gel electrophoresis (PAGE) purification), the sequences are listed in Table 1. 50 µl PCR reaction was composed of 0.5 µl template (5 ng), 2.5 µl of each primer (10 µM), 1µl dNTP mixture (10 mM) (Promega, France), 10 µl 5× Phusion HC buffer (New England Biolabs, France), 1.5 µl DMSO (New England Biolabs, France), 31.5 µl nuclease free H<sub>2</sub>O (B. Braun, France) and 0.5 µl Phusion high-fidelity DNA polymerase (2000 U/ml) (New England Biolabs, France). The PCR cycling parameters were 98°C 30 sec, (98°C 10sec, 72°C 1.5 min) × 30 cycles and 72°C 7 min.

Following the PCR reaction, 2 µl DpnI (10 U/µl) (Thermo Fisher Scientific, France) was added and incubated at 37 °C for 4 h to degrade the original unmodified plasmid templates. After DpnI digestion, 5µl of the mixture was used to transfect NEB 5-alpha competent *E. coli* cells (New England Biolabs, France) according to the manufacturer's instructions. Plasmid DNA was isolated using PureYield Miniprep Kit (Promega, France) and sequenced.

Primers	Modifications	Sequences (5' to 3')
<b>For-Fab-ID1</b>	Deletion of CH2 and CH3 domains	Phosphate-TGGCCAGCTCAGAGATGAGC
<b>Rev-Fab-ID1</b>	Deletion of CH2 and CH3 domains	Phosphate- ACAAGATTTGGGCTCAACTTTCTTGTC
<b>For-Fab-ID2</b>	Insertion of Tag2 into LC	TGGCCAGCTCAGAGATAGAGGGAGCCTGCA GGATTC
<b>Rev-Fab-ID2</b>	Insertion of Tag2 into LC	TCTCTGAGCTGGCCAACACTCTCCCCTGTTGA AGC
<b>For-scFv-ID3</b>	Insertion of Tag2	TGGCCAGCTCAGAGAGCCGCACATCACCATC ATCACCAT
<b>Rev-scFv-ID3</b>	Insertion of Tag2	TCTCTGAGCTGGCCATGCGGCCGCAGAAGA AACGGTAA

**Table 1. Primers used for the deletion CH2 and CH3 domains to create of Fab antibody fragment and the insertion of glutamine tag into LC of Fab and scFv.**

#### 4.1.2 Expression and purification of recombinant Fab

The recombinant antibody-binding fragments were transiently expressed in HEK293AD cells (ATCC). Cotransfection of LC and HC plasmids were carried out with Lipofectamin 3000 (Thermo Fisher Scientific, France) in Opti-MEM reduced serum media (Thermo Fisher Scientific, France) according to the manufacturer's instructions.

Cell culture supernatants were purified by protein-A-sepharose (GE Healthcare, France) (since the variable region of 4D5 clone belongs to VH3 family it can bind to protein-A), washed with 1x PBS (140 mM NaCl, 2.7 mM KCl, 10 mM Na<sub>2</sub>HPO<sub>4</sub>, 1.8 mM KH<sub>2</sub>PO<sub>4</sub>), eluted with 0.1 M glycine pH3 and immediately neutralized with 1M Tris-HCl pH 8. The buffer was exchanged against 1x PBS with Zebaspin desalting column (MWCO 40 kDa, Thermo Fisher Scientific, France). The purity of the rAbs was assessed by SDS-PAGE and silver nitrate staining. The average yield of the purified Fab was 10 mg/L.

### 4.1.3 Expression and purification of recombinant scFv

Recombinant scFv encoding in pET23NN plasmids were expressed in *E. coli* BL21(DE3) cells (New England Biolabs, France). Competent bacterial cell were transformed following the manufacturer's instructions, then a single colony was inoculated into 5 ml Luria-Bertani media (LB) containing 100µg/ml ampicillin and incubated (at 37 °C, 200 rpm) until the optical density (OD<sub>600</sub>) of the culture reached 0.4-0.6. The expression of scFv was initiated by auto-induction: 2.5 ml of the culture was transferred to 250 ml of LB (100 µg/ml ampicillin) supplemented with the auto-induction solutions (solution A: 25 mM Na<sub>2</sub>HPO<sub>4</sub>, 25 mM KH<sub>2</sub>PO<sub>4</sub>, 50 mM NH<sub>4</sub>Cl, 5 mM Na<sub>2</sub>SO<sub>4</sub>; solution B: 0.5 % (v/v) glycerol, 0.05 % (w/v) glucose, 0.2 % (w/v) α-lactose monohydrate; 2 mM MgSO<sub>4</sub>); Sigma, France) and incubated at 37 °C for 1.5 hours and subsequently for 20 h at 20 °C (200 rpm).

Bacteria cell were harvested by centrifugation at 4000 rpm for 10 min at 4 °C. Cytoplasmic scFv was extracted by the addition of the lysis buffer (10 mM HEPES, 0.5 mM EDTA, 30 mM NaCl, 0.65% (w/v) nonident-P40, 0.1 mg/ml lysozyme from chicken egg white, 2U/ml Dnase; Sigma, France) in 1:1 ration of the centrifuged culture volume and incubated for 1 hour at 4 °C under rotation. NaCl concentration was adjusted to 130 mM and the lysate was centrifuged at 10000 rpm for 30 min at 4 °C. Soluble fractions containing supernatant was collected and supplemented with 2mM PMSF and 1mM protease inhibitor (Sigma, France), then diluted 2 times by the addition of TBS 2X (100 mM Tris, 300 mM NaCl, Sigma) supplemented with 10 mM MgSO<sub>4</sub> and 10 mM imidazole (Sigama, France). The complemented supernatant was loaded onto Ni Sepharose column (GE Healthcare, Fane), which was equilibrated with the binding buffer (TBS 1X: 50 mM Tris, 150 mM NaCl; 10 mM imidazole; pH 7.5) before the purification. After washing (TBS 1X, 20 mM imidazole, pH 7.5), sample was eluted (TBS 1X, 200 mM imidazole, pH 7.5) and analysed by SDS-PAGE, silver nitrate staining and Western blotting. The average yield of the purified scFv was 100 mg/L.

#### **4.1.4 Enzymatic conjugation**

For conjugation of fluorescent tagged antibody fragments, the final antibody concentration was adjusted to 0.1 mg/ml (scFv) and 0.5 mg/ml (Ab and Fab) and incubated with 30-fold molar excess of AlexaFluor448-cadaverine (Thermo Fisher Scientific, France). The reaction was initiated by the addition of 4 U/mg antibody of microbial transglutaminase (Zedira, Darmstadt, Germany) and the reaction was O/N incubated at RT with gently agitation. The excess of the payloads and the enzyme were removed by protein-A purification (detailed in section 3.1.2). Fluorescent labeled conjugates were analyzed on 10% SDS-PAGE and visualized by UV-fluorescent detection and Silver-nitrate staining.

#### **4.1.5 Immunofluorescent staining**

Immunofluorescent staining with AlexaFluor488 conjugated different antibody formats (Ab, Fab, scFv) was performed on SKBR3 overexpressing HER2/neu and MCF-7 which cells express the receptor at normal level using cytospin samples. Neu-antibody(24D2)-PE (Santa Cruze Biotechnology, CA, USA) was used as a positive control. Frozen samples were fixed in 70 % (v/v) ice cold ethanol for 30 minutes at -20 C min and then rehydrated in PBS for 30 minutes at RT. Staining with 10 µg/ml of AlexaFluor488 tagged anti-HER2 antibody formats were diluted in PBS was carried out at RT for 1h in a humid chamber and the slides were subsequently washed with PBS. Nuclei were visualised with DAPI (Vectashield Mounting medium with DAPI, Vector laboratories, CA, USA) diluted in fluorescence mounting medium (Vectashield Mounting medium, Vector laboratories, CA, USA). Tumor sections were imaged by microscopy (Axio Imager 510 Upright Microscope, Zeiss, France).

#### **4.1.6 Fluorescent activated cell sorting**

The antigen binding ability of the site-specific conjugated different antibody formats was further determined on SKBR3 (HER2/neu positive) and MCF-7 (HER2/neu status normal) cell lines by fluorescent activated cell sorting (FACS). Cells harvested by trypsin/EDTA (Sigma, France) and washed with PBS were incubated with 10 µg/ml of AlexaFluor488 tagged anti-HER2 antibodies (Ab, Fab, scFv) and Neu-antibody(24D2)-PE (Santa Cruze Biotechnology, CA, USA) for 1 h at 4 °C. Following the washing with PBS, cells were resuspended in 150 µl of PBS complemented with 0.02% (w/v) EDTA and 3% (v/v) FBS then subjected to flow cytometry analysis (BD FACSCanto II, BD Bioscience). Data were analysed using BD FACSDiva software (BD Bioscience).

---

## 4.2 RESULTS AND DISCUSSION

### 4.2.1 Enzymatic conjugation

The functionality of Q-tag for site-specific modification of antibody fragment formats was demonstrated by conjugation of small molecular weight cadaverine derivatized fluorescent substrate (AlexaFluor488-cadaverine). The SDS-PAGE analysis of the tagged antibodies are shown in **Figure 2**. The reaction was monitored by fluorescent detection and the loaded protein were visualised by silver-nitrate staining.

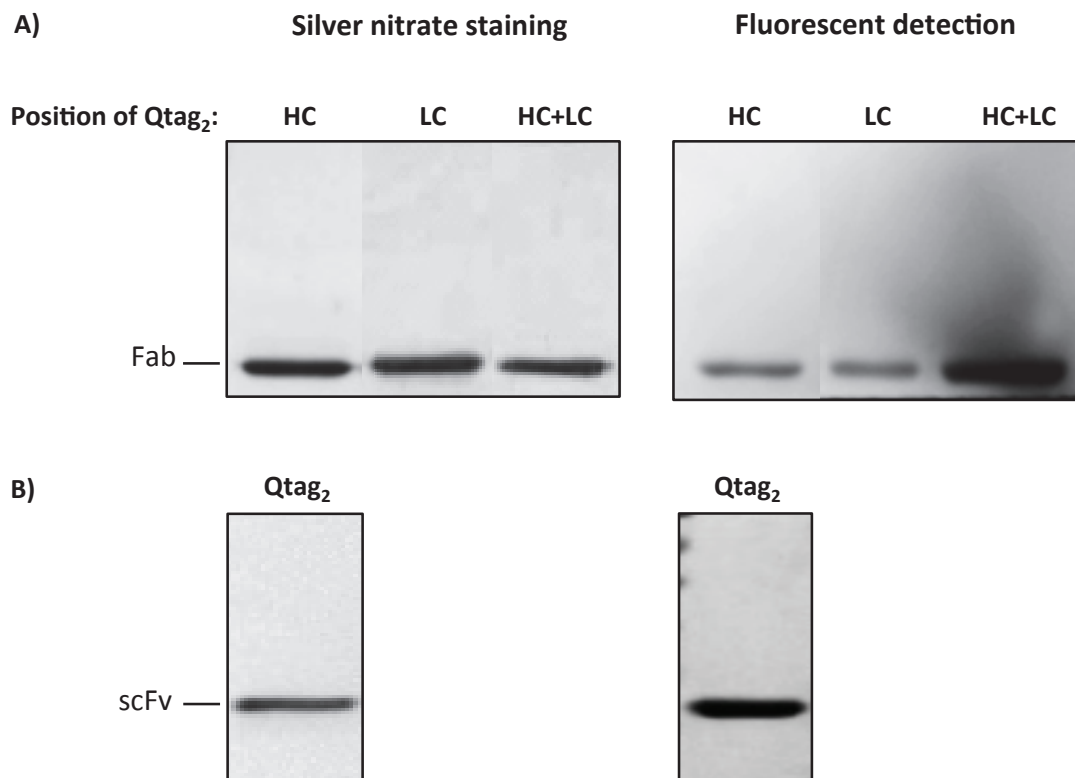


**Figure 2. Microbial transglutaminase mediated site-specific conjugation of Fab and scFv antibody fragments.** **A)** SDS-PAGE analysis of AlexaFluor488-cadaverine conjugated engineered Trastuzumab-Fab-Qtag<sub>2</sub>: Qtag on HC, Qtag on LC, Qtag on both HC and LC; and **B)** Trastuzumab-scFv-Qtag<sub>2</sub>. The conjugates were analysed by 10% SDS-PAGE upon non-reducing conditions, then visualised by fluorescent detection and silver nitrate staining. HC, heavy chain; LC, light chain.

To evaluate the relative efficacy of conjugation to C-terminus heavy (HC) and light chains (LC), Fab with LC-Qtag or HC-Qtag as well as with double Qtag (LC-Qtag and HC-Qtag) were constructed and produced (**Figure 2A**). As very similar fluorescent signal of LC and HC conjugated antibodies could be detected, suggesting that the investigated location does not affect the conjugation efficacy. In addition the higher labelling level of the Fab with double Qtag indicates that these engineered Fabs are appropriate for the generation of DAR1 as well as DAR2.

**Figure 2B** shows that glutamine tagged scFv was also approved for mTG mediated site specific conjugation of fluorescent compound.

#### 4.2.2 Immunoreactivity analysis

To study whether the conjugation interferes with the antigen binding, the cadaverine derivate of AlexaFluor448 was conjugated to full length antibody, Fab and scFv formats. The antigen binding ability of the conjugates was examined by immunofluorescent staining and flow cytometry. Cell lines with high (SKBR3) and normal expression level (MCF-7) of HER2/neu receptor were included in the assay.

Each antibody format showed very similar staining profile on HER2/neu positive cells, comparable to the commercially available control antibody (Neu242-PE). In addition target selectivity was confirmed by negative staining of the cell that express normal level of HER2/neu receptor (**Figure 3A**). Immunoreactivity and specificity were further demonstrated by FACS analysis (**Figure 3B**).

As expected, these results prove that the site-specific conjugation preserve the functionality of various antibody formats, since the conjugation site is distant from the antigen binding site.

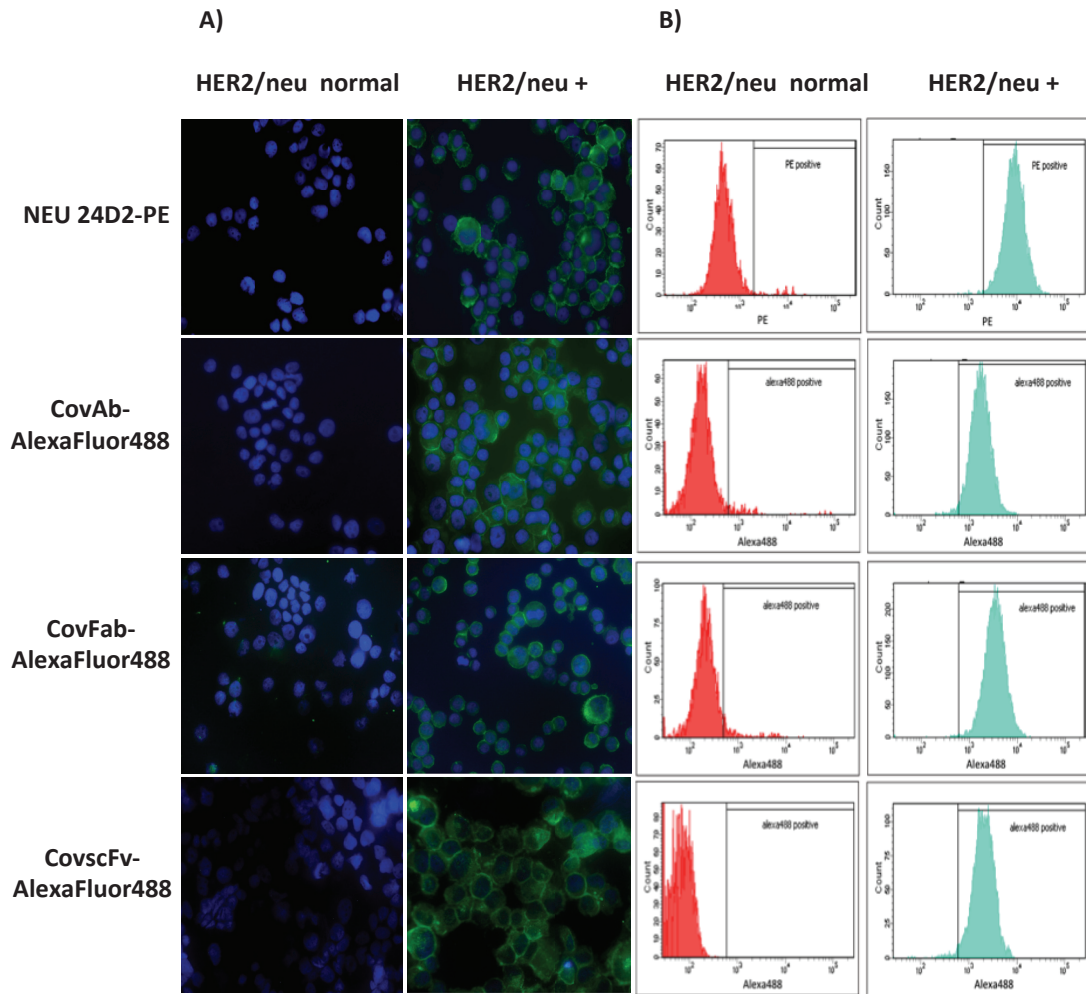


**Figure 3. Immunoreactivity analysis of site specific conjugated antibody formats.** A) Immunofluorescent staining and B) fluorescent activated cell sorting (FACS) analysis on SKBR3 (HER2/neu positive) and MCF-7 (HER2/neu status normal) cells. Glutamine tag engineered full length antibody (Ab), antigen-binding fragment (Fab) and single-chain variable fragment (scFv) antibody formats were conjugated with AlexaFluor488-cadaverine and the antigen binding profile was compared to the commercially available Neu-antibody(24D2)-PE. Green, AlexaFluor488 signal; blue, DAPI (nucleus).

## 5 OPTIMISED METHODS (SDS-PAGE AND LC-MS) REVEAL DEAMIDATION IN ANY TRANSGLUTAMINASES-MEDIATED REACTIONS

---

### AIM

Transglutaminases are known as nature's biological glue. These are a family of structurally and functionally related enzymes that catalyse the calcium dependent posttranslational modifications of proteins. Their transamidase activity includes protein-protein crosslinking (between specific  $\gamma$ -carboxiamide group of glutamine and  $\epsilon$ -amino group of a lysine residues) or amine incorporation. The resulted isopeptide bound is highly stable (against enzymatic, thermo and chemical degradation) that is beneficial for several biotechnological approaches. Their bacterial homologous has some further advantageous properties ( $\text{Ca}^{2+}$  independent activity, higher temperature and pH stability, low cost production) over the mammalian counterparts for the industrial applications. In addition to transamidation, TGs can catalyse deamidation that was considered for many years as a side reaction (in the absence of the primary amine or low pH), but recently substrate specific deamidations have been reported.

Our aim was to optimise the SDS-PAGE and LC-MS methods for the rapid and easy detection of both transamidated and deamidated peptides. In addition we further investigated how the ratio of deamidation to transamidation can be influenced by some reaction parameters, such as substrates affinity, amine donor concentration,  $\text{Ca}^{2+}$  concentration and pH.

Since we are using microbial transglutaminase as a tool for antibody conjugation, this study could help to better understand the enzymatic reaction and implicate this knowledge in the global project. Therefore, efficient ADC production the reaction conditions should be optimised to avoid deamidation.

## Optimised methods (SDS-PAGE and LC-MS) reveal deamidation in any transglutaminases-mediated reactions

Éva Sivadó<sup>1</sup>, Meddy El Alaoui<sup>1</sup>, Frédéric Delolme<sup>2</sup>, Robert Kiraly<sup>3</sup>, László Fesüs<sup>3</sup>, Saïd El Alaoui<sup>1\*</sup>

<sup>1</sup> Covalab S.A.S, Research Department, 11 Avenue Albert Einstein, 69100, Villeurbanne, Lyon, France

<sup>2</sup> Protein Science Facility, SFR BioSciences CNRS UMS 3444, Inserm US 8, UCBL, ENS, 69366 Lyon, France

<sup>3</sup> Department of Biochemistry and Molecular Biology, Faculty of Medicine, University of Debrecen, 4012 Debrecen, Hungary

Corresponding author:

Saïd El Alaoui,

Fax: +33 437 289 416.

\*: E-mail address: elalaoui@covalab.com

### Abstract

Transglutaminases (TGs) are a family of structurally and functionally related enzymes, which catalyse calcium dependent posttranslational modifications of proteins by generating protein-protein crosslink, amine incorporation or deamidation. For many years TGs mediated deamidation was considered to be a side-reaction, but recently substrate specific deamidations have been reported. Here we describe an optimised SDS-PAGE assay for the easy and rapid monitoring of the TG reaction with small peptides. The relative proportion of deamidation to transamidation was evaluated by densitometric analysis and confirmed by nanoLC-nano-ESI/MS. We addressed to further investigate the effect of reaction conditions on transamidation and deamidation reactions of TG1, TG2 and FXIII-A enzymes using a panel of glutamine containing peptides substrates. The ratio of transamidation to deamidation was enhanced at high excess of the acyl-acceptor substrate and increasing pH. In addition, it was influenced by peptides substrates as well. Whereas deamidation was favoured at low cadaverine concentrations and acidic pH, no significant effect of calcium was observed on the ratio of transamidation/deamidation. Under our experimental conditions particular deamidation always occurred *in vitro* even at high excess of the acyl-acceptor substrate, and the reaction outcome was shifted to deamidation at neutral pH. Our results provide clear evidence of the deamidation in transglutaminase reaction and may serve as an important approach for *in vivo* analysis of the deamidation to understand better the role of TGs in biological events.

### Keywords

Transglutaminases

Deamidation

Transamidation

Fluorescent-detection

SDS-PAGE

## Introduction

Transglutaminases (TGs; EC 2.3.2.13) are widely distributed enzymes with pleiotropic functions. Nine members have been described in mammals: keratinocyte (TG1), tissue (TG2), epidermal (TG3), prostate (TG4), type 5 (TG5), neuronal (TG6), type 7 (TG7), blood coagulation factor XIII-A subunit (FXIII-A), and the catalytically inactive erythrocyte band 4.2 protein (Griffin et al. 2002).

The distribution and physiological roles of TGs have been investigated in various cell types and tissues. TG2 is the most studied member of the TGs family. This multifunctional protein has diverse cellular localisation and is implicated in several physiological (regulation of cell survival/death processes, cell adhesion, migration, signal transduction, proliferation) and pathological processes (coeliac disease, neurodegenerative disorders, fibrosis, inflammatory diseases, metabolic diseases and cancer) (Fesus and Piacentini 2002). TG1 mainly exists in the upper spinous and granular layers of the skin, it is involved in the terminal differentiation of keratinocytes by the formation of the cross-linked cell envelope (Kim et al. 1995). Thrombin-activated factor FXIII-A (FXIII-A) plays essential role in the stabilisation of fibrin clots and in wound healing through the formation of isopeptide bonds (Ariëns et al. 2002).

TGs catalyse  $\text{Ca}^{2+}$ -dependent posttranslational modifications of proteins by generating protein-protein crosslink (between specific  $\gamma$ -carboxamide group of a glutamine and  $\epsilon$ -amino group of a lysine side chains), amine incorporation or deamidation. In the first step active site cysteine reacts with the  $\gamma$ -glutaminy group of the proteins or peptides leading to the formation of a thioester intermediate. In the second step the acyl group is transferred to an amine substrate resulting in the formation of isopeptide bond or the water can act as an alternative nucleophile leading to site-specific deamidation of the glutamine residue (Folk 1983; Lorand and Graham 2003). Many of these crosslinking reactions occur within 5 to 10 min, for example in case of FXIII-A between glutamine (Gln 398; 399) and lysine (Lys 406) residues of the fibrin  $\gamma$ -chains (Chen and Doolittle 1971). Whereas cross-linking of fibrin  $\alpha$ -chains involving Gln 221; 237; 328; 366 and Lys 208; 606 takes place more slower (Matsuka et al. 1996; Ariëns et al. 2002).

Deamidation of glutamine and asparagine residues is one of the most prevalent posttranslational modifications, which converts an uncharged amino acid to a negatively charged residue introducing alternations in the protein's conformation. The protein function can be changed as it is determined by its global structure and electrostatic protein-protein interaction can be modulated as well (Berg et al. 2002). Deamidation can occur in different ways (non-enzymatically, by glutamines or phosphate activated glutaminases) regulating several biological processes (Robinson and Robinson 2001; Hensley et al. 2013; Schousboe et al. 2014). Moreover cytotoxic necrotizing factors in *Escherichia coli* and necrotoxin in *Bordetella*, which are considered to be functional relatives of TGs, can induce the formation of stress fibers by the deamidation of Rho proteins (Schmidt et al. 1998).

Deamidation by TGs was believed to be a side-reaction and taking place only in the absence of primary amines or at low pH when their availability is limited (Fleckenstein et al. 2002). But, recently it has been reported that selective deamidation in small heat shock protein (Boros et al. 2006) and  $\beta$ B2,  $\beta$ B3-crystallins (Boros et al. 2008) can occur in a substrate specific manner. Respectively, the substrate affinity and reaction conditions can influence the propensity for deamidation and transamidation (Stamnaes et al. 2008). Many research works are focusing on the examination of transglutaminase cross-linking activity, which is linked to some diseases like fibrosis and neurodegeneration. So far TGs mediated deamidation activity has been related to coeliac disease (Folk 1983; Lorand and Graham 2003), and only few reports have been published on its role in other physiopathological processes (Nemes et al. 2000; Boros et al. 2008; Schmid et al. 2011; Iwai et al. 2014). These studies support the potential role of TGs dependent deamidation in the regulation of biological processes.

In this study we report an optimised sodium dodecyl sulphate polyacrylamide gel electrophoresis (SDS-PAGE) assay for the rapid and easy detection of both transamidated and deamidated peptides. TG1, TG2, FXIII-A enzymes and a panel of glutamine containing peptides were examined to determine how the ratio of deamidation to transamidation can be influenced by some reaction parameters, such as substrates affinity, amine donor concentration,  $\text{Ca}^{2+}$  concentration and pH. The identity and the relative quantity of the reaction products were confirmed by liquid chromatography–mass spectrometry (LC-MS) analysis. Our results are well correlated with the

published data, cited above. Unexpectedly, under our reaction conditions, we found that particular deamidation is always occurring in vitro, even at high excess of the acyl-acceptor substrates.

## Materials and methods

### *Materials*

All materials were obtained from Sigma-Aldrich (France), otherwise it is indicated. Recombinant human TG2 (rhu-TG2), recombinant human keratinocyte transglutaminase (TG1), and recombinant human blood coagulation factor XIII-A (FXIII-A) were purchased from Zedira (Darmstadt, Germany). Peptides were obtained from Covalab (Villeurbanne, France). MilliQ Water for mass spectrometry analysis was accessed from Elga system.

### *Synthetic peptides substrates*

FAM labeled peptides substrates were synthesized according to the standard method of Covalab. Isoenzyme specific glutamine containing peptides have been reported by Sugimura et al (2006, 2008) and used to develop specific TGs activity assays (Thomas et al. 2006; Perez Alea et al. 2009). K9 is a natural TG2 sequence based on  $\beta$ -casein (Cleary and Maurer 2006). Among the natural reactive glutamine sides in fibrinogen  $\alpha$ -chains a short peptide sequence containing Q238 (Matsuka et al. 1996) was chosen for our experiments. The corresponding deamidated control peptides were synthesized by Covalab (Table 1).

### *Transglutaminase reaction*

5  $\mu$ M of specific glutamine donor substrates labeled with FAM fluorescent and cadaverine (5-1000  $\mu$ M) as an acyl acceptor were incubated with their corresponding isoenzymes at 37 °C. 18 mU/ml of TG1, TG2, or thrombin (1U/ml) activated FXIII-A were applied in the assay buffer (20 mM Tris pH 7.2, 8.0 or MES pH 5.0, 6.0, 150 mM NaCl, 10 mM DTT) in the presence or absence of 10 mM EDTA. pH was 7.2, unless the effect of pH (5-8) was examined. The enzymatic reaction was initiated by the addition of 5 mM  $\text{CaCl}_2$  except in the experiments in which the effect of  $\text{Ca}^{2+}$  was investigated (0.1-5 mM).

### *SDS PAGE assay*

The assay was previously reported by Kenniston et al. (2013) and modified as briefly described below. After the incubation time the enzymatic reaction was stopped by boiling the sample in 6X SDS-loading buffer (9.3 w/w DTT, 12 wt.% SDS, 47 v/v% glycerol, 0.06 wt.% bromophenol blue in 0.5 M Tris-HCl, pH 6.8). The reaction products were run on SDS-PAGE (15% T, 2.6% C; T represents the total concentration of polyacrylamide monomer expressed in a g per 100 ml and C is the percentage of bis-polyacrylamide) and visualized by fluorescence detection (Luminescent Image Analyzer LAS-1000 plus, Fujifilm).

### *Liquid chromatography–mass spectrometry analysis (LC-MS)*

The samples were diluted 10 times in a solution of 0.1% formic acid before analysis. Mass spectrometry analysis were performed on a linear ion trap LTQ Velos (Thermo Scientific, San Jose California) with nano-Electrospray ionization source coupled in-line to a nanoRSLC system Ultimate 3000 (Thermo Scientific, Germering, Germany). 1  $\mu$ L of sample was injected via the autosampler. Samples were first desalted and concentrated on a reverse phase precolumn C18 PepMap100, 300  $\mu$ m i.d x 5 mm, 5  $\mu$ m, 100 Å (Thermo Scientific) for 3 min at 20  $\mu$ L/min with  $\text{H}_2\text{O}$ /Acetonitrile -98/2-0.1% Formic acid. Samples were then separated on a nanocolumn Acclaim C18, 15 cm x 75  $\mu$ m i.d, 2  $\mu$ m (Thermo Scientific). The HPLC gradient was 5-55% solvent B (A = 5% acetonitrile,

0.1% formic acid; B = 80% acetonitrile, 0.1% formic acid) in 30 min follow to 5 min 99% B. The total duration was set to 50 minutes at a flow rate of 300 nL/min. The oven temperature was kept constant at 40°C.

MS spectra were recorded in the mass range  $m/z$  500-1100 in positive ionisation mode, the enhanced scan rate was used for the full MS spectrum.

#### *Data analysis*

Relative intensity of fluorescent bands were analysed with ImageJ and plotted with GraphPad Prism 5 (GraphPad Software Inc., San Diego, CA, USA) software.

## **Results and discussion**

#### *Determination of transamidation and deamidation rates by transglutaminases*

Post-translational modifications (PTMs) behave as powerful regulatory elements that often define protein function through covalent modification. Because PTMs profoundly affect protein behavior, they are typically tightly controlled, and dysregulation is strongly associated with numerous diseases (Huang et al. 2014). Deamidation is an exception among PTMs due to its enzymatic and nonenzymatic and spontaneous nature.

Deamidation is the transformation of eligible glutamine and also asparagine residues into glutamate and aspartate/isoaspartate. Susceptibility for nonenzymatic deamidation is conditioned by the primary sequence, by the lack of three-dimensional structure, and is facilitated by high temperatures, extreme pH or high ionic strength. Deamidation affects a great number of proteins (calmodulin, tubulin, synapsin, Alzheimer's  $\beta$ -amyloid, histone H2B, cytochrome-C, ...), and has therefore wide biological repercussions because it can lead to structural changes and/or modify their life-span (Beaumat et al. 2016). Although there are select examples of deamidation serving functional roles, it is generally considered to represent degradation and is associated with a growing list of age-related, neurological, aggregation-prone, and autoimmune diseases (Lindner and Helliger 2001).

While *in vivo* deamidation of Asn to Asp was clearly established, transglutaminase mediated-deamidation of Gln is not fully understood and rather it was believed to be only a side-reaction, occurring when the second substrate is not available or at acidic pH. However, during about a decade many reports were focused on the study of the mechanism of hydrolysis of the specific Gln residues in order to elucidate the role of transglutaminases in the pathophysiology of some diseases and coeliac disease in particular.

In order to evaluate the deamidation reaction of transglutaminase to convert Gln to Glu, several methods were used depending on whether the Gln substrates were natural (e.g. proteins) or synthetic (e.g. peptides). In case of proteins, deamidations were analysed through molecular modelling and biological activity (Sjöström et al. 1998; Fleckenstein et al. 2002b) whereas synthetic peptides were analysed by various techniques such as mass spectrometry (MS & LC/MS), size exclusion chromatography (SEC), capillary electrophoresis (EC), HPLC, 2D gels, WB (Boros S, Quarsten H, Stammaes J, Heil A).

In this work we optimised an electrophoresis assay based on sodium dodecyl sulphate polyacrylamide gel (SDS-PAGE) for the rapid and easy detection of both transamidated and deamidated peptides. All reaction products of FAM fluorescein-labelled peptides could be simultaneously detected with high resolution and specificity. The relative ratio of deamidation and transamidation was evaluated by densitometric analysis (Fig. 1b,e). The identity and the proportion of the reaction products were confirmed by nanoLC-nano-ESI/MS analysis. The relative quantities were calculated from Extraction Ions Chromatogram Areas of the doubly charged ions of each species (Fig. 1c,f), assuming that all the species have the same response factors. The data obtained by LC-MS are in good

correlation with the results of densitometric analysis, indicating that the optimised SDS-PAGE assay is a reliable method for the semi-quantitative examination of both transamidated and deamidated reaction products.

*There is always deamidated substrate production during transglutaminase reaction*

In this study TG1, TG2, FXIII-A enzymes and five glutamine containing peptides (K5, T26, F11, K9 and  $\alpha$ C(Q328)) (Table 1) were examined to determine how the ratio of deamidation to transamidation can be influenced by some reaction parameters such as: the substrates affinity, amine donor concentration,  $\text{Ca}^{2+}$  concentration and pH. K5 (Sugimura et al. 2008), T26, F11 (Sugimura et al. 2006) were described as an isoenzyme preferred glutamine substrates having high affinity to TG1, TG2 and FXIII-A respectively, whereas K9 (Cleary and Maurer 2006) and fibrinogen  $\alpha$ C(Q328) peptides (Matsuka et al. 1996) are known as natural glutamine donor substrate for TG2 and FXIII-A.

Applying high excess of the amine donor substrate (cadaverine), the ratio of transamidation to deamidation was increased, whereas deamidation was favored at low cadaverine concentrations. In the absence of the second substrate no crosslinked product was detected (Fig. 2). In addition this effect appeared to be substrate dependent and confirm the results obtained by the group of Sollid L (Stamnaes J et al, 2008). TG2 transamidase activity was rather higher with K9 (Fig. 2b) than with T26 peptide (Fig. 2c) indicating better recognition of natural glutamine substrate. This difference was not observed with FXIII-A as the reactivity is higher with F11 than fibrinogen  $\alpha$ C(Q328) peptides. Indeed upon the same reaction conditions the relative ratio of deamidated/transamidated fibrinogen  $\alpha$ C(Q328) peptide was increased (Fig. 2e) whereas F11 peptide was preferred for transamidation (Fig. 2d). This slight difference in the deamidation/transamidation rate may be explained by the influence of the neighbouring amino acids relative to the targeted Gln and may effect the affinity of the enzymes. Indeed Boros et al (2005, 2008) reported that TG2 can process site-specific deamidation, and a proline at position +2 to the specific glutamine residue may positively influence deamidation (Fleckenstein et al. 2002b).

Moreover the results reveal that TG2 and FXIII-A catalysed substrate deamidation could always occur as an excess of primary amine did not completely inhibit deamidation (Fig. 1 b-e). However deamidation by TG1 is less obvious in all conditions studied and this could be explained that K5 may not be good substrate of this enzyme for deamidation (Fig. 1a). Using natural and good substrate for TG1 will be of interest to complete this work.

*Effect of pH on the transglutaminase catalysed deamidation*

Fleckenstein et al described that TG2 catalyzed reaction of gliadin substrate is strongly influenced by pH. Here we extended the investigation for two other isoenzymes and five peptide substrates as detailed in the materials & methods (Fig. 3). In all cases the transamidation and deamidation reactions were analysed in buffers with pH values ranging from 5 to 8. TG1 (Fig. 3a) and FXIII-A (Fig. 3 d,e) seem to not be active at acidic pH, however at pH 6.0 fibrinogen  $\alpha$ C(Q328) peptide was deamidated in the majority (Fig. 3e). At pH 8.0 all the peptides were converted to transamidate forms by all the corresponding enzymes. In the condition of neutral pH, TG1 was not active due probably to the low kinetic reaction, whereas TG2 and FXIII-A were able to convert the peptides to transamidated and deamidated products. The proportion of each product depends on the type of the enzyme and also the glutamine substrate. T26 was highly deamidated by TG2 whereas the natural substrate K9 was in the majority transamidated (Fig. 3b,c) and with FXIII-A the deamidation was more important to the transamidation for both substrates (Fig. 3d,e). These results further demonstrate that the rate of the transamidation reactions is significantly increased at alkaline pH indicating the importance of the nucleophilicity of the amine which must be unprotonated. As the pKa of the cadaverine amine is around 10 it's expected that the transamidation reaction can be favoured over deamidation. Indeed in the report of Fleckenstein (2002) using 5-BP as an amine donor with pKa around 10.5 they proposed a general base-catalyzed-deacylation mechanism for the transamidation reaction through the nucleophilic attack on the thiol ester intermediate. Increasing of the pH narrow the pKa of the base would decrease its protonation and consequently the competition by water molecules is blocked explaining the increase of transamidation rate.

### *Effect of Ca<sup>2+</sup> on the transglutaminase catalysed deamidation*

It is well known that Ca<sup>2+</sup> is required for the activation of transglutaminases through inducing a large conformational change in the enzyme structure (Di Venere et al. 2000; Pinkas et al. 2007). Because of the large difference in the open and closed conformations, we hypothesised that depending on Ca<sup>2+</sup> binding, more transient conformers with different hydrodynamic radius can be exhibited. Probably at lower Ca<sup>2+</sup> concentrations the substrate-binding channel could be particularly covered and the entrance of the second substrate can be inhibited resulting on the deamidation of the glutamine donor substrate via hydrolysis. Transamidation and deamidation were analysed with different Ca<sup>2+</sup> concentrations ranging from 0.1 to 5 mM as described in material & method (Fig. 4). At lower Ca<sup>2+</sup> concentration (0.1-0.2 mM) TG2 seems to not be active (Fig. 4 b,c) whereas TG1 converted the majority of K5 to transamidated product (Fig. 4a). With FXIII-A we observed high activity with F11 substrate (Fig. 4d) and low activity with natural substrate (Fig. 4e) that can be explained by the high affinity of the enzyme to the synthetic substrate. By increasing Ca<sup>2+</sup> concentration the enzymes were more active and both transamidation and deamidation occurred at different rate depending on the Gln substrate: transamidation was more observed with TG1 and TG2 using K5 and T26 substrates respectively and more deamidation was obtained with TG2 and FXIII-A using K9 and fibrinogen  $\alpha$ C(Q328). Based on these results no significant effect of calcium was obtained on the ratio of transamidation/deamidation.

In conclusion, our assay based on SDS-PAGE provides an easy and rapid method for monitoring the transglutaminase reaction with synthetic small peptides. The fractions of native, deamidated and transamidated peptides can be successfully separated and their rates were confirmed by nanoLC-nano-ESI/MS. Under our experimental conditions we noticed that particular deamidation always occurs, even at high molar concentration (148-200 fold molar excess) of amine donor substrate and it is preferred at low to neutral pH. These data provide further evidence for the simultaneous reactions of transamidation and deamidation, however further work should be confirmed *in vitro* and *in vivo* at the endogenous proteins level. Knowledge about the *in vivo* regulation of the transamidation versus deamidation is therefore crucial for the elucidation of the transglutaminase enigma. Most of the transglutaminase activity assays are based on detection of the transamidated products. Since the deamidation is no longer believed as a side reaction, TG activity cannot be accurately evaluated only by detecting the cross-linked products.

### **Acknowledgments**

We would like to thank Agnès Degiuli (University Lyon 1, CNRS, INSA, CPE-Lyon, Institute for Molecular and Supramolecular Chemistry and Biochemistry) to provide free access for Luminescent Image Analyzer (LAS-1000 plus, Fujifilm). E.S. was supported by a Marie Curie research grant (“TRANSPATH”, FP7 No 289964) and R.K. was supported by Janos Bolyai Research Fellowship of the Hungarian Academy of Science.

### Figure captions

**Fig. 1** Relative quantification of transglutaminase reaction products using SDS-PAGE analysis and fluorescent detection. TG2 was incubated with FAM-K9 peptide (a, b, c), thrombin activated FXIIIa with FAM-fibrinogen  $\alpha C_{(325-336)}$  peptide (d, e, f) and with cadaverine in the presence of  $Ca^{2+}$  for 20 min (TG2) or 5 h (FXIII-A) at 37 °C. Q: reactive glutamine containing control peptide, E: deamidated control peptide. (b, e) Densitometry analysis of the SDS-PAGE. (c, f) Relative quantification of the reaction products by nanoLC-nano-ESI/MS

**Fig. 2** Monitoring of transglutaminase reaction at different cadaverine concentrations by SDS-PAGE analysis. TG1 was incubated with FAM-K5 (a), TG2 with FAM-T26 (b) and FAM-K9 (c), thrombin activated FXIII-A with FAM-F11 (d), FAM-fibrinogen  $\alpha C_{(325-336)}$  (e) glutamine donor peptides and with cadaverine in the presence of  $Ca^{2+}$  for 20 min (a,b,c,d) or 5 h (e) at 37 °C. The reaction products were separated by SDS-PAGE and visualised by fluorescence detection. Q: reactive glutamine containing control peptide, E: deamidated control peptide

**Fig. 3** Monitoring of transglutaminase reaction at different pH by SDS-PAGE analysis. TG1 was incubated with FAM-K5 (a), TG2 with FAM-T26 (b) and FAM-K9 (c), thrombin activated FXIII-A with FAM-F11 (d), FAM-fibrinogen  $\alpha C_{(325-336)}$  (e) glutamine donor peptides and with cadaverine as acyl-acceptor in the presence (-EDTA) or absence (+ EDTA) of  $Ca^{2+}$  at pH 5-8 for 20 min (a,b,c,d) or 5 h (e) at 37 °C. The reaction products were separated by SDS-PAGE and visualised by fluorescence detection. Q: reactive glutamine containing control peptide, E: deamidated control peptide

**Fig. 4** Monitoring of transglutaminase reaction at different  $Ca^{2+}$  concentrations by SDS-PAGE analysis. TG1 was incubated with FAM-K5 (a), TG2 with FAM-T26 (b) and FAM-K9 (c), thrombin activated FXIII-A with FAM-F11 (d), FAM-fibrinogen  $\alpha C_{(325-336)}$  (e) glutamine donor peptides and with cadaverine as acyl-acceptor at different  $Ca^{2+}$  concentrations for 20 min (a,b,c,d) or 5 h (e) at 37 °C. The reaction products were separated by SDS-PAGE and visualised by fluorescence detection. Q: reactive glutamine containing control peptide, E: deamidated control peptide

**Table 1** Sequence of the glutamine containing amine acceptor- and deamidated control peptides

**Table 1**

Peptides	Sequence
T26	5-FAM- <sup>1</sup> HQSYVDPWMLDH <sup>12</sup> -CONH <sub>2</sub>
T26 (Q2E)	5-FAM- <sup>1</sup> HESYVDPWMLDH <sup>12</sup> -CONH <sub>2</sub>
K9(K7L) <sup>a</sup>	5-FAM- <sup>1</sup> LGPGQSLVIG <sup>10</sup> -COOH
K9 (K7L,Q5E)	5-FAM- <sup>1</sup> LGPGESLVIG <sup>10</sup> -COOH
K5	5-FAM- <sup>1</sup> YEQHKLPDSWPF <sup>12</sup> -COOH
K5 (Q3E)	5-FAM- <sup>1</sup> YEEHKLPDSWPF <sup>12</sup> -COOH
F11	5-FAM- <sup>1</sup> DQMMLPWPAVAL <sup>12</sup> -COOH
F11 (Q2E)	5-FAM- <sup>1</sup> DEMMLPWPAVAL <sup>12</sup> -COOH
Fibrinogen αC	5-FAM- <sup>325</sup> TGNQNP <sup>336</sup> GS <sup>336</sup> PRPG <sup>336</sup> -COOH
Fibrinogen αC (Q328E)	5-FAM- <sup>325</sup> TGNE <sup>328</sup> NP <sup>336</sup> GS <sup>336</sup> PRPG <sup>336</sup> -COOH

**Fig. 1**

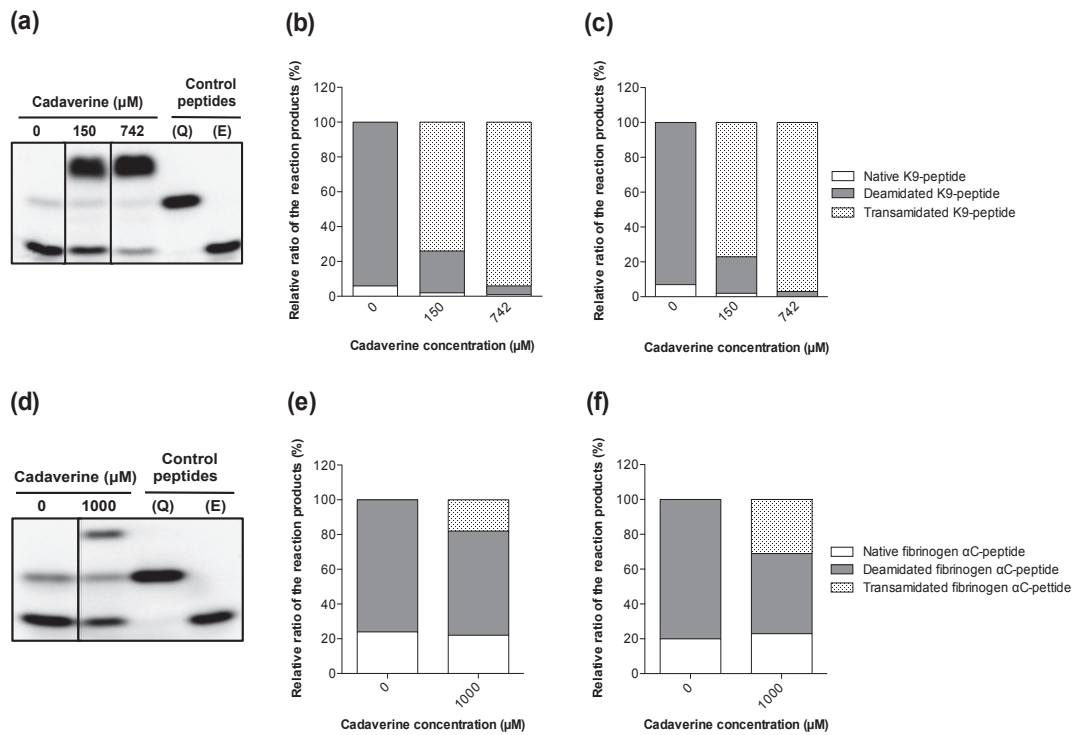


Fig. 2

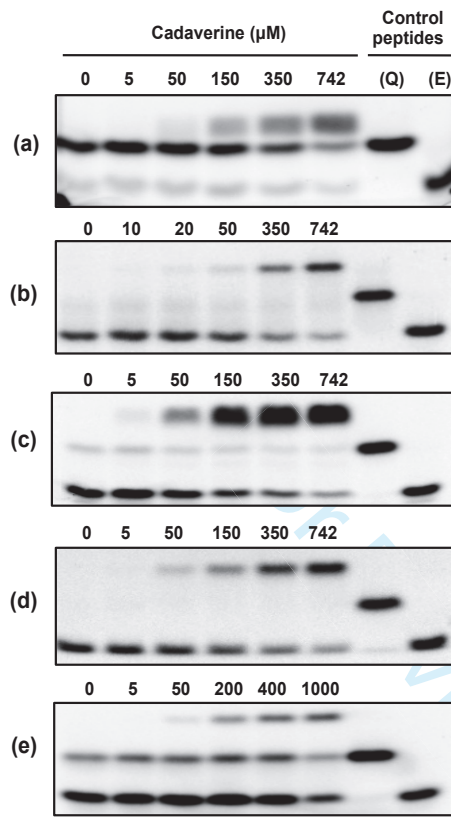


Fig. 3

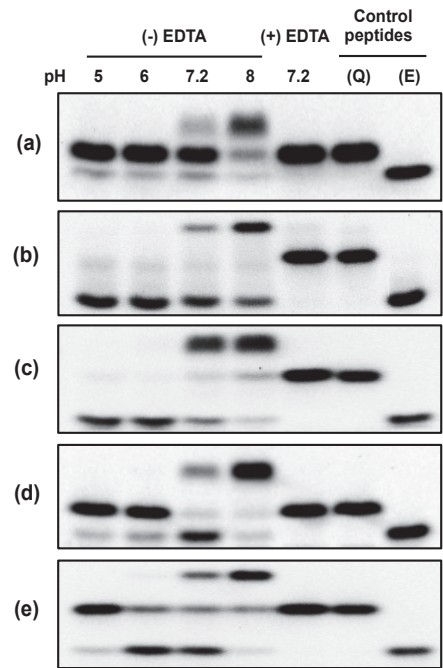
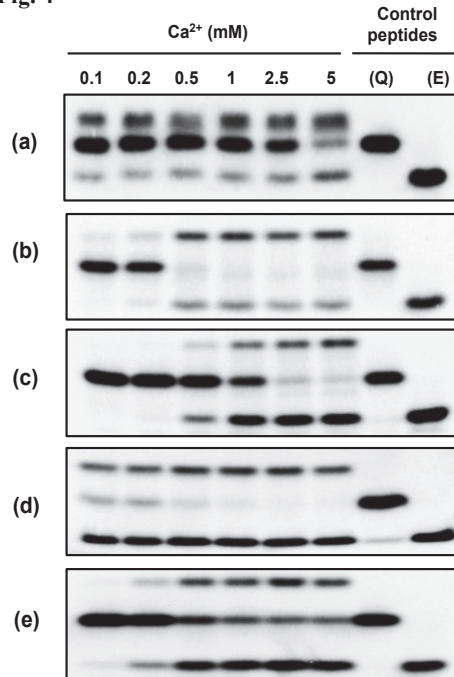


Fig. 4



## References

- Ariëns R a S, Lai T, Weisel JW, et al (2002) Role of factor XIII in fibrin clot formation and effects of genetic polymorphisms. Review article Role of factor XIII in fibrin clot formation and effects of genetic polymorphisms. *Blood* 100:743–754. doi: 10.1182/blood.V100.3.743
- Beaumat F, Dhaybi M El, Lasserre J, et al (2016) N52 monodeamidated Bcl - x L properties in vivo and in vitro shows impaired oncogenic. *Oncotarget* 7:17129–17143. doi: 10.18632/oncotarget.7938
- Berg J, Tymoczko J, Stryer L (2002) *Biochemistry*. Biochem 5th Ed Jeremy M Berg, John L Tymoczko, Lubert Stryer New York W H Free 2002 ISBN 0-7167-3051-0 319–344.
- Boros S, Åhrman E, Wunderink L, et al (2006) Site-specific transamidation and deamidation of the small heat-shock protein Hsp20 by tissue transglutaminase. *Proteins Struct Funct Genet* 62:1044–1052. doi: 10.1002/prot.20837
- Boros S, Wilmarth PA, Kamps B, et al (2008) Tissue transglutaminase catalyzes the deamidation of glutamines in lens  $\beta$ B2- and  $\beta$ B3-crystallins. *Exp Eye Res* 86:383–393. doi: 10.1016/j.exer.2007.11.011
- Chen R, Doolittle RF (1971) Gamma-gamma cross-Linking Sites in Human and Bovine Fibrin. *Biochemistry* 10:4486–4491. doi: 10.1021/bi00800a021
- Cleary DB, Maurer MC (2006) Characterizing the specificity of activated Factor XIII for glutamine-containing substrate peptides. 1764:1207–1217. doi: 10.1016/j.bbapap.2006.05.003
- Di Venere a, Rossi A, De Matteis F, et al (2000) Opposite effects of Ca(2+) and GTP binding on tissue transglutaminase tertiary structure. *J Biol Chem* 275:3915–3921.
- Fesus L, Piacentini M (2002) Transglutaminase 2 : an enigmatic enzyme with diverse functions. *TRENDS Biochem Sci* 27:534–539.
- Fleckenstein B, Molberg Ø, Qiao S, et al (2002a) Gliadin T Cell Epitope Selection by Tissue Transglutaminase in. 277:34109–34116. doi: 10.1074/jbc.M204521200
- Fleckenstein B, Molberg Ø, Qiao SW, et al (2002b) Gliadin T cell epitope selection by tissue transglutaminase in celiac disease. Role of enzyme specificity and pH influence on the transamidation versus deamidation reactions. *J Biol Chem* 277:34109–34116. doi: 10.1074/jbc.M204521200
- Folk JE (1983) Mechanism and basis for specificity of transglutaminase-catalyzed  $\epsilon$ -( $\gamma$ -glutamyl) lysine bond formation. *Adv Enzymol Relat Areas Mol Biol* 54:1–56. doi: 10.1002/9780470122990.ch1
- Griffin M, Casadio R, Bergamini CM (2002) Transglutaminases: nature's biological glues. *Biochem J* 368:377–96. doi: 10.1042/BJ20021234
- Hensley CT, Wasti AT, Deberardinis RJ (2013) Glutamine and cancer: cell biology, physiology, and clinical opportunities. *J Clin Invest* 123:3678–3684. doi: 10.1172/JCI69600.3678
- Huang Q, Chang J, Cheung MK, et al (2014) Human proteins with target sites of multiple post-translational modification types are more prone to be involved in disease. *J Proteome Res* 13:2735–2748. doi: 10.1021/pr401019d
- Iwai K, Shibukawa Y, Yamazaki N, Wada Y (2014) Transglutaminase 2-dependent deamidation of glyceraldehyde-3-phosphate dehydrogenase promotes trophoblastic cell fusion. *J Biol Chem* 289:4989–4999. doi: 10.1074/jbc.M113.525568
- Kim SY, Chung SI, Yoneda K, Steinert PM (1995) Expression of transglutaminase I in human epidermis. *J Invest Dermatol* 104:211–7.
- Lindner H, Helliger W (2001) Age-dependent deamidation of asparagine residues in proteins. *Exp Gerontol* 36:1551–1563. doi: 10.1016/S0531-5565(01)00140-1
- Lorand L, Graham RM (2003) Transglutaminases: crosslinking enzymes with pleiotropic functions. *Nat Rev Mol Cell Biol* 4:140–156. doi: 10.1038/nrm1014
- Matsuka Y V., Medved L V., Migliorini MM, Ingham KC (1996) Factor XIIIa-catalyzed cross-linking of recombinant alpha C fragments of human fibrinogen. *Biochemistry* 35:5810–5816. doi: 10.1021/bi952294k

- Nemes Z, Demény M, Marekov LN, et al (2000) Cholesterol 3-sulfate interferes with cornified envelope assembly by diverting transglutaminase I activity from the formation of cross-links and esters to the hydrolysis of glutamine. *J Biol Chem* 275:2636–2646. doi: 10.1074/jbc.275.4.2636
- Perez Alea M, Kitamura M, Martin G, et al (2009) Development of an isoenzyme-specific colorimetric assay for tissue transglutaminase 2 cross-linking activity. *Anal Biochem* 389:150–156. doi: 10.1016/j.ab.2009.03.029
- Pinkas DM, Strop P, Brunger AT, Khosla C (2007) Transglutaminase 2 Undergoes a Large Conformational Change upon Activation. *5:2788–2796*. doi: 10.1371/journal.pbio.0050327
- Robinson NE, Robinson a B (2001) Molecular clocks. *Proc Natl Acad Sci U S A* 98:944–949. doi: 10.1073/pnas.98.3.944
- Schmid AW, Condemni E, Tuchscherer G, et al (2011) Tissue transglutaminase-mediated glutamine deamidation of  $\beta$ -amyloid peptide increases peptide solubility, whereas enzymatic cross-linking and peptide fragmentation may serve as molecular triggers for rapid peptide aggregation. *J Biol Chem* 286:12172–12188. doi: 10.1074/jbc.M110.176149
- Schmidt G, Selzer J, Lerm M, Aktories K (1998) The Rho-deamidating cytotoxic necrotizing factor 1 from *Escherichia coli* possesses transglutaminase activity: Cysteine 866 and histidine 881 are essential for enzyme activity. *J Biol Chem* 273:13669–13674. doi: 10.1074/jbc.273.22.13669
- Schousboe A, Scafidi S, Bak LK, Waagepetersen HS MM (2014) Glutamate Metabolism in the Brain Focusing on Astrocytes. *Adv Neurobiol* 11:11–30. doi: 10.1007/978-3-319-08894-5
- Sjöström H, Lundin KEA, Molberg, et al (1998) Identification of a gliadin T-cell epitope in coeliac disease: General importance of gliadin deamidation for intestinal T-cell recognition. *Scand J Immunol* 48:111–115. doi: 10.1046/j.1365-3083.1998.00397.x
- Stamnaes J, Fleckenstein B, Sollid LM (2008) The propensity for deamidation and transamidation of peptides by transglutaminase 2 is dependent on substrate affinity and reaction conditions. *Biochim Biophys Acta - Proteins Proteomics* 1784:1804–1811. doi: 10.1016/j.bbapap.2008.08.011
- Sugimura Y, Hosono M, Kitamura M, et al (2008) Identification of preferred substrate sequences for transglutaminase 1 - Development of a novel peptide that can efficiently detect cross-linking enzyme activity in the skin. *FEBS J* 275:5667–5677. doi: 10.1111/j.1742-4658.2008.06692.x
- Sugimura Y, Hosono M, Wada F, et al (2006) Screening for the Preferred Substrate Sequence of Transglutaminase Using a Phage-displayed Peptide Library IDENTIFICATION OF PEPTIDE SUBSTRATES FOR TGASE 2 AND FACTOR XIIIa \*. *281:17699–17706*. doi: 10.1074/jbc.M513538200
- Thomas V, El Alaoui S, Massignon D, et al (2006) Development and evaluation of a modified colorimetric solid-phase microassay for measuring the activity of cellular and plasma (Factor XIII) transglutaminases. *Biotechnol Appl Biochem* 43:171–179. doi: 10.1042/BA20050161

## 6 CONCLUSION & PERSPECTIVES

---

Antibody-drug conjugates have proved their potential over the naked therapeutic antibodies or chemotherapies in different clinical trials. Although the basic concept of this approach is simple, over the past 30 years so far, only four ADCs have reached the clinic and the therapeutic window remained narrow. This is the consequence of the chemical conjugation leading to heterogeneous mixtures that negatively influence the pharmacokinetics and *in vivo* performance<sup>44</sup>. In ADC design, besides the selection of the optimal target, antibody, linker and payloads, the conjugation technology and the optimal drug loading is also very important to improve the safety, efficacy and toxicity profiles. In order that ADCs can deliver their full potential and simplify the manufacturing challenges, the development of efficient site-specific conjugation methods is essential. Recently several important developments have been achieved to advance their potency, including the establishment of site-specific technologies.

In this thesis, we report the development of CovIsoLink™ technology for the generation of homogenous immunoconjugates using a novel glutamine donor peptides (Q-tag). It has been demonstrated that mTG allows the site-specific conjugation of multiple drugs to IgG1 antibody. Upon deglycosylation of the antibody, a glutamine in the heavy chain at 295 position can be recognised by the enzyme and the further mutation of N297 to glutamine permits the conjugation of 4 substrates<sup>120-122</sup>. However deglycosylation can alter the stability, aggregation rate and effector functions of the antibodies<sup>126</sup>. Strop *et al.* constitute a conjugation site by engineering a glutamine tag substrate (LLQG) in the constant region at different position to investigate the impact of location on the stability and pharmacokinetics, and they found that the C-terminal position of the LC and HC is the most suitable<sup>49</sup>.

Previously, Covalab has designed a synthetic peptide library and four potential peptides have been selected with improved affinity compared to the known peptides (ZQG, LLQG)<sup>127,128</sup>. As a proof of concept, the peptides sequences were introduced into the heavy chain C-terminal of Trastuzumab antibody and antibody fragments (Fab

and scFv). Since the Q-tag was engineered into distant region from the antigen-binding site, this conjugation technology preserve the functionality of the ADC, as it was confirmed in different binding assays. The coupling of structurally different amine containing payloads required unique optimisation. We demonstrated that this conjugation strategy led to reproducible stoichiometry without the presence of DAR0, which prevents competitive interaction between naked antibodies and conjugates particularly interesting when the targeted antigen expression is low. Comparative evaluation of CovADCs revealed that our immunoconjugates display similar *in vivo* tumor cell killing potency as the FDA approved T-DM1, even with lower DAR.

Currently, several site-specific conjugation methods have been developed and the number of ADCs undergoing in clinical trials are rapidly increasing, confirming the need for further advancements and optimisations. According to the indications, the paradigm of the future ADC design may change. Currently, the traditional antibody driven ADC design is applied: following target identification and antibody generation, the linker and the payload are selected for ADC construction.

The new dogma is based on payload driven design. At first, the cytotoxic compound is characterised for the deep understanding of its mechanism of action and examine in which subpopulation of patients is the most efficient. Afterwards, the antibody, which targets this subpopulation, is selected for ADC generation. Moreover the design should trend towards the selection and adaptation of the optimal site-specific conjugation methods depending on the individual ADC considering the antibody, the linker and the payload.

The present ADC medications are quite expensive, thus additionally the cost-effective production is also an important point that should be taken into account during the development of novel technologies. Among them, the mTG-mediated enzymatic approach provides several advantages, including mild-reaction conditions preventing the antibody structure and functionality, highly stable linkages *via* isopeptide bond, site-specific conjugation using engineered peptide substrates and mass-production of mTG by conventional fermentation at low cost. Since the reaction selectivity is determined mainly by the glutamine donor substrate, the conjugation efficacy can be improved by the modification of the Q-tag sequences, as we demonstrated. Since the affinity and the accessibility is strongly determined by the

neighbouring amino acids and the global structure, these peptide sequences could be potentially further optimised considering the scaffold. Furthermore the mutation of mTG active site can be other option to improve the kinetic parameters of the enzymatic reaction or the specificity to the determined sequence as it was shown for peptidase technology (EnzyPep BV, personal communication).

While developing an ADC, the basic principle of targeted tumor cell killing through the cellular mechanism of the payloads is considered. The local destruction of the tumors is very important during the therapy, but to trigger long lasting tumor-response and avoid relapse, the interaction of the immune system is crucial. As it was shown for naked mAbs therapeutic effect of the ADCs is also mediated by ADCC since Fc region of T-DM1 retains its ability to bind to FcγR<sup>77</sup>. Moreover, recent studies have revealed that certain cytotoxic drugs including DM1<sup>129</sup> and MMAE have direct immunomodulatory effects, inducing the activation of dendritic cells and potentiating tumor-specific T cells response *in vivo*<sup>130</sup>. Using an immunocompetent and Trastuzumab-resistant mouse model, Müller *et al.* demonstrated that the therapeutic activity of T-DM1 is particularly due to its anti-tumor immunity effect induced by the payload. The combined treatment of T-DM1 with immune checkpoint blockade therapy lead to increase the tumor-infiltration of effector T-cells, complete regression and immune memory formation<sup>129</sup>. These results potentiate the combination of immunotherapies with targeted therapies.

There are numerous potential combinations of the mAb, linker and drug that gives lots of opportunities for the construct optimisation but also, increase the complexity of this approach. Thus, the deep understanding and characterisation of the each individual ADC and their therapeutic implications is very important.

Besides the technical issues, there are several considerable clinical challenges, including linker stability, off-target toxicity, development of resistance against the cytotoxic compounds, penetration into the tumor and reaching the target of the payload, development of antibodies against the antigens which do not sufficiently internalised. Therefore, the target, linker and payload are key challenging success factors.

First, the level of expression and tumor distribution of the targeted antigen is really important for efficient delivery of the payload in the tumor cells. Considering

that only 0.0003-0.8% of in *in vivo* injected antibody dose is present per gram of tumor, therefore the efficient internalisation and the high cytotoxic potency of the payloads are crucial. The internalisation properties of the mAbs can directly be influenced by the epitope. As it was demonstrated in case of the antibodies targeting distinct epitopes of HER2 receptor, depending on the recognition site the characteristics of the mAbs such as inhibition of downstream signal transduction pathway were different<sup>131</sup>. The epitope also determines the sequences of hyper variable regions that can influence the global structure and the physicochemical properties of the antibody. This can be more substantial in case of smaller antibody fragments having smaller ratio of the antigen recognition to the framework sequences. Furthermore the antibody cross reactivity among different species has concerned impact, since it is beneficial during the *in vivo* toxicity and activity studies<sup>132</sup>.

The affinity and the size of the antibody have also significant impact on the penetration. The localisation and type of the tumor can determine the selection of the best format. Three of the four FDA approved ADCs are targeting hematopoietic or lymphoid tumors and among the ADC that are undergoing in clinical trials, there are fewer number of solid tumors targeting conjugates. This may represent the difficulties to efficiently destroy solid tumors by antibody approach using the full-length format. Moreover, mAbs cannot cross or exhibit poor penetration through the blood-brain barrier, therefore they are not efficient against glioblastomas. The development of smaller antibody fragments (Fab, scFv, nanobody) conjugates may overcome these issues. Or in case of glioblastomas, bispecific antibodies targeting specific receptors on the luminal side for the transcytosis can be a possible therapeutic way.

The potent targeting is especially challenging in case of hypoxic, solid tumors. Thus targeting of the tumor microenvironment by the conjugation of immunomodulatory payloads such as chemokines, glucocorticoids, pattern recognition receptors (PRR) agonist or viral (oncolytic or not) proteins could be a potential approach to activate the immune system. For this approach, antibody fragments, which diffuse into the tumor mass more efficiently, could be probably more capable vehicles. This can also be combined with  $\beta$ -glucuronidase linker optimizing release of the drug in the microenvironment (see chapter 1.2.2). In hypoxic environment the concentration of nutrients such as glucose are lower and the cells stop or slow down

their rate of proliferation. However, about 80% of the ADCs in the pipeline are conjugated with anti-mitotic agents, thus they are more efficient against rapidly dividing cells. Therefore, DNA damaging agents may be better therapeutic effect in the hypoxic solid tissues.

Over past the few years, ADC approach has archived considerably innovations especially in case of the conjugation technologies. The linker and payload developments show slower progress. In addition to the improvement of PK properties by the generation of site-specific-homogeneous ADCs, the release of cytotoxic compounds at the right time in the right place is very important especially considering that approximately still there is 40% off-target effect. The need of identification of highly potent ( $IC_{50}$  in picomolar range) compounds that are acting on different mechanisms and overcoming resistances should be also festinated. Targeting tumors with distinct but not too high expression level of therapeutic target would recommend the delivery of powerful drugs.

We can conclude that using novel glutamine donor peptides, our technology provides an alternative enzymatic conjugation strategy for the engraftment of various payloads, using different antibody formats resulting in homogeneous batches, without unconjugated species.

## 7 REFERENCES

---

1. Adams, G. P. & Weiner, L. M. Monoclonal antibody therapy of cancer. *Nat. Biotechnol.* **23**, 1147–1157 (2005).
2. Grillo-López, A. J., Hedrick, E., Rashford, M. & Benyunes, M. Rituximab: Ongoing and future clinical development. *Semin. Oncol.* **29**, 105–112 (2002).
3. Chames, P., Van Regenmortel, M., Weiss, E. & Baty, D. Therapeutic antibodies: Successes, limitations and hopes for the future. *Br. J. Pharmacol.* **157**, 220–233 (2009).
4. Carter, P. J. & Lazar, G. A. Next generation antibody drugs: Pursuit of the ‘high-hanging fruit’. *Nat. Rev. Drug Discov.* **17**, 197–223 (2018).
5. Carter, P. Antibody-Based Cancer Therapies. **1**, 118–129 (2001).
6. Kholodenko, Roman V Kalinovsky, D. V., Doronin, I. I., Ponomarev, E. D. & Kholodenko, I. V. Antibody Fragments as Potential Biopharmaceuticals for Cancer Therapy: Success and Limitations. *Curr. Med. Chem.* (2017). doi:10.2174/0929867324666170817152554
7. Holliger, P. & Hudson, P. J. Engineered antibody fragments and the rise of single domains. *Nat. Biotechnol.* **23**, 1126–1136 (2005).
8. Müller, D. *et al.* Improved pharmacokinetics of recombinant bispecific antibody molecules by fusion to human serum albumin. *J. Biol. Chem.* **282**, 12650–12660 (2007).
9. Nelson, A. L. Antibody fragments: hope and hype. *Landes Biosci.* **2**, 77–83 (2010).
10. Strebhardt, K. & Ullrich, A. Paul Ehrlich ’ s magic bullet concept : 100 years of progress. *Nat. Rev. cancer* **8**, 473–480 (2008).
11. Senter, P. D. & Sievers, E. L. The discovery and development of brentuximab vedotin for use in relapsed Hodgkin lymphoma and systemic anaplastic large cell lymphoma. *Nat. Biotechnol.* **30**, 631–637 (2012).
12. Schrama, D., Reisfeld, R. A. & Becker, J. C. Antibody targeted drugs as cancer therapeutics. *Nat. Rev. Drug Discov.* **5**, 147–159 (2006).
13. Damelin, M., Zhong, W., Myers, J. & Sapra, P. Evolving Strategies for Target Selection for Antibody-Drug Conjugates. *Pharm. Res.* **32**, 3494–3507 (2015).
14. Panowski, S., Bhakta, S., Raab, H., Polakis, P. & Junutula, J. R. Site-specific antibody drug conjugates for cancer therapy. *MAbs* **6**, 34–45 (2014).
15. Rudnick, S. I. *et al.* Influence of Affinity and Antigen Internalization on the

- Uptake and Penetration of Anti-HER2 Antibodies in Solid Tumors. **71**, 2250–2259 (2012).
16. Rudnick, S. I. *et al.* Influence of affinity and antigen internalization on the uptake and penetration of anti-HER2 Antibodies in Solid Tumors. *Cancer Res.* **71**, 2250–2259 (2011).
  17. Liu, L. Pharmacokinetics of monoclonal antibodies and Fc-fusion proteins. *Protein Cell* **9**, 15–32 (2018).
  18. Perrino, E. *et al.* Curative properties of noninternalizing antibody-drug conjugates based on maytansinoids. *Cancer Res.* **74**, 2569–2578 (2014).
  19. Zhang, Y. & Pastan, I. High shed antigen levels within tumors: An additional barrier to Immunoconjugate therapy. *Clin. Cancer Res.* **14**, 7981–7986 (2008).
  20. Pak, Y., Zhang, Y., Pastan, I. & Lee, B. Antigen shedding may improve efficiencies for delivery of antibody-based anticancer agents in solid tumors. *Cancer Res.* **72**, 3143–3152 (2012).
  21. Jiang, X. R. *et al.* Advances in the assessment and control of the effector functions of therapeutic antibodies. *Nat. Rev. Drug Discov.* **10**, 101–110 (2011).
  22. Sapra, P. & Shor, B. Monoclonal antibody-based therapies in cancer: Advances and challenges. *Pharmacol. Ther.* **138**, 452–469 (2013).
  23. Erickson, H. K. *et al.* Antibody-maytansinoid conjugates are activated in targeted cancer cells by lysosomal degradation and linker-dependent intracellular processing. *Cancer Res.* **66**, 4426–4433 (2006).
  24. Lyon, R. P. *et al.* Reducing hydrophobicity of homogeneous antibody-drug conjugates improves pharmacokinetics and therapeutic index. *Nat. Biotechnol.* **33**, 733–735 (2015).
  25. Chari, R. V. J., Miller, M. L. & Widdison, W. C. Antibody-Drug Conjugates: An Emerging Concept in Cancer Therapy. *Angew. Chemie Int. Ed.* **53**, 3796–3827 (2014).
  26. Pillay, C. S., Elliott, E. & Dennison, C. Endolysosomal proteolysis and its regulation. *Biochem. J.* **363**, 417–429 (2002).
  27. Hamann, P. R. *et al.* An anti-CD33 antibody - Calicheamicin conjugate for treatment of acute myeloid leukemia. Choice of linker. *Bioconjug. Chem.* **13**, 40–46 (2002).
  28. Griffith, O. W. Biologic and pharmacologic regulation of mammalian glutathione synthesis. *Free Radic. Biol. Med.* **27**, 922–935 (1999).
  29. Traverso, N. *et al.* Role of Glutathione in Cancer Progression and Chemoresistance. *Oxid. Med. Cell. Longev.* **2013**, (2013).
  30. Appenzeller-Herzog, C. & Ellgaard, L. The human PDI family: Versatility packed

- into a single fold. *Biochim. Biophys. Acta - Mol. Cell Res.* **1783**, 535–548 (2008).
31. Dubowchik, G. M. & Firestone, R. A. Cathepsin b-sensitive dipeptide prodrugs. 1. A model study of structural requirements for efficient release of doxorubicin. *Bioorg. Med. Chem. Lett.* **8**, 3341–3346 (1998).
  32. Caculitan, N. G. *et al.* Cathepsin B is dispensable for cellular processing of cathepsin B-cleavable antibody–drug conjugates. *Cancer Res.* **77**, 7027–7037 (2017).
  33. de Graaf, M., Boven, E., Scheeren, H. W., Haisma, H. J. & Pinedo, H. M. Beta-Glucuronidase-Mediated Drug Release. *Curr. Pharm. Des.* **8**, 1391–1403 (2002).
  34. Jeffrey, S. C. *et al.* Development and Properties of  $\beta$ -Glucuronide Linkers for Monoclonal Antibody–Drug Conjugates. *Bioconjugate Chem.* **17**, 831–840 (2006).
  35. Dan, N. *et al.* Antibody-drug conjugates for cancer therapy: Chemistry to clinical implications. *Pharmaceuticals* **11**, (2018).
  36. Sedlacek, H.-H., Seemann, G., Hoffmann, D., Czech, J. & Lorenz, P. Antibodies as carriers of cytotoxicity. *Contrib. to Oncol.* **43**, 1–145 (1992).
  37. Beck, A., Goetsch, L., Dumontet, C. & Corvaia, N. Strategies and challenges for the next generation of antibody-drug conjugates. *Nat. Rev. Drug Discov.* **16**, 315–337 (2017).
  38. Elias, D. J. *et al.* Phase I clinical comparative study of monoclonal antibody KS1/4 and KS1/4-methotrexate immunconjugate in patients with non-small cell lung carcinoma. *Cancer Res.* **50**, 4154–4159 (1990).
  39. Petersen, B. H., Deherdt, S. V, Schneck, D. W. & Bumol, T. F. The Human Immune Response to KS1/4-Desacetylvinblastine (LY256787) and KS1/4-Desacetylvinblastine Hydrazide (LY203728) in Single and Multiple Dose Clinical Studies. *Cancer Res.* **51**, 2286–2290 (1991).
  40. Trail, P. *et al.* Cure of xenografted human carcinomas by BR96-doxorubicin immunoconjugates. *Science (80- )*. **261**, 212–215 (1993).
  41. Alley, S. C., Okeley, N. M. & Senter, P. D. Antibody-drug conjugates: Targeted drug delivery for cancer. *Curr. Opin. Chem. Biol.* **14**, 529–537 (2010).
  42. Wang, L., Amphlett, G., Bla, W. A., Lambert, J. M. & Zhang, W. E. I. Structural characterization of the maytansinoid – monoclonal antibody immunoconjugate , huN901 – DM1 , by mass spectrometry. *Protein Sci.* **14**, 2436–2446 (2005).
  43. Salfeld, J. G. Isotype selection in antibody engineering. *Nat. Biotechnol.* **25**, 1369–1372 (2007).
  44. Junutula, J. R. *et al.* Site-specific conjugation of a cytotoxic drug to an antibody improves the therapeutic index. *Nat. Biotechnol.* **26**, 925–932 (2008).

45. Hamblett, K. J. *et al.* Effects of Drug Loading on the Antitumor Activity of a Monoclonal Antibody Drug Conjugate Effects of Drug Loading on the Antitumor Activity of a Monoclonal Antibody Drug Conjugate. *Clin. Cancer Res.* **10**, 7063–7070 (2004).
46. Pillow, T. H. *et al.* Site-specific trastuzumab maytansinoid antibody-drug conjugates with improved therapeutic activity through linker and antibody engineering. *J. Med. Chem.* **57**, 7890–7899 (2014).
47. Mehrling, T. & Soltis, D. Challenges in Optimising the Successful Construction of Antibody Drug Conjugates in Cancer Therapy. *Antibodies* **7**, 11 (2018).
48. Shen, B. Q. *et al.* Conjugation site modulates the in vivo stability and therapeutic activity of antibody-drug conjugates. *Nat. Biotechnol.* **30**, 184–189 (2012).
49. Strop, P. *et al.* Location matters: Site of conjugation modulates stability and pharmacokinetics of antibody drug conjugates. *Chem. Biol.* **20**, 161–167 (2013).
50. Kline, T. *et al.* Methods to Make Homogenous Antibody Drug Conjugates. *Pharm. Res.* **32**, 3480–3493 (2015).
51. Moek, K. L., de Groot, D. J. A., de Vries, E. G. E. & Fehrmann, R. S. N. The antibody-drug conjugate target landscape across a broad range of tumour types. *Ann. Oncol.* **28**, 3083–3091 (2017).
52. Norsworthy, K. *et al.* FDA Approval Summary: Mylotarg for Treatment of Patients with Relapsed or Refractory CD33-Positive Acute Myeloid Leukemia. *Oncologist.* (2018). doi:10.1634/theoncologist.2017-0604
53. Akkapeddi, P. *et al.* Construction of homogeneous antibody-drug conjugates using site-selective protein chemistry. *Chem. Sci.* **7**, 2954–2963 (2016).
54. Ricart, A. D. Antibody-drug conjugates of calicheamicin derivative: Gemtuzumab ozogamicin and inotuzumab ozogamicin. *Clin. Cancer Res.* **17**, 6417–6427 (2011).
55. Olejniczak, S. H., Stewart, C. C., Donohue, K. & Czuczman, M. S. A quantitative exploration of surface antigen expression in common B-cell malignancies using flow cytometry. *Immunol. Invest.* **35**, 93–114 (2006).
56. Francisco, J. A. *et al.* cAC10-vcMMAE, an anti-CD30-monomethyl auristatin E conjugate with potent and selective antitumor activity. *Blood* **102**, 1458–1465 (2003).
57. Deutsch, Y. E., Tadmor, T., Podack, E. R. & Rosenblatt, J. D. CD30: an important new target in hematologic malignancies. *Leuk. Lymphoma* **52**, 1641–54 (2011).
58. Forero-Torres, A. *et al.* A Phase II study of SGN-30 (anti-CD30 mAb) in Hodgkin lymphoma or systemic anaplastic large cell lymphoma. *Br. J. Haematol.* **146**, 171–179 (2009).
59. Donato, E. M., Fernández-Zarzoso, M., Hueso, J. A. & Rubia, J. de la.

- Brentuximab vedotin in hodgkin lymphoma and systemic anaplastic large-cell lymphoma. *Onco. Targets. Ther.* **11**, 4583–4590 (2018).
60. Ferlay, J. *et al.* Estimates of worldwide burden of cancer in 2008: GLOBOCAN 2008. *Int. J. Cancer* **127**, 2893–2917 (2010).
  61. Way, T.-D. & Lin, J.-K. Role of HER2/HER3 co-receptor in breast carcinogenesis. *Futur. Oncol* **1**, 841–849 (2005).
  62. Citri, A., Skaria, K. B. & Yarden, Y. The deaf and the dumb: The biology of ErbB-2 and ErbB-3. *EGF Recept. Fam. Biol. Mech. Role Cancer* **284**, 57–68 (2003).
  63. Owens, M. A., Horten, B. C. & Da Silva, M. M. HER2 amplification ratios by fluorescence in situ hybridization and correlation with immunohistochemistry in a cohort of 6556 breast cancer tissues. *Clin. Breast Cancer* **5**, 63–69 (2004).
  64. Gravalos, C. & Jimeno, A. HER2 in gastric cancer: A new prognostic factor and a novel therapeutic target. *Ann. Oncol.* **19**, 1523–1529 (2008).
  65. Pauletti, G., Godolphin, W., Press, M. & Slamon, D. Detection and quantitation of HER-2/neu gene amplification in human breast cancer archival material using fluorescence in situ hybridization. *Oncogene.* **13**, 63–72 (1996).
  66. Muller, W. J., Ho, J. & Siegel, P. M. Oncogenic activation of Neu/ErbB-2 in a transgenic mouse model for breast cancer. *Biochem Soc Symp* **63**, 149–157 (1998).
  67. Wang, S. E. *et al.* HER2 kinase domain mutation results in constitutive phosphorylation and activation of HER2 and EGFR and resistance to EGFR tyrosine kinase inhibitors. *Cancer Cell* **10**, 25–38 (2006).
  68. Berchuck, A. *et al.* Overexpression of HER-2 / neu Is Associated with Poor Survival in Advanced Epithelial Ovarian Cancer1. 4087–4091 (1990).
  69. Rolitsky, C., Theil, K., McGaughy, V., Copeland, L. & Niemann, T. HER-2/neu amplification and overexpression in endometrial carcinoma. *Int J Gynecol Pathol.* **18**, 138–143. (1999).
  70. Coogan, C. L., Estrada, C. R., Kapur, S. & Bloom, K. J. HER-2/neu protein overexpression and gene amplification in human transitional cell carcinoma of the bladder. *Urology* **63**, 786–790 (2004).
  71. Bunn, P. A. *et al.* Expression of Her-2 / neu in Human Lung Cancer Cell Lines by Immunohistochemistry and Fluorescence in Situ Hybridization and its Relationship to in Vitro Cytotoxicity by Trastuzumab and Chemotherapeutic Agents Expression of Her-2 / neu in Human Lung Cance. **7**, 3239–3250 (2001).
  72. Slamon, D. J. *et al.* Numb Er 11 Use of Chemotherapy Plus a Monoclonal Antibody Against Her2. *English J.* **344**, 783–792 (2001).
  73. Vogel, C. *et al.* First-line, single-agent Herceptin® (trastuzumab) in metastatic breast cancer: A preliminary report. *Eur. J. Cancer* **37**, S25–S29 (2001).

74. Luo, Y., Lacroix, J. J. & Prabhu, S. in *Antibody-Drug Conjugates*. 203–223 (Springer, Cham, 2015). doi:[https://doi.org/10.1007/978-3-319-13081-1\\_12](https://doi.org/10.1007/978-3-319-13081-1_12)
75. Partida-Martinez, L. P. & Hertweck, C. Pathogenic fungus harbours endosymbiotic bacteria for toxin production. *Nature* **437**, 884–888 (2005).
76. Junttila, T. T. *et al.* Ligand-Independent HER2/HER3/PI3K Complex Is Disrupted by Trastuzumab and Is Effectively Inhibited by the PI3K Inhibitor GDC-0941. *Cancer Cell* **15**, 429–440 (2009).
77. Junttila, T. T., Li, G. & Parsons, K. Trastuzumab-DM1 ( T-DM1 ) retains all the mechanisms of action of trastuzumab and efficiently inhibits growth of lapatinib insensitive breast cancer. **1**, 347–356 (2011).
78. Barok, M., Tanner, M., Köninki, K. & Isola, J. Trastuzumab-DM1 causes tumour growth inhibition by mitotic catastrophe in trastuzumab-resistant breast cancer cells in vivo. *Breast Cancer Res.* **13**, R46 (2011).
79. Recondo, G. *et al.* Novel approaches to target HER2-positive breast cancer: Trastuzumab emtansine. *Cancer Manag. Res.* **8**, 57–65 (2016).
80. Barok, M., Joensuu, H. & Isola, J. Trastuzumab emtansine: Mechanisms of action and drug resistance. *Breast Cancer Res.* **16**, 1–12 (2014).
81. Folk, J. & Finlayson, J. The epsilon-(gamma-glutamyl)lysine crosslink and the catalytic role of transglutaminases. *Adv Protein Chem* 1–133 (1977).
82. Cheng, X.-F. Hydrolysis of gamma :epsilon Isopeptides by Cytosolic Transglutaminases and by Coagulation Factor XIIIa. *J. Biol. Chem.* **272**, 10311–10317 (1997).
83. Fesus, L. & Piacentini, M. Transglutaminase 2 : an enigmatic enzyme with diverse functions. *TRENDS Biochem. Sci.* **27**, 534–539 (2002).
84. Folk, J. No Title Mechanism and basis for specificity of transglutaminase-catalyzed epsilon-(gamma-glutamyl) lysine bond formation. *Adv Enzym. Relat Areas Mol Biol.* 1–56. (1983).
85. Lorand, L. & Graham, R. M. Transglutaminases: crosslinking enzymes with pleiotropic functions. *Nat. Rev. Mol. Cell Biol.* **4**, 140–156 (2003).
86. Griffin, M., Casadio, R. & Bergamini, C. M. Transglutaminases: nature’s biological glues. *Biochem. J.* **368**, 377–96 (2002).
87. Mehta, K. & Eckert, R. *Transglutaminases: Family of Enzymes with Diverse Functions. Progress in experimental tumor research* **38**, (2005).
88. Greenberg, C., Birckbichler, P. & Rice, R. Transglutaminases : multifunctional cross-linking enzymes that stabilize tissues. **5**, 3071–3077 (1991).
89. Schmidt, G., Selzer, J., Lerm, M. & Aktories, K. The Rho-deamidating Cytotoxic Necrotizing Factor 1 from *Escherichia coli* Possesses Transglutaminase Activity. *J.*

- Biol. Chem.* **273**, 13669–13674 (1998).
90. Makarova, K. S., Aravind, L. & Koonin, E. V. A superfamily of archaeal, bacterial, and eukaryotic proteins homologous to animal transglutaminases. *Protein Sci.* **8**, 1714–1719 (1999).
  91. Plácido, D. *et al.* Auto-induction and purification of a *Bacillus subtilis* transglutaminase (Tgl) and its preliminary crystallographic characterization. *Protein Expr. Purif.* **59**, 1–8 (2008).
  92. Ando, H. *et al.* Purification and characteristics of a novel transglutaminase derived from microorganisms. *Agric. Biol. Chem.* **53**, 2613–2617 (1989).
  93. Sato, H. Enzymatic procedure for site-specific pegylation of proteins. *Adv. Drug Deliv. Rev.* **54**, 487–504 (2002).
  94. Zhu, Y., Rinzema, A., Tramper, J. & Bol, J. Microbial transglutaminase – a review of its production and application in food processing. *Appl Microbiol Biotechnol* **44**, 277–282 (1995).
  95. Mariniello, L. & Porta, R. in *Transglutaminases: Family of Enzymes with Diverse Functions* (eds. Mehta, K. & Ckert, R.) 174–191 (Prog Exp Tum Res., 2005).
  96. Pasternack, R. *et al.* Bacterial pro-transglutaminase from *Streptoverticillium mobaraense* - Purification, characterisation and sequence of the zymogen. *Eur. J. Biochem.* **257**, 570–576 (1998).
  97. Kashiwagi, T. *et al.* Crystal structure of microbial transglutaminase from *Streptoverticillium mobaraense*. *J. Biol. Chem.* **277**, 44252–44260 (2002).
  98. Zhang, L. *et al.* Enzymatic characterization of transglutaminase from *Streptomyces mobaraensis* DSM 40587 in high salt and effect of enzymatic cross-linking of yak milk proteins on functional properties of stirred yogurt. *J. Dairy Sci.* **95**, 3559–3568 (2012).
  99. Pedersen, L. C. *et al.* Transglutaminase factor XIII uses proteinase-like catalytic triad to crosslink macromolecules. *Protein Sci.* **3**, 1131–1135 (1994).
  100. Kanaji, T. *et al.* Primary structure of microbial transglutaminase from *Streptoverticillium* sp. strain s-8112. *J. Biol. Chem.* **268**, 11565–11572 (1993).
  101. Folk, J. & Chung, S. Molecular and catalytic properties of transglutaminases. *Adv Enzym. Relat Areas Mol Biol.* 109–191 (1973).
  102. Fleckenstein, B. *et al.* Gliadin T cell epitope selection by tissue transglutaminase in celiac disease. Role of enzyme specificity and pH influence on the transamidation versus deamidation reactions. *J. Biol. Chem.* **277**, 34109–34116 (2002).
  103. Pasternack, R. *et al.* A fluorescent substrate of transglutaminase for detection and characterization of glutamine acceptor compounds. *Anal. Biochem.* **249**, 54–60 (1997).

104. Nonaka, M., Sawa, A., Matsuura, Y., Motoki, M. & Nio, N. Deamidation of Several Food Proteins Using Free and Immobilized Ca<sup>2+</sup>-Independent Microbial Transglutaminase. *Biosci Biotechnol Biochem.* **60**, 532–533 (1996).
105. Ohtsuka, T., Umezawa, Y., Nio, N. & Kubota, K. Comparison of deamidation activity of transglutaminases. *J. Food Sci.* **66**, 25–29 (2001).
106. Shimba, N., Yokoyama, K. I. & Suzuki, E. I. NMR-based screening method for transglutaminases: Rapid analysis of their substrate specificities and reaction rates. *J. Agric. Food Chem.* **50**, 1330–1334 (2002).
107. Tagami, U. *et al.* Substrate specificity of microbial transglutaminase as revealed by three-dimensional docking simulation and mutagenesis. *Protein Eng. Des. Sel.* **22**, 747–752 (2009).
108. Taguchi, S. *et al.* Substrate specificity analysis of microbial transglutaminase using proteinaceous protease inhibitors as natural model substrates. *J. Biochem.* **128**, 415–425 (2000).
109. Mero, a, Spolaore, B., Pasut, G., Veronese, F. M. & Fontana, A. Transglutaminase-Mediated PEGylation of Proteins: Direct Identification of the Sites of Protein Modification by Mass Spectrometry using a Novel Monodisperse PEG. 384–389 (2009).
110. Stachel, I., Schwarzenbolz, U., Henle, T. & Meyer, M. Cross-linking of type I collagen with microbial transglutaminase: Identification of cross-linking sites. *Biomacromolecules* **11**, 698–705 (2010).
111. Nonanaka, M., Matsuura, Y. & Motoki, M. Incorporation of Lysine-and Lysine Dipeptides into  $\alpha$ 1-Casein by Ca<sup>2+</sup>-independent Microbial Transglutaminase. **60**, 131–133 (1996).
112. Esposito, C. & Caputo, I. Mammalian transglutaminases: Identification of substrates as a key to physiological function and physiopathological relevance. *FEBS J.* **272**, 615–631 (2005).
113. Spolaore, B. *et al.* Local unfolding is required for the site-specific protein modification by transglutaminase. *Biochemistry* **51**, 8679–8689 (2012).
114. Ota, M., Sawa, A., Nio, N. & Ariyoshi, Y. Enzymatic ligation for synthesis of single-chain analogue of monellin by transglutaminase. *Biopolymers* **50**, 193–200 (1999).
115. Ohtsuka, T., Ota, M., Nio, N. & Motoki, M. Comparison of Substrate Specificities of Transglutaminases Using Synthetic Peptides as Acyl donors. *Bioscience, Biotechnology, and Biochemistry* **64**, 2608–2613 (2000).
116. Sugimura, Y., Yokoyama, K., Nio, N., Maki, M. & Hitomi, K. Identification of preferred substrate sequences of microbial transglutaminase from *Streptomyces mobaraensis* using a phage-displayed peptide library. *Arch. Biochem. Biophys.* **477**, 379–383 (2008).

117. Malešević, M., Andreas, M., Hertel, T. C. & Pietzsch, M. A Fluorescence-Based Array Screen for Transglutaminase Substrates. *Chembiochem* **26**, 1169–1174 (2015).
118. Ohtsuka, T., Sawa, A., Kawabata, R., Nio, N. & Motoki, M. Substrate specificities of microbial transglutaminase for primary amines. *J. Agric. Food Chem.* **48**, 6230–6233 (2000).
119. Gundersen, M., Keillor, J. & Pelletier, J. Microbial transglutaminase displays broad acyl-acceptor substrate specificity. *Appl Microbiol Biotechnol.* **98**, 219–230 (2014).
120. Mindt, T. L. *et al.* Modification of different IgG1 antibodies via glutamine and lysine using bacterial and human tissue transglutaminase. *Bioconjug. Chem.* **19**, 271–278 (2008).
121. Jeger, S. *et al.* Site-specific and stoichiometric modification of antibodies by bacterial transglutaminase. *Angew. Chemie - Int. Ed.* **49**, 9995–9997 (2010).
122. Dennler, P. *et al.* Transglutaminase-based chemo-enzymatic conjugation approach yields homogeneous antibody-drug conjugates. *Bioconjug. Chem.* **25**, 569–578 (2014).
123. Knogler, K. *et al.* Copper-67 radioimmunotherapy and growth inhibition by anti-L1-cell adhesion molecule monoclonal antibodies in a therapy model of ovarian cancer metastasis. *Clin. Cancer Res.* **13**, 603–611 (2007).
124. Siegmund, V. *et al.* Locked by Design: A Conformationally Constrained Transglutaminase Tag Enables Efficient Site-Specific Conjugation. *Angew. Chemie - Int. Ed.* **54**, 13420–13424 (2015).
125. Spidel, J. L. *et al.* Site-Specific Conjugation to Native and Engineered Lysines in Human Immunoglobulins by Microbial Transglutaminase. *Bioconjug. Chem.* **28**, 2471–2484 (2017).
126. Zheng, K., Bantog, C. & Bayer, R. The impact of glycosylation on monoclonal antibody conformation and stability. *MAbs* **3**, 568–576 (2011).
127. PCT/EP2014/0792278.
128. Perez Alea, M. *et al.* Development of an isoenzyme-specific colorimetric assay for tissue transglutaminase 2 cross-linking activity. *Anal. Biochem.* **389**, 150–156 (2009).
129. Müller, P. *et al.* Trastuzumab emtansine ( T-DM1 ) renders HER2 + breast cancer highly susceptible to CTLA-4 / PD-1 blockade. *Sci. Transl. Med.* **7**, 315ra188-315ra188 (2015).
130. Muller, P. *et al.* Microtubule-Depolymerizing Agents Used in Antibody-Drug Conjugates Induce Antitumor Immunity by Stimulation of Dendritic Cells. *Cancer Immunol. Res.* **2**, 741–755 (2014).

131. De Goeij, B. E. *et al.* HER2 monoclonal antibodies that do not interfere with receptor heterodimerization-mediated signaling induce effective internalization and represent valuable components for rational antibody-drug conjugate design. *MAbs* **6**, 392–402 (2014).
132. Loisel, S. *et al.* Relevance, advantages and limitations of animal models used in the development of monoclonal antibodies for cancer treatment. *Crit. Rev. Oncol. Hematol.* **62**, 34–42 (2007).

## Development of a sandwich ELISA assay for quantification of human tissue transglutaminase in cell lysates and tissue homogenates

Éva Sivadó<sup>1</sup> · Sabrina Lareure<sup>1</sup> · Valérie Attuil-Audenis<sup>1</sup> · Saïd El Alaoui<sup>1</sup> · Vincent Thomas<sup>1</sup>

Received: 11 September 2016 / Accepted: 4 October 2016 / Published online: 19 October 2016  
© Springer-Verlag Wien 2016

**Abstract** Tissue transglutaminase (tTG) belongs to the multigene transglutaminase family of Ca<sup>2+</sup>-dependent protein cross-linking enzymes. There is a strong evidence that tTG is involved in pathology, such as neurodegenerative diseases, cancer, and celiac disease. To study physiopathological implication of tTG, a sandwich immunoassay has been developed with a new monoclonal antibody for the capture and polyclonal antibody both generated in house. Using this ready to use assay, the tTG protein level can be measured in human tissue homogenates and cells extracts easily in about 4 h. The limit of detection is 1.7 ng/ml; the coefficients of intra- and inter-assay variations range from 1 to 2 % and from 7 to 10 %, respectively. The assay is specific to tTG, and no cross reactivity with TG1, TG3, TG6, TG7, or factor XIIIa was observed. Finally, in the addition to the tTG activity assay previously developed, this assay should be a valuable tool to increase our knowledge of the tTG involvement in physiological and pathological states.

**Keywords** Tissue transglutaminase · Sandwich ELISA · Monoclonal antibody · Polyclonal antibody

### Introduction

Transglutaminases (TGs; EC 2.3.2.13) are a family of structurally and functionally related enzymes that catalyze

calcium-dependent post-translational modifications of proteins. This transamidase activity consists of protein cross-linking via isopeptide bonds (between a specific glutamine and a lysine residue) and also of the incorporation of low-molecular weight amines (Folk and Finlayson 1977). In the absence of amine donors, the enzyme is able to catalyze site-specific deamidation (Lorand and Graham 2003).

In mammals, nine distinct TG members have been identified: TG1, TG2, TG3, TG4, TG5, TG6, TG7, factor XIIIa, and the enzymatically inactive erythrocyte band 4.2 protein (Griffin et al. 2002). TG2, also known as tissue transglutaminase (tTG), is the most studied and widely distributed member of the TGs family in various cellular locations. It is mainly localized in the cytosol, but it can be represented in the extracellular matrix, in the nucleus, and associated with the mitochondria and plasma membrane as well (Gundemir et al. 2011). Besides the transamidation activity that stabilizes tissues, it can bind and hydrolyze GTP and ATP that regulate signal transduction as a G protein (Lai et al. 1998), it has intrinsic kinase activity (Mishra and Murphy 2004), and it exhibits protein disulphide isomerase activity (Hasegawa et al. 2003).

tTG is constitutively expressed in several tissues, while its expression is induced by external stimuli or as part of their differentiation in some other types of cells (Zemskov et al. 2006). The control of tTG primarily occurs at the transcription level (Griffin et al. 2002). Retinoids are well-known regulators of the enzyme (Nagy et al. 1996). Moreover, response elements for transforming growth factor- $\beta$ 1 (Ritter and Davies 1998) and stress-induced transcription factors (NF- $\kappa$ B, hypoxia inducible factor) are located in the tTG promoter (Mirza et al. 1997; Jang et al. 2010). This multifunctional protein has diverse cellular localization and displays diverse functions in several physiological (e.g., signal transduction, proliferation, cell adhesion, migration,

Handling Editors: S. Beninati, M. Piacentini, C. M. Bergamini.

✉ Vincent Thomas  
vthomas@covalab.com

<sup>1</sup> Research Department, Covalab S.A.S, 11 Avenue Albert Einstein, 69100 Villeurbanne, France

regulation of cell survival/death processes), and pathological processes (fibrosis, inflammatory diseases, neurodegenerative disorders, metabolic diseases, coeliac disease, and cancer) (Fesus and Piacentini 2002).

In previous studies, we developed different assays for measuring tTG and other TG isoenzymes activities. These assays (now commercially available) can be used to quantify transglutaminase specific activities in different biological samples (Thomas et al. 2006; Perez Alea et al. 2009). However, to address a better correlation between the presence of the enzymes and their functions, the quantification of both enzyme activity and enzyme level is needed. Moreover, the measurement of enzyme activity alone will not reflect the presence of possible inactive form of TG proteins in tissues, as it was published by Siegel et al. (2008). Since it is evident, a test measuring active and non-active tTG should be a tool of interest to study the enzyme involvement in different biological processes.

Attempts were made by few groups to measure tTG protein level in various sources of samples. The analytical sensitivity of these assays was 0.1 ng/ml (Brevé et al. 2008) and 40 pg/ml (Wolf et al. 2011). However, in the first case, the authors used polyclonal antibodies that cannot be used for routine assay development due to the limited availability of the antibody and the variability from batch to batch production. In the second publication, the main problem of the use of fluorimetric assay is the interference of the relative fluorescence with the biological material, such as blood. In the present study, we developed and validated a sandwich enzyme-linked immunosorbent assay (ELISA) for the quantitative detection of tTG protein level using our newly developed monoclonal and polyclonal antibodies. However, the analytical sensitivity of this assay is around 2 ng/ml, which is less sensitive but more accurate and robust test. Our new and ready to use assay represents an easy tool for the detection and quantification of tTG in various human and guinea pig samples, including serums, tissue homogenates, and cell extracts. This ELISA assay can be used to study the expression and function of tTG and complement the data obtained by tTG activity assay, respectively.

## Materials and methods

### Chemicals

Recombinant human tTG (rhu-tTG), recombinant human keratinocyte transglutaminase (TG1), recombinant human epidermal transglutaminase (TG3), recombinant human neuronal transglutaminase (TG6), recombinant human transglutaminase 7 (TG7), and recombinant human factor

XIII (FXIII) were obtained from Zedira (Darmstadt, Germany). Horseradish peroxidase (HRP) conjugated goat anti-rabbit IgG (H + L) was purchased from Jackson ImmunoResearch Europe Ltd. (Suffolk, UK). Corning immuno 96-stripwell flat-bottom plates and cell culture dishes, protease inhibitor cocktail, phenylmethanesulfonyl fluoride (PMSF), bovine serum albumin (BSA), hypoxanthine-aminopterin-thymidine medium (HAT), DMEM medium, culture media and supplements, protease inhibitor cocktail, Freund's complete adjuvant and Freund's incomplete adjuvants were obtained from Sigma-Aldrich (France). Tetramethylbenzidine (TMB) staining solution, Covalight chemiluminescent reagent, and blocking buffer were obtained from Covalab (Villeurbanne, France).

### Generation of monoclonal antibodies

Mouse monoclonal IgG antibodies (Mabs) against tTG were prepared by immunizing 6–8-week-old female Balb/c mice with rhu-tTG. The immunization, the fusion of murine myeloma cell line (Sp2/O-Ag-14) and spleen cells from the best responding animal, respectively, HAT (hypoxanthine-aminopterin-thymidine medium) selection of hybridomas were performed according to the standard method of Covalab (Villeurbanne, France) described by El Alaoui et al. (1991).

### Generation of polyclonal antibodies

Rabbit polyclonal IgG antibodies against tTG were prepared by immunizing 3-month-old white female New Zealand rabbits with rhu-tTG according to the standard method of Covalab (Villeurbanne, France).

### Selection of tTG antibody couple

To achieve the best signal-to-noise ratio for the sensitivity level desired in sandwich ELISA, a panel of monoclonal and polyclonal antibodies was examined by check board titration, using rhu-tTG as antigen (data not shown). After selection of 3F3 monoclonal and Cov2005 polyclonal antibodies, ELISA assay condition was optimized.

### Cell culture

HEK293AD cell line stable transfected with rhu-tTG was kindly provided by Dr. Laszlo Fesus and Dr. Katalin Kanchan (Department of Biochemistry and Molecular Biology, University of Debrecen, Hungary) (Kanchan et al. 2013). HEK293AD-tTG cells were grown in DMEM supplemented with 10 % fetal bovine serum (FBS), L-glutamine (300 mg/ml), and penicillin/streptomycin

(100 U/ml) at 37 °C in an atmosphere of 5 % CO<sub>2</sub>. SHEP neuroblastoma cell extracts were kindly provided by Dr. Sandrine Wittmann (Centre Léon Bérard, France). To initiate retinoic acid-mediated differentiation, cells were grown in the low-serum medium containing 10 μM retinoic acid.

#### Sample preparation

Both cell types were collected and washed twice with phosphate-buffered saline (PBS), resuspended in RIPA buffer [50 mM Tris/HCl (pH 7.5), 150 mM NaCl, 1 mM EDTA, 1 mM DTT, 0.5 % Nonidet P40, 10 % glycerol, and protease inhibitor cocktail] and incubated for 30 min with gentle agitation at 4 °C. The cells were sonicated twice on ice and finally centrifuged at 10000 *g* for 10 min at 4 °C.

Livers were surgically removed from guinea pigs and washed with 140 mM NaCl. Liver homogenates were prepared in ice-cold buffer containing 140 mM NaCl, 40 mM Tris/HCl (pH 7.5), 3 mM EDTA, 2 mM DTT, 1 mM PMSF, and protease inhibitor cocktail. Supernatant was collected after centrifugation at 25000 *g* for 30 min at 4 °C.

Erythrocytes were separated by centrifugation at 2000 rpm for 5 min at 4 °C. The red blood cell (RBC) containing pellet was washed three times with ice-cold PBS. Followed by lysis of isolated RBC in lysis buffer [5 mM NaHPO<sub>4</sub> (pH 8.5), 0.3 mM PMSF, 1 mM EDTA, and protease inhibitor cocktail] and centrifuged at 3500 rpm for 20 min at 4 °C. Protein content was determined by the Bradford method using BSA as standard. Samples were stored at -80 °C.

#### Western blotting

Tissue transglutaminase expression levels in different samples were evaluated also by western blot (WB). Cell lysates, tissue homogenates (20 or 50 μg of total protein), human red blood cell lysates (200 μg), and rhu-tTG were electrophoresed on a 10 % polyacrylamide gel (SDS-PAGE) and transferred to nitrocellulose membranes (Amersham) according to the manual of wet-transfer (Bio-Rad). The membranes were blocked with 5 % non-fat dried milk in PBS for 1 h at 37 °C and then incubated with mouse monoclonal 3F3, 7D2, 6F1, 6B5, or rabbit polyclonal Cov2005 antibodies (5 μg/ml dilution in 1 % non-fat milk/TBST) overnight at 4 °C. After washing with TBST, HRP-conjugated secondary anti-mouse or anti-rabbit antibodies were added and incubated for 1 h at 37 °C. After the final washing, immunoblots were visualized by the incubation of the membranes with chemiluminescence solution.

Luminescence was measured using ImageMaster VDS-CL (GE Healthcare).

#### Assay procedure

The microplate wells were coated overnight at 4 °C with 100 μl of 15 μg/ml 3F3 mouse anti-transglutaminase Mab diluted in 50 mM bicarbonate buffer (pH 9.5) and were blocked for 3 h at room temperature (RT) with 300 μl blocking buffer. Plates were stored and desiccated at 4 °C until examination.

To prepare an ELISA standard curve, serial dilution of rhu-tTG was prepared in the range of 15.6–1000 ng/ml. 100 μl of rhu-tTG or protein samples (ranging from 13.2 to 250 ng/ml of total protein), diluted in wash/dilution buffer (TBS with 0.05 % Tween 20, pH 7.4), were added to the wells and incubated for 2 h at 37 °C with gentle shaking. After washing with wash/dilution buffer, 100 μl of 2 μg/ml Cov2005 rabbit anti-transglutaminase polyclonal antibody diluted in wash/dilution buffer was added for 1 h at 37 °C with gentle shaking. Subsequently, the wells were incubated with 100 μl of HRP-conjugated goat anti-rabbit IgG (H + L) diluted 1/10000 in wash/dilution buffer. After the final washing step, 100 μl of TMB staining solution was added to the wells and incubated for 5 min at RT. Color development was stopped by the addition of 100 μl 0.5 N H<sub>2</sub>SO<sub>4</sub>, and the absorbance was determined at 450 nm using a microplate reader (Multiskan, Labsystem, Helsinki, Finland).

#### Specificity

For the determination of the antigen specificity of the assay, a serial dilution of recombinant human tTG, TG1, TG3, TG6, TG7, and FXIIIa was prepared in a concentration range of 15.6–1000 ng/ml; then, the same ELISA protocol was applied as described above.

#### Evaluation of accuracy

For the estimation of intra-assay variation, three dilutions of guinea pig liver homogenates were prepared and measured tenfold within one ELISA cycle. The inter-assay variation was assessed by measuring each of the three diluted liver samples fourfold on five different days.

#### Data analysis

Values are reported as mean ± SD. Data were analyzed with GraphPad Prism 5 (GraphPad Software Inc., San Diego, CA, USA).

## Results

### Selection and differential screening of Mabs to tTG

To select the best Mabs specific to tTG which will react with the enzyme in various samples from different species, two types of tests (ELISA and WB) were made using rhu-tTG, cell extracts, and tissue homogenates. Therefore we undertook a differential screening with these samples of clones preselected for their secretion of antibodies reacting positively with tTG. Of seven clones tested for further screening on the tTG from different samples, only four (clones: 3F3, 7D2, 6B5, and 6F1) secreted Mabs with restricted specificity to human, mouse, and guinea pig tTG. They were typed as an IgG1 (6F1, 6B5), IgG2a (3F3), and IgG3 (7D2) with kappa light chain.

In Fig. 1, the selected four Mabs and the polyclonal antibody Cov2005 were analyzed by western blot against rhu-tTG. 3F3 and 7D2 showed clear reactivity with rhu-tTG whereas 6F1 and 6B5 had low immuno-reactivity (Fig. 1a). To investigate the cross reactivity of the antibodies with the tTG from other species, liver homogenates from mouse, rat, and guinea pig were used to test the antibodies. It is apparent from Fig. 1b that 3F3 was specific to rhu-tTG and guinea pig tTG, whereas 7D2 and Cov2005 showed good reactivity with rhu-tTG, mouse, rat, and guinea pig tTG.

For further investigation of the specificity to human, mouse, and guinea pig, we tested the Mabs for their

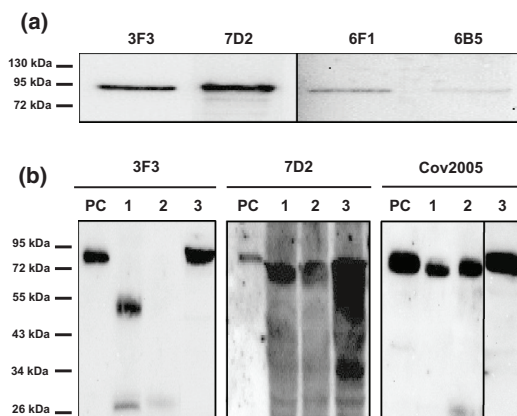


**Fig. 1** Characterization of the generated antibodies by western blot. **a** Verification of the immuno-reactivity of the selected mouse monoclonal 3F3, 7D2, 6F1, and 6B5 antibodies against rhu-tTG. **b** Determination of the genus specificity of the monoclonal 3F3, 7D2, and polyclonal Cov2005 antibodies. *PC* rhu-tTG positive control, *lane 1* mouse liver homogenate, *lane 2* rat liver homogenate, *lane 3* guinea pig liver homogenate. 0.1  $\mu$ g of rhu-tTG and 50  $\mu$ g of protein per slot were applied

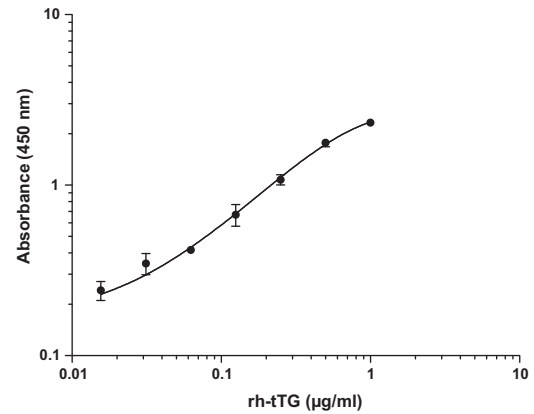


**Fig. 2** Standard curve of tTG sandwich ELISA with recombinant human tTG. The standard curve was linear up to 0.5  $\mu$ g/ml. The limit of detection was 1.77 ng/ml. Blank absorbance subtracted was  $0.132 \pm 0.017$ . Values are mean  $\pm$  standard deviation of three experiments performed as duplicates

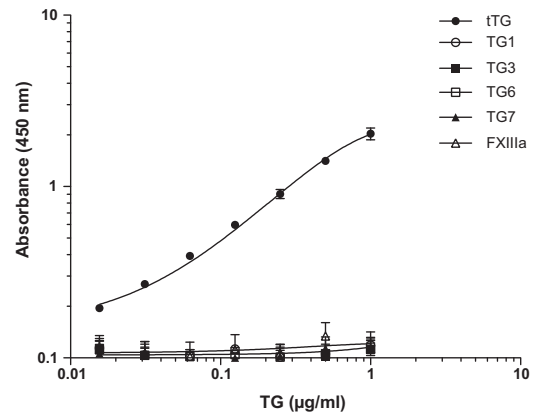


**Fig. 3** Specificity of the immunoassay for tTG comparing with TG1, TG3, TG6, TG7, and FXIIIa. Values are mean  $\pm$  standard deviation of three experiments performed as duplicates

use as captured antibodies in sandwich ELISA assay. Indeed, a comparison of the immuno-reactivity of the antibodies was tested for their (1) affinity and specificity to tTG from human, mouse, and guinea pig; (2) stability during their adsorption in the microtiter plates; and (3) sensitivity. Under our experimental procedures, mouse and rat tTGs could not be detected efficiently in liver and blood samples, and hence, the specificity of our assay was limited to human and guinea pig samples (data not shown).

**Table 1** Intra- and inter-assay variations of tTG sandwich ELISA assay

Sample/well ( $\mu\text{g}$ )	<i>n</i>	tTG ( $\mu\text{g/ml}$ )		% CV
		Mean	SD	
Intra-assay variation				
5	10	0.231	0.01	2
10	10	0.536	0.01	1
20	10	0.802	0.02	2
Inter-assay variation				
5	5	0.219	0.02	7
10	5	0.538	0.04	8
20	5	0.820	0.08	10

### Development of the sandwich ELISA assay, sensitivity, and accuracy of the test

Among the four Mabs studied, the combination of 3F3 as capture antibody with rabbit polyclonal Cov2005 detection antibody led to the best signal-to-noise ratio and was chosen for all further experiments. The absorbance of the blank, containing all reagents expect rhu-tTG, was  $0.132 \pm 0.017$ .

There is a linear relationship between absorbance and concentration of rhu-tTG up to  $0.5 \mu\text{g/ml}$  (Fig. 2). The limit of detection (LOD), defined as mean plus three times, the SD of the background optical density was  $1.77 \text{ ng/ml}$ .

### Specificity

Having good immuno-reactivity of 3F3 antibody to rhu-tTG, we sought to define the specificity of this antibody using the available recombinant TG isoforms (TG1, TG3, TG6, TG7, and FXIIIa). Serial dilutions of each TG were prepared and used as described in "Materials and methods".

The antigen specificity of the assay was determined using purified human recombinant tTG, TG1, TG3, TG6, TG7, and FXIIIa. No cross reactivity was observed up to  $1 \mu\text{g/ml}$  (Fig. 3), indicating the specificity of the two antibodies (3F3 and Cov2005) for tTG. The use of high-specific antibodies to tTG is crucial as in cell lysates or tissue

homogenates other isoenzymes of TG family are expressed (e.g., erythrocytes, neuronal cells or tissues, and lung tissues), particularly during the investigation of the role of tTG in the pathogenesis of neurodegeneration or fibrosis, in which other isoenzymes can be involved as well. These results were confirmed by WB (results not shown).

### Reproducibility

To determine the reproducibility of sandwich ELISA, intra- and inter-assay coefficients of variation (%CV) were calculated in the range from 1 to 2 and 7 to 10 % (Table 1) depending on tTG concentrations in the dilutions of HEK293AD-tTG cell lysates.

The recovery of tTG in crude samples was estimated by spiking HEK293AD-tTG and human red blood cell lysates with  $0.05$  or  $0.1 \mu\text{g/ml}$  of rhu-tTG. The mean recoveries were between 80 and 97 % (Table 2).

### Stability

For the stability, study plates were stored for 3 and 12 month at  $4^\circ\text{C}$  to analyze the variation of the sandwich ELISA system and all the reagents. No significant loss in signal intensity was detected, and the storage of 3F3 Mab-coated plates over prolonged periods does not affect the quality of tTG detection (data not shown).

### Measurement of tTG levels in samples

The immunoassay assay was evaluated on tissues and cell homogenates (guinea pig liver homogenate, SHEP and HEK293AD-tTG cell lysates, and human red blood cell lysates) for the determination of tTG level. The results were confirmed by Western blot using both the capture and detection antibodies (Fig. 4). The tTG protein level visualized by immunoblotting related well correlated with the enzyme concentration obtained by the immunoassay (Fig. 4b, c). Recombinant tTG was detected at the same position than the sample bands, confirming that full length was detected. The detectable concentration of tTG in human red blood cell lysate was low (Fig. 4a), but the

**Table 2** Recovery of recombinant human tTG

	tTG in sample ( $\mu\text{g/ml}$ )	rhu-tTG in spiked sample ( $\mu\text{g/ml}$ )	Total tTG ( $\mu\text{g/ml}$ )	Spiking recovery (%)
HEK293AD-tTG (10 $\mu\text{g}$ )	0.084	0.052	0.124	83
	0.084	0.124	0.201	93
HEK293AD-tTG (30 $\mu\text{g}$ )	0.376	0.045	0.427	97
	0.376	0.085	0.454	94
Human RBC lysate (1000 $\mu\text{g}$ )	0.05	0.06	0.079	80
	0.05	0.1	0.122	95

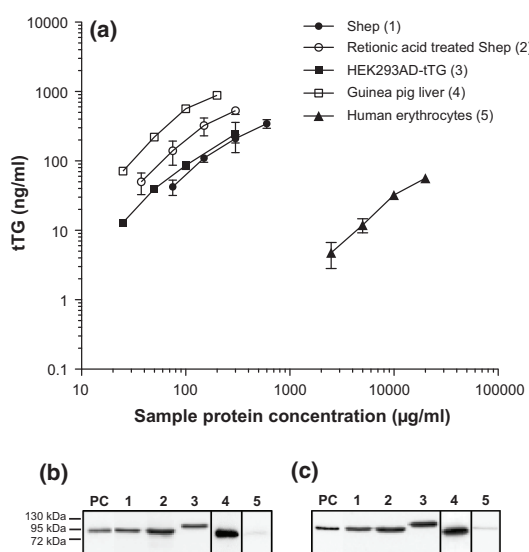


**Fig. 4** Detection of tTG in cultured mammalian cells, isolated human erythrocytes lysates, and guinea pig liver homogenates. **a** Sandwich ELISA assay. Values are mean  $\pm$  standard deviation of three experiments performed as duplicates. **b** Western blot with mouse monoclonal 3F3 antibody. **c** Western blot with rabbit polyclonal Cov2005 antibody. 20  $\mu$ g (lane 1–4) and 200  $\mu$ g (lane 5) of protein per slot were applied. PC rhu-tTG positive control

obtained curve was linear up to 2 mg/ml dilution, indicating that there was no interference with matrix components. In guinea pig liver homogenate, the highest level of tTG was obtained. The stable-transfected HEK293AD-tTG cell line expresses around 710 ng tTG per mg of protein, which is in similar range than what it was determined in SHEP cells. Whereas, upon retinoic acid treatment, we observed approximately three times increase in the enzyme level in SHEP cell lysates.

## Discussion

To investigate the role of tTG in health and disease, an accurate, reliable and quantitative test measuring the enzyme level is needed. This is of importance to address expression and functional questions with regard to members of the TG family. Despite some effort to develop such assay (Brevé et al. 2008; Wolf et al. 2011), no test was reported to be used as a gold standard. In this respect, new assay was developed and evaluated for measuring tTG level in different samples thanks to the new antibodies (monoclonals and polyclonal).

To develop the sandwich ELISA, the monoclonal and polyclonal antibodies were tested by check board titration

to reach the best signal-to-noise ratio and specificity for tTG. The combination of mouse monoclonal 3F3 as a capture antibody and rabbit polyclonal Cov2005 as detecting antibody was proved to be the best. Our assay is highly specific for tTG isoform without any cross-reactivity with TG1, TG3, TG6, TG7, and FXIIIa. This result is important for the investigation of the specific role of tTG. Indeed, it is well established that several TG isoforms are expressed in the same tissue, such as liver, brain, and skin, in which tTG, TG1, TG3, TG5, and TG6 are found, and in blood, tTG and FXIII are well present.

The assay was validated by measuring the intra- and inter-assay variations. The coefficients of intra- and inter-assay variations spanned from 1 to 2 % and from 7 to 10 %, respectively, which were proved to be within the appropriate range (Taverniers et al. 2004). The analytical sensitivity of our assay was up to 1.77 ng/ml. This value of LOD is not so low as that described by Brevé et al. (2008). However, the optimized conditions are the result of a tradeoff between incubation time of different steps and assay sensitivity. Therefore, using the ready to use assay, the ELISA protocol can be performed in a reasonable time (4 h) and the sensitivity should be enough to measure tTG in biological samples. However, to increase the sensitivity of our sandwich ELISA, the development of a second generation of this assay using fluorescence or chemiluminescence is planned in the future.

In this study, we demonstrated that using our sandwich ELISA assay, tTG could be measured in cell lysates, tissue homogenates, and red blood cell lysates. We chose cell lines which naturally express tTG (Human neuroblastoma SHEP) and a transfected one (HEK293AD-tTG) to measure the change of the enzyme level during the experimental treatments. Moreover, these cell lines express high amount of tTG. In the case of the neuroblastoma cell line, the high expression level can be correlated with the pathological processes (Liu et al. 2007). In addition, retinoids are well-known regulators of tTG (Nagy et al. 1996), which modulate the transcription level of the enzyme through binding to the retinoic acid receptors. Indeed, we observed a significant increase in tTG protein level in neuroblastoma cells after retinoic acid treatment. Guinea pig liver is known to express quite high level of tTG (Folk and Cole 1966), and thus, it is widely used and accepted as a standard reference of the endogenous tTG. Moreover, guinea pig models can be used for the investigation of diseases correlated with tTG, such as cartilage hypertrophy in the spontaneous guinea pig model of osteoarthritis (Huebner et al. 2009). Using our test, we quantified the highest level of tTG in guinea pig liver homogenate confirming the existing data. In addition to liver, tTG is well expressed in red blood cells (Bergamini et al. 1999); however, our test was not as sensitive (as described by others), as we found the lowest

tTG content in human erythrocytes lysates. This can be explained by the loss of the enzyme protein during the sample preparation as confirmed by WB (Fig. 4) when using the monoclonal 3F3 (a) and the polyclonal Cov2005 (b). These results were confirmed several times with different blood samples using a mixture of protease inhibitors. The other limitations of our Mab 3F3 was the lack of the cross reactivity with the mouse and rat tTG. Indeed, recognizing the importance of rodent models, the development of a specific immunoassay to measure mouse and rat tTG will be proposed.

In conclusion, our validated sandwich ELISA assay presents a reliable, sensitive, and highly specific tool for the detection and quantification of human and guinea pig tTG in several sources of samples, such as cell lysates, tissue homogenates, and erythrocytes lysates to investigate the contribution of tTG in the physiological and pathological processes.

**Acknowledgments** We would like to thank Prof László Fésüs (Department of Biochemistry and Molecular Biology, Hungary) and Sandrine Wittmann (Centre Léon Bérard, France) for cell samples. E.S. was supported by a Marie Curie research grant ("TRANS-PATH", FP7 No 289964).

#### Compliance with ethics requirements

**Conflict of interest** Éva Sivadó declares that she has no conflict of interest, Sabrina Lareure declares that she has no conflict of interest, and Valérie Attuïl-Audenis declares that she has no conflict of interest. Saïd El Alaoui declares that he has no conflict of interest, and Vincent Thomas declares that he has no conflict of interest.

**Study with human subjects** All procedures followed were in accordance with the ethical standards of the responsible committee on human experimentation (institutional and national) and with the Helsinki Declaration of 1975, as revised in 2008 (5). Informed consent was obtained from all patients for being included in the study.

**Study with animals** All institutional and national guidelines for the care and use of laboratory animals were followed.

## References

- Bergamini CM, Dean M, Matteucci G, Hanau S, Tanfani F, Ferrari C, Boggian M, Scatturin A (1999) Conformational stability of human erythrocyte transglutaminase. Patterns of thermal unfolding at acid and alkaline pH. *Eur J Biochem* 266:575–582
- Brevé JJ, Drukarch B, van Strien M, van Dam AM (2008) Validated sandwich ELISA for the quantification of tissue transglutaminase in tissue homogenates and cell lysates of multiple species. *J Immunol Methods* 332:142–150
- El Alaoui S, Legastelois S, Roch AM, Chantepie J, Quash G (1991) Transglutaminase activity and N epsilon (gamma glutamyl) lysine isopeptide levels during cell growth: an enzymic and immunological study. *Int J Cancer* 48:221–226
- Fesus L, Piacentini M (2002) Transglutaminase 2: an enigmatic enzyme with diverse functions. *Trends Biochem Sci* 27:534–539
- Folk JE, Cole PW (1966) Mechanism of action of guinea pig liver transglutaminase. I. Purification and properties of the enzyme: identification of a functional cysteine essential for activity. *J Biol Chem* 241:5518–5525
- Folk JE, Finlayson JS (1977) The epsilon-(gamma-glutamyl)lysine crosslink and the catalytic role of transglutaminases. *Adv Protein Chem* 31:1–133
- Griffin M, Casadio R, Bergamini CM (2002) Transglutaminases: nature's biological glues. *Biochem J* 368:377–396
- Gundemir S, Colak G, Tucholski J, Johnson GV (2011) Transglutaminase 2: a molecular Swiss army knife. *Biochim Biophys Acta* 1823:406–419
- Hasegawa G, Suwa M, Ichikawa Y, Ohtsuka T, Kumagai S, Kikuchi M, Sato Y, Saito Y (2003) A novel function of tissue-type transglutaminase: protein disulphide isomerase. *Biochem J* 373:793–803
- Huebner JL, Johnson KA, Kraus VB, Terkeltaub RA (2009) Transglutaminase 2 is a marker of chondrocyte hypertrophy and osteoarthritis severity in the Hartley guinea pig model of knee OA. *Osteoarthr Cartilage* 17:1056–1064
- Jang GY, Jeon JH, Cho SY, Shin DM, Kim CW, Jeong EM, Bae HC, Kim TW, Lee SH, Choi Y, Lee DS, Park SC, Kim IG (2010) Transglutaminase 2 suppresses apoptosis by modulating caspase 3 and NF-kappaB activity in hypoxic tumor cells. *Oncogene* 29:356–367
- Kanchan K, Ergülen E, Király R, Simon-Vecsei Z, Fuxreiter M, Fésüs L (2013) Identification of a specific one amino acid change in recombinant human transglutaminase 2 that regulates its activity and calcium sensitivity. *Biochem J* 455:261–272
- Lai TS, Slaughter TF, Peoples KA, Hettasch JM, Greenberg C (1998) Regulation of human tissue transglutaminase function by magnesium-nucleotide complexes. Identification of distinct binding sites for Mg-GTP and Mg-ATP. *J Biol Chem* 273:1776–1781
- Liu T, Tee AE, Porro A, Smith SA, Dwarto T, Liu PY, Iraci N, Sekyere E, Haber M, Norris MD, Diolaiti D, Della Valle G, Perini G, Marshall GM (2007) Activation of tissue transglutaminase transcription by histone deacetylase inhibition as a therapeutic approach for Myc oncogenesis. *Proc Natl Acad Sci* 104:18682–18687
- Lorand L, Graham RM (2003) Transglutaminases: crosslinking enzymes with pleiotropic functions. *Nat Rev Mol Cell Biol* 4:140–156
- Mirza A, Liu SL, Frizell E, Zhu J, Maddukuri S, Martinez J, Davies P, Schwarting R, Norton P, Zern MA (1997) A role for tissue transglutaminase in hepatic injury and fibrogenesis, and its regulation by NF-kappaB. *Am J Physiol* 272:G281–G288
- Mishra S, Murphy LJ (2004) Tissue transglutaminase has intrinsic kinase activity: identification of transglutaminase 2 as an insulin-like growth factor-binding protein-3 kinase. *J Biol Chem* 279:23863–23868
- Nagy L, Saydak M, Shipley N, Lu S, Basilion JP, Yan ZH, Syka P, Chandraratna RA, Stein JP, Heyman RA, Davies PJ (1996) Identification and characterization of a versatile retinoid response element (retinoic acid receptor response element-retinoid X receptor response element) in the mouse tissue transglutaminase gene promoter. *J Biol Chem* 271:4355–4365
- Perez Alea M, Kitamura M, Martin G, Thomas V, Hitomi K, El Alaoui S (2009) Development of an isoenzyme-specific colorimetric assay for tissue transglutaminase 2 cross-linking activity. *Anal Biochem* 389:150–156
- Ritter SJ, Davies PJ (1998) Identification of a transforming growth factor-beta1/bone morphogenetic protein 4 (TGF-beta1/BMP4) response element within the mouse tissue transglutaminase gene promoter. *J Biol Chem* 273:12798–12806

- Siegel M, Strnad P, Watts RE, Choi K, Jabri B, Omary MB, Khosla C (2008) Extracellular transglutaminase 2 is catalytically inactive, but is transiently activated upon tissue injury. *PLoS One* 3:e1861
- Taverniers I, De Loose M, Van Bockstaele E (2004) Trends in quality in the analytical laboratory. II. Analytical method validation and quality assurance. *Trends Anal Chem* 23:535–552
- Thomas V, El Alaoui S, Massignon D, Clement S, Simonet F, Quash G (2006) Development and evaluation of a modified colorimetric solid-phase microassay for measuring the activity of cellular and plasma (Factor XIII) transglutaminases. *Biotechnol Appl Biochem* 43:171–179
- Wolf J, Lachmann I, Wagner U, Osman AA, Mothes T (2011) Quantification of human tissue transglutaminase by a luminescence sandwich enzyme-linked immunosorbent assay. *Anal Biochem* 419:153–160
- Zemskov EA, Janiak A, Hang J, Waghary A, Belkin AM (2006) The role of tissue transglutaminase in cell-matrix interactions. *Front Biosci* 11:1057–1076

# Oncolytic properties of Rotavirus Vaccines overcome Resistance to Immune Checkpoint Blockade Therapy

Tala Shekarian<sup>1,2,3</sup>, Stéphane Depil<sup>1,2,3</sup>, Eva Sivado<sup>2,3</sup>, Anne-Catherine Jallas<sup>1,2</sup>, Nadège Goutagny<sup>1,2,3</sup>, Christophe Bergeron<sup>2,6</sup>

Sandrine Valsesia-Wittmann<sup>\*2,3</sup>, Christophe Caux<sup>\*1,2</sup>, Aurélien Marabelle<sup>\*2,4,5,6</sup>

<sup>1</sup> Centre de Recherche en Cancérologie de Lyon (CRCL), UMR INSERM U1052 CNRS 5286  
Université de Lyon, F- 69008 Lyon, France

<sup>2</sup> Centre de Lutte contre le Cancer Léon Bérard, F-69008 Lyon, France

<sup>3</sup> Université Claude Bernard Lyon 1

<sup>4</sup> INSERM U1015, F-94805 Villejuif, France

<sup>5</sup> Gustave Roussy, Université Paris-Saclay, DITEP, Villejuif, F-94805, France

<sup>6</sup> Institut d'Hématologie et d'Oncologie Pédiatrique, Centre Léon Bérard, F-69008 Lyon,  
France

\* co-last

Corresponding author: Aurélien Marabelle. Gustave Roussy, 114 rue Edouard-Vaillant, Villejuif, F  
94805, France

**One sentence summary:** We have discovered that rotavirus commercial vaccines have oncolytic properties and that they can overcome resistance to and synergize with immune checkpoint antibodies upon intratumoral injections.

**In revision in Science Translational Medicine, Manuscript ID: aat5025**

## **Abstract:**

Immune checkpoint targeted therapies against PD-1, PD-L1 and CTLA-4 are currently revolutionizing cancer care. However, only a minority of patients develop objective responses to these treatments. Therefore, new therapeutic interventions are needed to increase the immunogenicity of tumors in order to overcome the resistance to these novel immunotherapies. Oncolytic properties of common viruses can be exploited for the priming of anti-tumor immunity and such oncolytic viruses (OVs) are currently in active clinical development in combination with immune checkpoint targeted therapies. However the routine implementation of these therapies is limited by their manufacturing constraints, the risk of exposure of clinical staff and the ongoing regulations on GMOs. We sought to determine if anti-infectious vaccines could be used as a commercially available source of immunostimulatory agents for cancer immunotherapy. We have found that Rotavirus vaccines have both immunostimulatory and oncolytic properties. These pediatric vaccine virus have pro-inflammatory properties and can activate the NF- $\kappa$ B pathway in a toll-like receptor and IRF3 independent manner. Moreover they can directly kill cancer cells with features of immunogenic cell death. In vivo, intra-tumoral rotavirus therapy has anti-tumor effects which are mainly immune mediated. Interestingly, in several immunocompetent murine tumor models, intra-tumoral rotavirus overcome resistance to and synergize with immune checkpoint targeted therapy. Rotavirus vaccines are pediatric and adult clinical grade products. Therefore, in situ immunization strategies with intra-tumoral attenuated rotavirus could be implemented quickly in the clinic.

## **Introduction:**

Immune checkpoint targeted therapies (ICT) against PD-1, PDL-1 and CTLA-4 have demonstrated their clinical activity in multiple cancers, including melanoma, lung, head and neck, bladder, renal cell carcinoma, Merkel-cell carcinoma, mismatch repair deficient tumors, hepatocarcinoma, gastric cancers and Hodgkin's lymphoma(1). However, only a minority of patients actually develop objective tumor responses with

these new treatments. Several factors have been identified to correlate with the effectiveness of ICT, notably the high proportion of tumor infiltrating T-cells (2), and the existence of neo-epitopes generated by a high level of somatic point mutations in the cancer cells genome (3, 4). Other elements have been shown to contribute to the resistance to ICT such as immunosuppressive myeloid cells (5, 6), mutations in JAK1/2 (7) and the absence of MHC-I expression by tumor cells (8). In this context, pediatric cancers which display low levels of T-cell infiltrates, high levels of myeloid cell infiltrates, and usually low mutational load, are poorly responsive to these immunotherapies (9–14). Intra-tumoral injections of oncolytic viruses (OVs), toll-like receptor agonists, or STING agonists are in situ immunotherapy strategies currently in active clinical development with the aim of stimulating pattern recognition receptors (PRRs) for the priming of the anti-tumor immunity by turning non-infiltrated “cold” tumors into immune-infiltrated “hot” tumors (15). Intra-tumoral stimulation of PRRs has shown promising results in cancer patients by inducing effective anti-tumor immune responses, in both injected and non-injected sites (so called “abscopal effect”) (16–18). Also, intra-tumoral PRR agonists and OVs can overcome ICT resistance in syngeneic tumor models (19–22) and patients with melanoma (23, 24).

Since the pediatric clinical development of PRR agonists will only start many years after their adult development, we sought to use anti-infectious vaccines as a potential source of clinical grade PRR agonists to prime the anti-tumor immunity of pediatric cancers.

Upon screening of most commercially available anti-infectious vaccines, we have identified that rotavirus containing vaccines (Rotarix® and Rotateq®) have the ability *in vitro* to simultaneously activate NF-κB in a TLR-independent manner and induce immunogenic cell death of multiple cancer cell lines. *In vivo*, intratumoral injections of rotavirus vaccines, results in type I interferon-response and immune cell activation, which can culminate in regression of large, established pediatric ICT resistant tumors in mice. Of utmost importance, oncolytic Rotavirus vaccines synergize with anti-CTLA4 antibodies resulting in complete regressions and abscopal responses curing the vast majority of tumor-bearing mice and protecting them upon re-challenge.

## Results:

### ***Pro-inflammatory features of Rotavirus vaccines***

Because anti-infectious vaccines contain pathogens or pathogens extracts, we assessed whether they could be used as a clinical grade source of PRR agonists. To evaluate the intrinsic ability of anti-infectious vaccines to stimulate Toll-like receptors (TLRs), a major family of PRRs, we used transgenic cell lines cotransfected individually with the different TLRs and a luciferase reporter plasmid under the control of a NF- $\kappa$ B binding site. We incubated 10 different serial dilutions of 14 viral and bacterial anti-infectious vaccines with these transgenic cell lines and measured 12 hours later the Luciferase bioluminescence intensity proportionally correlated to the NF- $\kappa$ B induction. In these assays, we found that among the 14 evaluated vaccines, the Typhoid Fever vaccine (Tyavax<sup>®</sup>) and Mycobacterium tuberculosis vaccine (BCG Pasteur<sup>®</sup>) were potent activators of TLR4 and TLR2, respectively (Fig.1a,b). More surprisingly, we found that, when used at median range concentrations, the two rotavirus vaccines (Rotarix<sup>®</sup> and Rotateq<sup>®</sup>) were activating NF- $\kappa$ B in all the transgenic cell lines, including the parental cell line devoid of TLR transgene. This suggest that these rotavirus vaccines were able to activate the NF- $\kappa$ B pathway independently of any TLR (Fig. 1c,d,e) and Supplementary Figure 1).

### ***Rotavirus vaccines have antitumor activity against pediatric tumor models resistant to anti-CTLA-4 and anti-PD-1 (L1)***

The vaccines leading to NF- $\kappa$ B activation were then evaluated for their therapeutic activity in syngeneic models of Neuroblastoma (Neuro2a) that are resistant to anti-CTLA-4, anti-PD-1, anti-PD-L1 or their combinations (Figure. 2a). Although the Tyavax<sup>®</sup> and BCG<sup>®</sup> vaccines can activate TLR4 and TLR2, we could not evidence any significant therapeutic activity in these syngeneic pediatric tumor models upon intratumoral injections compared to PBS injection (Fig. 2b). In contrast, when injected intratumorally, the Rotavirus vaccines (Rotarix<sup>®</sup> or Rotateq<sup>®</sup>) had a significant anti-tumor activity

observed in 50 % of the Neuro2a Neuroblastoma tumor bearing mice (Fig.2b). We observed in previous experiments that the NF- $\kappa$ B activation of Rotavirus vaccines in vitro was dose dependent and decreased upon dilutions of the vaccine (Fig.1c, d). However, at high concentrations of Rotavirus vaccine, we noticed a loss of NF- $\kappa$ B activation due to low cell viability. We hypothesized that the vaccine might have direct cytotoxic effects at high concentration. Using the sulforhodamine B (SRB) cell viability assay, we found that Rotavirus vaccines (Rotarix shown, Rotateq not shown) were able to kill 293T cells at vaccines dilutions of 1/2, 1/4 and 1/10 (Fig.S2). In order to confirm the intrinsic cytotoxic properties of Rotavirus and eliminate the potential osmotic effects of the vaccines' excipients, we tested the cytotoxic effects of the original rotavirus strain obtained from the manufacturer of the Rotateq<sup>®</sup> vaccine (Merck Sharp & Dohme corp, USA). These five viral Rotavirus strains contain higher virus titers (100x to 1000x higher than in the Rotateq<sup>®</sup> commercial vaccine) and are free of excipient. Excipient of Rotateq<sup>®</sup> vaccine is mostly composed of concentrated carbohydrates and has partial osmotic cytotoxic effects at high concentrations (1/20) with no effect at lower dose (see FigS3). Most importantly, increasing concentrations of the rotavirus viral strains showed dose dependent intrinsic cytotoxicity of Rotavirus against human Neuroblastoma (SH-SY5Y) (IC<sub>50</sub>=1/200000) with higher efficacy compare to vaccines confirming a direct role of the virus on cell cytoxicity (Fig2c). As the Rotateq<sup>®</sup> is composed of five different Rotavirus vaccine strains (G1, G2, G3, G4 and P1), we analyzed the cytotoxic properties of each individual strain on the human NB cancer cell line SH-SY5Y. We found that all five strains have important cytotoxic properties (Fig.S4) IC<sub>50</sub>= from 1/200,000- 1/2000). To generalize the cytotoxic properties of Rotavirus against other tumor cell lines, we repeated SRB cytotoxic assay using human breast carcinoma MDA-MB-231 and murine tumor models (Fig2d,e). We found that the Rotavirus strain has dose dependent cytotoxic effect on all cancer cell lines tested although at lower efficacy (IC<sub>50</sub>=1/2000) for Neuro2a and A20 murine cell lines (Fig.2d). These results confirmed a potent higher cytotoxic properties against human cancer cell lines IC<sub>50</sub>=1/200000). With the aim to evaluate the oncolytic specificity of rotavirus strain, we further used HMEC primary mammary epithelial cells and different primary fibroblasts for SRB cytotoxic assay using same rotavirus strain dilutions and timing (Fig.2e). We observed lower cytotoxic abilities on untransformed cells (IC<sub>50</sub>=1/200 for fibroblasts, 1/20 HMEC). All together, these

results suggest the ability of rotavirus strains to preferentially kill cancer cells (IC50= 1/200000) over normal cells which is a common feature of oncolytic virus.

### ***In vitro oncolytic properties of Rotavirus strains translate into in vivo anti-tumor immunity***

We then studied the *in vivo* anti-tumor effects of different dilutions of Rotavirus strain on different tumor models (Fig3a). Following three consecutive intra-tumoral injections every 3 days in the syngeneic A20 Lymphoma model, we observed a potent antitumoral effect of Rotavirus reaching 70% of complete tumor regression whatever the dose, even the lowest dose (1/100 dilution) gave rise to faster regression. This potent anti-tumor effect lead to a benefice in overall survival as shown in Fig3a right panel. Working further at the 1/100 Rotavirus dilution, we observed anti-tumor activity in 30-40% of the mice in the Neuroblastoma NXS2 (Fig.3b) and Neuro2a (Fig.3c) syngenic tumor models with significant benefice in overall survival observed only in the Neuro2a tumor model (Fig3b). To discriminate between direct cytolytic anti-tumoral effect and immune mediated activity of the Rotavirus we repeated the experiments in NSG immunodeficient mice. The antitumor effect was almost abolished in NSG mice without any complete tumor rejection, thus demonstrating a major contribution of the immune system in the antitumor effect of the Rotavirus (Fig.3d).

### ***Immunostimulatory properties of intra-tumoral Rotavirus injections***

To further demonstrate the role of the immune system in the *in vivo* anti-tumor activity of rotavirus, we analyzed by flow cytometry the tumor-infiltrating cells in the Neuro2a (Neuroblastoma) tumor model. Briefly, 24 hours after the first intratumoral rotavirus injection, we quantified CD11+ myeloid cell, CD4+ and CD8+ T cell proportion in tumor infiltrates reported as % of total CD45+ cells in tumors. As shown in figure 4a, we observed that injection of rotavirus led to a remarkable increase in tumor infiltrating myeloid cells from 30% to 70% of tumor immune infiltrate with no major variation in CD4 and CD8 T cell proportion. Most importantly, a significant proportion of these CD11b+ myeloid cells switched to an activated phenotype, expressing high levels of the costimulatory molecule CD86 compared to PBS treated tumors, suggesting a strong

inflammatory response to virus injection. Although the frequency of CD8+ T cell infiltrate remained stable, an highly significant proportion of these CD8+ T-cells had upregulated activation markers such as OX40 (50%) and CD137 (30%) on their surface suggesting a CD8 switch to anti-tumoral phenotype (Fig. 4a). Interestingly the inhibitory immune checkpoint CTLA-4 was also strongly up-regulated at the cell surface of both CD8+ and Foxp3+ CD4+ Regulatory T cells probably due to a negative feedback regulation (Fig.4a). To further analyse the local immune response we evaluated the activation of the IFN-I pathway by analyzing the expression of the interferon-inducible MxA protein by immunofluorescence into the tumors of treated mice compared to PBS control mice in A20 lymphoma model (Fig.4b). High proportion of MxA positive cells was observed for all tumors tested compare to control, confirming type-I IFN production induce by the virus. Then, we studied the immunogenic properties of the in vitro cellular death induced by Rotavirus. We found hallmarks of immunogenic cell death both in human and murine cell lines with an extra-cellular release of ATP (Fig.4c) and calreticulin upregulation (not shown).

### ***Intratumoral Rotavirus overcomes and synergizes with anti-CTLA-4 to generate a CD8+ T-cell anti-tumor immune response***

The upregulation of CTLA4 and CD86 respectively on T cells and myeloid cells (Fig. 4a), provided the rationale for combination experiments between intratumoral Rotavirus and systemic anti-CTLA-4 antibodies. Interestingly, although the Neuro2a Neuroblastoma model was resistant to anti-CTLA-4 and transiently responsive to rotavirus single therapies (Fig.5a), we found that the combination of intratumoral Rotavirus + systemic anti CTLA-4 was highly synergistic with a 100% complete response rate with no relapse (Fig.5a). Similarly, 100% complete tumor regression was also observed in the A20 lymphoma model (Fig.5b) with the combination while only (50-70%) of tumor rejection was observed with Rotavirus or (10-20%) with anti-CTLA4 single agent. We also looked at the effect of the commercial Rotavirus vaccine combination with CTLA-4 antibodies in these two tumor mice models. We still observed a synergistic effect of Rotavirus vaccine with anti-CTLA-4 in Neuroblastoma (60% of complete regression) (Fig.5c) and in the lymphoma model (70% of complete regression) (Fig.5d).

To assess the contribution of T-cells in this therapeutic synergy we depleted CD4+ and CD8+ T cells in Balb/c mice transplanted with the A20 murine lymphoma. We observed that in the CD8+ depleted mice the anti-tumoral effect of the combination therapy was drastically abolished. In contrast, the depletion of the CD4+ T cells had virtually no impact on the therapeutic response. This demonstrated the major role played by the CD8+ T-cells in response to the treatment (Fig.5e). We also observed that all of the cured mice were protected upon rechallenge with the same tumor cells, demonstrating induction of an adaptive immune memory response in cured mice (Fig.5f). Balb/c mice cured from A20 lymphoma were re-challenged with both A20 lymphoma cells and irrelevant 4T1 breast cancer carcinoma cells in two separated flanks. The 4T1 breast carcinoma tumors developed in these cured mice whereas A20 lymphoma tumor did not, illustrating the specificity of the anti-tumor immune response generated by the combination therapy (fig5g). Then, to measure the T cell anti-tumor response induced by the anti CTLA-4 + Rotavirus combination, splenocytes from A20 lymphoma (Fig.5h) and Neuro2a Neuroblastoma cured mice (Fig.5i) were exposed in vitro respectively to the A20 or Neuro2a cell lines. After 4 days, CD8+ T cells were stained for intracellular IFN- $\gamma$ , and surface CD137 and OX40 activation markers and analysed by FACS. We observed that splenocytes from mice cured from either tumor model produced 2 to 3 times (5% to 10-15%) more levels of intracellular IFN $\gamma$  compared to control and expressed up-regulated surface activation marker such as CD137 and OX40 compared to control mice (Fig.5h,i).

### ***Intratumoral Rotavirus generates abscopal and durable tumor-specific immunity***

To assess whether the Rotavirus + anti-CTLA-4 combination therapy could also induce an antitumor effect on distant non-injected tumors (abscopal effect), we set up two tumors mice model by injecting tumor cells on both flanks. Rotavirus was injected in one of the two tumor sites and anti-CTLA-4 antibody was injected systemically (i.p). Despite the aggressive features of the two tumor models, the combination could cure 100% of the mice with complete regression of both injected and non-injected tumors both in A20 lymphoma model (Fig.6a) and in Neuro2a Neuroblastoma model (Fig.6b). These results

suggest a systemic antitumor immunity response leading to a complete regression of the injected and non-injected tumor lesion leading to a complete survival rate for both tumor models. We studied the effects of this combination therapy on the immune infiltrating cells at the injected and distant tumors.

Although Neuro2a Neuroblastoma tumors contained more myeloid cells, we observed similar impact on both tumor models (Fig6c-d) of Rotavirus (1/100) injection (analysed 24 hours after the second intratumoral injection): i) myeloid cells were activated (as shown by CD86 upregulation) in both the injected and distant tumors with and without anti-CTLA-4, ii) CD8 T cells were increased in number both in injected and distant tumor in particular in the Neuro2a models after Rotavirus + CTLA4 combination therapy and iii) high CD8 T cell activation was observed with OX40 upregulation in both models, both the injected and distant tumors.

### **Discussion:**

Immune checkpoint targeted antibodies are currently revolutionizing cancer patient treatment. However, a majority of patients remain resistant to these immunotherapies. This study was designed to evaluate clinical grade strategies to overcome such resistance. We previously showed that the intra-tumoral injection of PRRs agonist can induce an anti-tumor immune stimulation that can synergize with ICT mAbs (22). Commercially available anti-infectious vaccines represent a potential alternative source of PRRs agonists, notably in the context of pediatric cancers that are currently shown to be resistant to ICT mAbs (25) (26). While evaluating the TLR stimulating capacity of different viral and bacterial based vaccine, we identified that Rotavirus vaccines have the capacity to stimulate NF- $\kappa$ B independently of TLRs and IRFs. The mechanism by which Rotavirus activate NF- $\kappa$ B remains unclear. It may be directed by one of the viral structural or non-structural protein. Indeed, it has been shown that viral proteins interact with host proteins implicated in the type I IFN response (27). This activation might be indirect via vaccine-induced cytotoxicity on tumor cells resulting in the release of DAMPs or the production of cytokines and the activation of different pathways that lead to NF- $\kappa$ B activation. Even if the cell death induced by Rotavirus is not yet fully

characterized it harbors features of immunogenic cell death through the release of ATP and CRT cell surface translocation (not shown). We show that the Rotavirus has tumor cells specific cytotoxicity since it induces cell lysis of all evaluated tumor lines at low dose (1/200 000-1/2000) but affects normal fibroblasts and primary HMEC viability only at much higher dose (1/20-1/200). As shown by MXa detection the in vivo injection of Rotavirus leads to intra-tumor type I IFN induction that may contribute to the immune response induced by the Rotavirus. The source of type I IFN leading to Mxa protein expression may originate from cancer cells or tumor infiltrating immune cells. In this context, we also observed an activation of tumor infiltrating myeloid cells and CD8 T lymphocytes, which demonstrates the immune stimulating properties of the virus.

This activation of the immune response by the virus leads to a potent therapeutic activity when combined with i.p. anti-CTLA4 in ICT resistant pediatric tumor models. As expected the therapeutic activity of the combination of Rotavirus and anti-CTLA-4 was mainly CD8 T cell-dependent and CD8 specific anti-tumor immunity was demonstrated. The use of mice bearing tumors on two different sites allowed to demonstrate a clear abscopal effect of the combination of i.t. Rotavirus with i.p. anti-CTLA-4 with complete regression of both the injected and non-injected tumors in 100% of mice. In addition, we observed an immune cell activation in both tumor sites. Our work is in concordance with the work of Prof Jim Allison's lab reporting that intratumoral injections of New castle disease murine oncolytic virus could overcome a systemic resistance to anti-CTLA-4 therapy in a mouse melanoma model (20) and also with the recent work of Prof Antony Ribas et al which has shown that the talimogene laherparepvec (T-VEC) virotherapy might improve anti PD-1 immunotherapy in patients with metastatic melanoma(28). Through the induction of tumor immunogenic cell death and the production of type I IFN, i.t Rotavirus injection is leading to an activation of the myeloid antigen presenting cells likely resulting to CD8 T cell priming. CTLA4 and it ligands (CD80, CD86) are upregulated upon rotavirus injections on T cells and myeloid cells respectively, supporting the potent synergy seen between Rotavirus and anti-CTLA4. In addition, anti-CTLA4 may also alter the Treg suppressive function induced after virus infection. As we observed a very high induction of CTLA-4 on Tregs after Rotavirus injection (Fig.4a)

Intratumoral injections of rotavirus should prevent the side effects of systemic exposure. Furthermore, like for T-VEC, intratumoral injections of a high viral load should prevent virus neutralization in Rotavirus immunized patients.

Altogether, our results provide the pre-clinical rationale in favor of intratumoral rotavirus to overcome anti-CTLA-4 cancer immunotherapy resistance, notably in pediatric cancers. Such clinical translation should be feasible with the use of Rotavirus vaccines which represent a clinical grade, pediatric approved, non-genetically modified, source of oncolytic virus.

### **Material and methods:**

#### **Reagents:**

Commercially available Rotavirus vaccines Rotarix®(GSK) and Rotateq®(Merck) have been both tested in the experiments and will be referred as Rotavirus vaccine throughout the manuscript. Because multiple of infections (MOI) cannot be established for these commercial vaccines, dilutions in culture media of pure vaccines/virus have been used for *in vitro* experiments. Pure vaccines and also rotavirus vaccinal strain stock and pure excipient were provided by Merck (Merck Sharp & Dohme corp, USA).

### **Cell culture:**

SH-SY5Y cells (ATCC–CRL2266) were cultured in RPMI 1740 medium (Gibco-life technologies) supplemented with 10% of heat inactivated fetal bovine serum (FBS), 1% Glutamine, 1% antibiotic (penicillin and streptomycin) (Life technologies). Transgenic hTLR-LUC cell lines were seeded in DMEM (Gibco-life technologies) supplemented as described before. Each cell line was selected by its respective antibiotic (TLR2, 4 by Zeocin, Hygromycin, Blastidicin and TLR3, 5, 6, 7, 8, 9 by Zeocin, Blastidicin and LUC by Zeocin) (Invivogen). All cell lines were incubated at 37 °; 5% CO<sub>2</sub>. A20 cell lines were a kind gift from Prof Ronald Levy lab, Stanford University, California, USA and were cultured with RPMI supplemented as mentioned above. Neuro2a (ATCC®CCL-131™) and NXs2 (previously described by Lode JNCI 1997) were cultured in DMEM supplemented as mentioned above. Skin fibroblast cell lines from Caucasian individuals were obtained from the cell culture collections of the Centre de Biotechnologie Cellulaire, CBC-Biotec, CRB-Hospices Civils de Lyon, France. Primary mammary epithelial cells (HMEC) (ATCC-PCS-600-010) cell lines were cultured in Mammary epithelial cell basal Medium (ATCC-PCS-600-03) enriched with Mammary epithelial cell growth kit (ATCC-PCS-600-040). MDA-MB-231 (ATCC® HTB26™) cell lines were cultured in DMEM supplemented as mentioned above.

### **Bioluminescence assay:**

Human embryonic kidney cells 293 (HEK 293) were stably transfected with plasmid allowing the constitutive expression of TLRs of human origin (hTLR) (InvivoGen San Diego, CA, USA). To generate reporter model of TLR activation, HEK-293 stably expressing hTLRs or control HEK293 cells were then stably transfected with the NF-κB inducible reporter plasmid pNiFty-luc (Invivogen) using the Calcium phosphate method. Stable transfectants were selected in the presence of 100 µg/ml Zeocin (Invivogen). For stimulation assay, cells were seeded in DMEM supplemented on flat-bottom 96 well plates. The next day, medium was replaced by fresh medium and respective ligands. 18-20 hours later, cells were lysed in 30 µl of 5x lysis buffer (Promega). Firefly luciferase activity was quantified using 20 µl lysate by integrated measurement of flash

luminescence over 1 sec (Bethold Tristar LB941, Grenier) in 96 wells after injection of 20  $\mu$ l 1x "In-House" luciferase revelation buffer (20 mM Tris Ph7.8, 1.07 mM MgCl<sub>2</sub>, 2.7 mM MgSO<sub>4</sub>, 0.1 mM EDTA, 33.3 mM DTT, 470  $\mu$ M luciferine, 530  $\mu$ M ATP and 270  $\mu$ M CoEnzyme A) by TECAN spectra plate reader machine.

### **Cytotoxicity test (Sulforhodamine B assay):**

SRB assay (Sigma-Aldrich TOX6-1KT) was used to evaluate the cytotoxicity activity of different dilution of Rotavirus vaccine/strain on human tumoral cells. Triton 0.1% was used as the positive control. Briefly, cancer cells (10,000) were plated in a 96-well plate and then treated with serial dilution of Rotavirus vaccine/virus in medium for 3 to 5 days. The treated cells were fixed with 50  $\mu$ l of 10% cold trichloroacetic acid solution for 1 h at 4 °C, washed with distilled water five times, then dried at room temperature. The dried cells were stained with 50  $\mu$ l of 0.4% SRB for 10 min and rinsed with 1% acetic acid solution five times. Finally dye was dissolved in 10 mM Tris buffer and measured at 565 nm on a TECAN spectra plate reader machine.

### **Mice:**

6 to 8 weeks femelle A/J and Balb/C mice were provided from Harlan, the NSG mice from Charles Rivers. All the experiences have been done in Leon Berard Center animal laboratory with the approval number: C69 388 0202. All the experiments were validated through ethics comity with approval number: CECCAPP-CLB-2016-009.

### **Tumor transplantation :**

5x10<sup>6</sup> of Neuro2a, Nxs2, A20 and 1x10<sup>6</sup> of 4T1 tumor cell lines in 100  $\mu$ l of PBS, were transplanted subcutaneously to the mice. Tumor sizes were monitored with a digital caliper (Mitutoyo) every 2 to 3 days and expressed as surface (length  $\times$  width). Mice were killed when s.c. tumor size reached 2 cm<sup>2</sup>.

### **Tumor immunotherapy treatment:**

Treatment started when tumors reached 0.7–1 cm in largest diameter, usually around day 7 after tumor inoculation. Intratumoral injection of rotavirus vaccine/strain (100µl of the vaccine and 100µl of 1/100 virus dilution) 3 times every 3 days, combined with i.p injection of anti-CTLA-4 at the concentration of 200µg in 100 µl of PBS, 4 times every 3 days(10 mice /group in each experiments).

### **CD4 and CD8 T cell depletions:**

Anti-CD4 (rat IgG2b; Clone:GK1.5) and anti-CD8a (rat IgG2b; Clone:2.43) depleting mAbs were obtained from Bioxcell laboratory, 200µg of these antibodies were injected intraperitoneally 2 and 1 day before treatment and 5 and 8 days after beginning of the therapy.

### **Immune cell processing and transplant:**

Tumors, lymph nodes, and spleens were turned into single cell suspensions by processing them through a 70-µm cell strainer (BD Biosciences).

### **Flow cytometry:**

1 x 10<sup>6</sup> cells were surface stained in PBS with 1 µg antibodies, mouse Fc receptors were blocked with 1 µg FcγRIII/II-specific antibody (clone 2.4G2, rat IgG2b κ; BD Bioscience). CD45 (clone 30-f11), CD8 (clone 53-6.7), CD4 (GK1.5), Foxp3 (cloneFJK-16S), CTLA-4 (clone UC10-4B9), Ox40 (clone ox-86), CD137 (clone-17B5) and IFNγ (clone XMG1.2) intracellular staining was done using Foxp3 staining kit (00-5523-00) and intracellular Fixation and permeabilisation buffer (88-8824-00). Brefeldin A (00-4506-51) provided by eBioscience, CD3 (clone 17A2) and CD11B (clone M1/70) was provided by Biolegend. All the staining was acquired and analysed by flow cytometry on a FACS Canto II (BD Bioscience).

### **Immunofluorescence in situ:**

Immunofluorescence staining was done on frozen tumor samples, using mouse anti Mxa (2G12; NPB1-47859) provided by Novus and goat anti mouse antibody conjugated to FITC (00030748) provided from Dako. The incubation time for each staining step was maximum 1 hour. The mean of immunofluorescence intensity is measured using image J software.

### **Splenocyte stimulation with cancer cells:**

Splenocytes from cured and control mice were exposed to tumor cell line for 4 days *in vitro*. The ratio of splenocytes to tumor cell line was 1000:1 in RPMI/DMEM medium. After 4 days, cells were treated with Brefedin A for 5 hours in 37 °. Then the surface markers and intracellular IFN  $\gamma$  (intracellular Fixation and permeabilization buffer (88-8824-00) provided by eBioscience), were stained by the antibodies. (The reference were mentioned before in the flow cytometry part) and were analysed by flow cytometry.

### **ATP release study:**

ATP release was studied by CellTiter-Glo<sup>®</sup> Luminescent Cell Viability Assay kit provided by Promega.

### **Statistics:**

Prism software version 6.0 (GraphPad) was used to analyze tumor growth and to determine the statistical significance of differences between groups by applying 2-tailed Student t tests (paired or unpaired depending on the settings of the experiment). Comparisons of means between more than 2 groups were done by ANOVA. Kaplan-Meier plots were used to analyze survival. Comparisons of survival curves were made using the log-rank test. *P* values of less than 0.05 were considered significant.

1. S. L. Topalian, J. M. Taube, R. A. Anders, D. M. Pardoll, Mechanism-driven biomarkers to guide immune checkpoint blockade in cancer therapy, *Nat. Rev. Cancer* **16**, 275–287 (2016).
2. P. C. Tumeh, C. L. Harview, J. H. Yearley, I. P. Shintaku, E. J. M. Taylor, L. Robert, B. Chmielowski, M. Spasic, G. Henry, V. Ciobanu, A. N. West, M. Carmona, C. Kivork, E. Seja, G. Cherry, A. J. Gutierrez, T. R. Grogan, C. Mateus, G. Tomasic, J. A. Glaspy, R. O. Emerson, H. Robins, R. H. Pierce, D. a. Elashoff, C. Robert, A. Ribas, PD-1 blockade induces responses by inhibiting adaptive immune resistance, *Nature* **515**, 568–571 (2014).
3. A. Snyder, V. Makarov, T. Merghoub, J. Yuan, J. M. Zaretsky, A. Desrichard, L. A. Walsh, M. a. Postow, P. Wong, T. S. Ho, T. J. Hollmann, C. Bruggeman, K. Kannan, Y. Li, C. Elipenahli, C. Liu, C. T. Harbison, L. Wang, A. Ribas, J. D. Wolchok, T. a. Chan, Genetic basis for clinical response to CTLA-4 blockade in melanoma., *N. Engl. J. Med.* **371**, 2189–99 (2014).
4. N. A. Rizvi, M. D. Hellmann, A. Snyder, P. Kvistborg, V. Makarov, J. J. Havel, W. Lee, J. Yuan, P. Wong, T. S. Ho, M. L. Miller, N. Rekhtman, A. L. Moreira, F. Ibrahim, C. Bruggeman, B. Gasmi, R. Zappasodi, Y. Maeda, C. Sander, E. B. Garon, T. Merghoub, J. D. Wolchok, T. N. Schumacher, T. A. Chan, Mutational landscape determines sensitivity to PD-1 blockade in non-small cell lung cancer, *Science (80-. )*. **348** (2015).
5. E. Romano, M. Kusio-Kobialka, P. G. Foukas, P. Baumgaertner, C. Meyer, P. Ballabeni, O. Michielin, B. Weide, P. Romero, D. E. Speiser, Ipilimumab-dependent cell-mediated cytotoxicity of regulatory T cells ex vivo by nonclassical monocytes in melanoma patients., *Proc. Natl. Acad. Sci. U. S. A.* **112**, 6140–5 (2015).
6. C. Gebhardt, A. Sevko, H. Jiang, R. Lichtenberger, M. Reith, K. Tarnanidis, T. Holland-Letz, L. Umansky, P. Beckhove, A. Sucker, D. Schadendorf, J. Utikal, V. Umansky, Myeloid Cells and Related Chronic Inflammatory Factors as Novel Predictive Markers in Melanoma Treatment with Ipilimumab., *Clin. Cancer Res.* **21**, 5453–9 (2015).
7. D. S. Shin, J. M. Zaretsky, H. Escuin-Ordinas, A. Garcia-Diaz, S. Hu-Lieskovan, A. Kalbasi, C. S. Grasso, W. Hugo, S. Sandoval, D. Y. Torrejon, N. Palaskas, G. Abril Rodriguez, G. Parisi, A. Azhdam, B. Chmielowski, G. Cherry, E. Seja, B. Berent-Maoz, I. P. Shintaku, D. T. Le, D. M. Pardoll, L. A. Diaz, P. C. Tumeh, T. G. Graeber, R. S. Lo, B. Comin-Anduix, A. Ribas, Primary Resistance to PD-1 Blockade Mediated by JAK1/2 Mutations, *Cancer Discov.* (2016), doi:10.1158/2159-8290.CD-16-1223.
8. J. M. Zaretsky, A. Garcia-Diaz, D. S. Shin, H. Escuin-Ordinas, W. Hugo, S. Hu-Lieskovan, D. Y. Torrejon, G. Abril-Rodriguez, S. Sandoval, L. Barthly, J. Saco, B. Homet Moreno, R. Mezzadra, B. Chmielowski, K. Ruchalski, I. P. Shintaku, P. J. Sanchez, C. Puig-Saus, G. Cherry, E. Seja, X. Kong, J. Pang, B. Berent-Maoz, B. Comin-Anduix, T. G. Graeber, P. C. Tumeh, T. N. M. Schumacher, R. S. Lo, A. Ribas, Mutations Associated with Acquired Resistance to PD-1 Blockade in Melanoma., *N. Engl. J. Med.* **375**, 819–29 (2016).
9. J. Vakkila, R. Jaffe, M. Michelow, M. T. Lotze, Pediatric cancers are infiltrated predominantly by macrophages and contain a paucity of dendritic cells: a major nosologic difference with adult tumors., *Clin. Cancer Res.* **12**, 2049–54 (2006).
10. S. Asgharzadeh, J. A. Salo, L. Ji, A. Oberthuer, M. Fischer, F. Berthold, M. Hadjidaniel, C. W.-Y. Liu, L. S. Metelitsa, R. Pique-Regi, P. Wakamatsu, J. G. Villablanca, S. G. Kreissman, K. K. Matthay, H. Shimada, W. B. London, R. Sposto, R. C. Seeger, Clinical Significance of Tumor-Associated Inflammatory Cells in Metastatic Neuroblastoma., *J. Clin. Oncol.* (2012), doi:10.1200/JCO.2011.40.9169.

11. J. J. Molenaar, J. Koster, D. A. Zwijnenburg, P. van Sluis, L. J. Valentijn, I. van der Ploeg, M. Hamdi, J. van Nes, B. A. Westerman, J. van Arkel, M. E. Ebus, F. Haneveld, A. Lakeman, L. Schild, P. Molenaar, P. Stroeken, M. M. van Noesel, I. Ora, E. E. Santo, H. N. Caron, E. M. Westerhout, R. Versteeg, Sequencing of neuroblastoma identifies chromothripsis and defects in neuritogenesis genes., *Nature* **483**, 589–93 (2012).
12. T. J. Pugh, O. Morozova, E. F. Attiyeh, S. Asgharzadeh, J. S. Wei, D. Auclair, S. L. Carter, K. Cibulskis, M. Hanna, A. Kiezun, J. Kim, M. S. Lawrence, L. Lichtenstein, A. McKenna, C. S. Pdamallu, A. H. Ramos, E. Shefler, A. Sivachenko, C. Sougnez, C. Stewart, A. Ally, I. Birol, R. Chiu, R. D. Corbett, M. Hirst, S. D. Jackman, B. Kamoh, A. H. Khodabakshi, M. Krzywinski, A. Lo, R. A. Moore, K. L. Mungall, J. Qian, A. Tam, N. Thiessen, Y. Zhao, K. A. Cole, M. Diamond, S. J. Diskin, Y. P. Mosse, A. C. Wood, L. Ji, R. Sposto, T. Badgett, W. B. London, Y. Moyer, J. M. Gastier-Foster, M. A. Smith, J. M. G. Auvil, D. S. Gerhard, M. D. Hogarty, S. J. M. Jones, E. S. Lander, S. B. Gabriel, G. Getz, R. C. Seeger, J. Khan, M. A. Marra, M. Meyerson, J. M. Maris, The genetic landscape of high-risk neuroblastoma., *Nat. Genet.* **45**, 279–84 (2013).
13. R. Lee, C. Stewart, S. Carter, A remarkably simple genome underlies highly malignant pediatric rhabdoid cancers, *J. Clin. Invest.* **122**, 2983–88 (2012).
14. T. Fujiwara, J. Fukushi, S. Yamamoto, Y. Matsumoto, N. Setsu, Y. Oda, H. Yamada, S. Okada, K. Watari, M. Ono, M. Kuwano, S. Kamura, K. Iida, Y. Okada, M. Koga, Y. Iwamoto, Macrophage infiltration predicts a poor prognosis for human ewing sarcoma., *Am. J. Pathol.* **179**, 1157–70 (2011).
15. M. A. Aznar, N. Tinari, A. J. Rullán, A. R. Sánchez-Paulete, M. E. Rodríguez-Ruiz, I. Melero, Intratumoral Delivery of Immunotherapy-Act Locally, Think Globally., *J. Immunol.* **198**, 31–39 (2017).
16. J. D. Brody, W. Z. Ai, D. K. Czerwinski, J. A. Torchia, M. Levy, R. H. Advani, Y. H. Kim, R. T. Hoppe, S. J. Knox, L. K. Shin, I. Wapnir, R. J. Tibshirani, R. Levy, In situ vaccination with a TLR9 agonist induces systemic lymphoma regression: a phase I/II study., *J. Clin. Oncol.* **28**, 4324–32 (2010).
17. Y. H. Kim, D. Gratzinger, C. Harrison, J. D. Brody, D. K. Czerwinski, W. Z. Ai, A. Morales, F. Abdulla, L. Xing, D. Navi, R. J. Tibshirani, R. H. Advani, B. Lingala, S. Shah, R. T. Hoppe, R. Levy, In situ vaccination against mycosis fungoides by intratumoral injection of a TLR9 agonist combined with radiation: a phase 1/2 study., *Blood* **119**, 355–63 (2012).
18. R. H. I. Andtbacka, H. L. Kaufman, F. Collichio, T. Amatruda, N. Senzer, J. Chesney, K. A. Delman, L. E. Spitler, I. Puzanov, S. S. Agarwala, M. Milhem, L. Cranmer, B. Curti, K. Lewis, M. Ross, T. Guthrie, G. P. Linette, G. A. Daniels, K. Harrington, M. R. Middleton, W. H. Miller, J. S. Zager, Y. Ye, B. Yao, A. Li, S. Doleman, A. VanderWalde, J. Gansert, R. Coffin, Talimogene Laherparepvec Improves Durable Response Rate in Patients With Advanced Melanoma., *J. Clin. Oncol.* **33**, 2780–8 (2015).
19. J. Fu, D. B. Kanne, M. Leong, L. H. Glickman, S. M. McWhirter, E. Lemmens, K. Mechette, J. J. Leong, P. Lauer, W. Liu, K. E. Sivick, Q. Zeng, K. C. Soares, L. Zheng, D. A. Portnoy, J. J. Woodward, D. M. Pardoll, T. W. Dubensky, Y. Kim, STING agonist formulated cancer vaccines can cure established tumors resistant to PD-1 blockade., *Sci. Transl. Med.* **7**, 283ra52 (2015).
20. D. Zamarin, R. B. Holmgaard, S. K. Subudhi, J. S. Park, M. Mansour, P. Palese, T. Merghoub, J. D. Wolchok, J. P. Allison, Localized Oncolytic Virotherapy Overcomes Systemic Tumor Resistance to Immune Checkpoint Blockade Immunotherapy, *Sci. Transl. Med.* **6**, 226ra32–226ra32 (2014).
21. R. Houot, R. Levy, T-cell modulation combined with intratumoral CpG cures lymphoma in a mouse model without the need for chemotherapy., *Blood* **113**, 3546–52 (2009).
22. A. Marabelle, H. Kohrt, I. Sagiv-Barfi, B. Ajami, R. Axtell, G. Zhou, R. Rajapaksa, M. R. Green, J.

Torchia, J. Brody, R. Luong, M. D. Rosenblum, L. Steinman, H. I. Levitsky, V. Tse, R. Levy, Depleting tumor-specific Tregs at a single site eradicates disseminated tumors, *J. Clin. Invest.* **Jun 3; 123**, 2447–2463 (2013).

23. I. Puzanov, M. M. Milhem, D. Minor, O. Hamid, A. Li, L. Chen, M. Chastain, K. S. Gorski, A. Anderson, J. Chou, H. L. Kaufman, R. H. I. Andtbacka, Talimogene Laherparepvec in Combination With Ipilimumab in Previously Untreated, Unresectable Stage IIIB-IV Melanoma, *J. Clin. Oncol.* , JCO671529 (2016).

24. G. V Long, R. Dummer, A. Ribas, I. Puzanov, A. VanderWalde, R. H. I. Andtbacka, O. Michielin, A. J. Olszanski, J. Malvehy, J. S. Cebon, E. Fernandez, J. M. Kirkwood, T. Gajewski, C. K. Gause, L. Chen, K. Gorski, A. Anderson, D. R. Kaufman, J. Chou, F. S. Hodi, Efficacy analysis of MASTERKEY-265 phase 1b study of talimogene laherparepvec (T-VEC) and pembrolizumab (pembro) for unresectable stage IIIB-IV melanoma., *ASCO Meet. Abstr.* **34**, 9568 (2016).

25. M. S. Merchant, M. Wright, K. Baird, L. H. Wexler, C. Rodriguez-Galindo, D. Bernstein, C. Delbrook, M. Lodish, R. Bishop, J. D. Wolchok, H. Streicher, C. L. Mackall, Phase I Clinical Trial of Ipilimumab in Pediatric Patients with Advanced Solid Tumors., *Clin. Cancer Res.* **22**, 1364–70 (2016).

26. B. Georger, C. Bergeron, L. Gore, L. Sender, I. J. Dunkel, C. Herzog, L. Brochez, O. Cruz, K. Nysom, E. Berghorn, B. Simsek, J. Shen, A. Pappo, Phase II study of ipilimumab in adolescents with unresectable stage III or IV malignant melanoma, *Eur. J. Cancer* **86**, 358–363 (2017).

27. M. Barro, J. T. Patton, Rotavirus NSP1 Inhibits Expression of Type I Interferon by Antagonizing the Function of Interferon Regulatory Factors IRF3, IRF5, and IRF7, *J. Virol.* **81**, 4473–4481 (2007).

28. A. Ribas, R. Dummer, I. Puzanov, A. VanderWalde, R. H. I. Andtbacka, O. Michielin, A. J. Olszanski, J. Malvehy, J. Cebon, E. Fernandez, J. M. Kirkwood, T. F. Gajewski, L. Chen, K. S. Gorski, A. A. Anderson, S. J. Diede, M. E. Lassman, J. Gansert, F. S. Hodi, G. V. Long, Oncolytic Virotherapy Promotes Intratumoral T Cell Infiltration and Improves Anti-PD-1 Immunotherapy, *Cell* **170**, 1109–1119.e10 (2017).

## Acknowledgements:

Paul Berchard, Melissa Husson and Valentin Dettling, technical students for their helps.  
IHOP, La Ligue contre le cancer, Lyric and INCA for fundings.

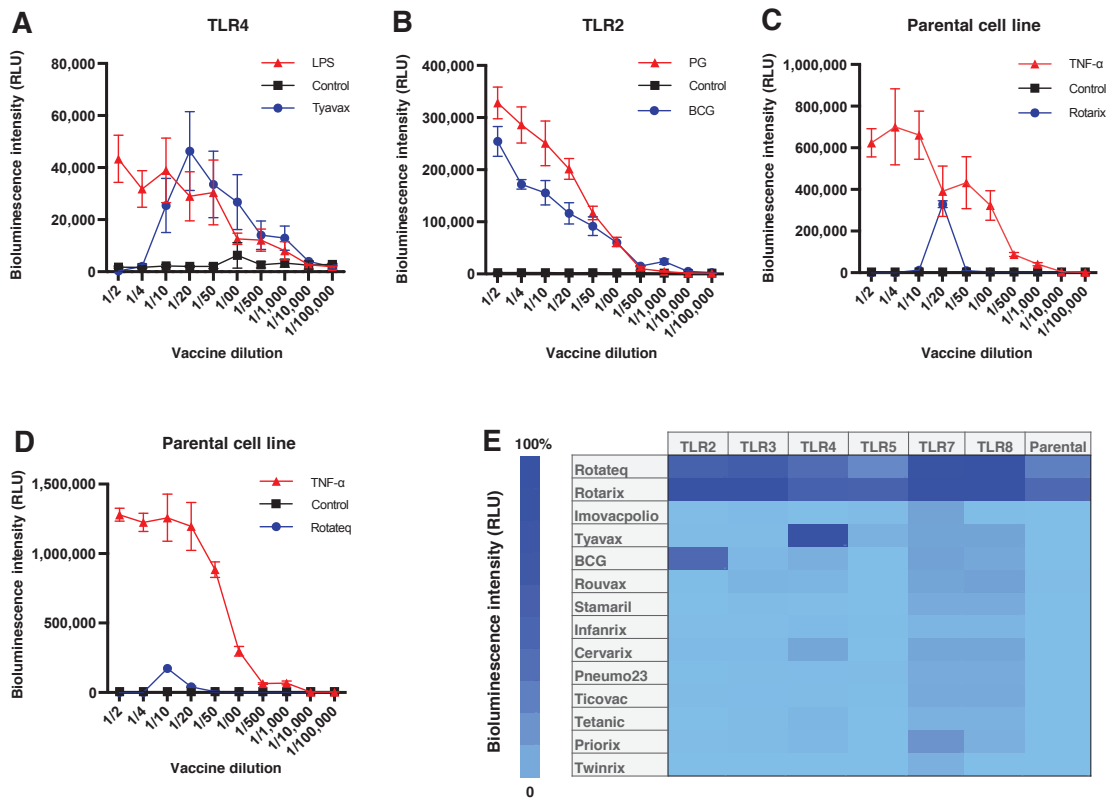


**Fig1) Proinflammatory features of Rotavirus vaccines:** NF-κB activation in transgenic cell lines expressing specific Toll-like receptors (TLR) and NF-κB-Luc reporter system by different dilutions of **A)** the Typhoid Fever vaccine (Tyavax®) **B)** Mycobacterium tuberculosis vaccine (BCG Pasteur®). Data are represented as RLU bioluminescence intensity. Red line represents natural ligand of the TLR, blue line represents the vaccine and the black line is negative control (medium). **C-D)** NF-κB activation in 293 T parental cell line that doesn't express any TLR but contains NF-κB reporter system by **C)** Rotarix and **D)** Rotateq. Data are (mean ± s.e.m), n=3 well per dilution. **E)** Heat map of NF-κB activation capacity of 14 anti-infectious vaccines at optimal dilution using transgenic reporter cell lines expressing specific Toll-like receptors (TLR) and NF-κB-Luc reporter system. The normalization is done using the corresponding natural TLR ligand at optimal dilution as a positive control (100%). The highest bioluminescence intensity is represented in dark blue and lowest in light blue. TLR9 and TLR6 cell lines were equally activated by rotavirus vaccines but the ratio have not been depicted because of the lack of positive control activation of the corresponding NF-κB cell lines by synthetic ligands (supplementary data 1).

**Fig 1**

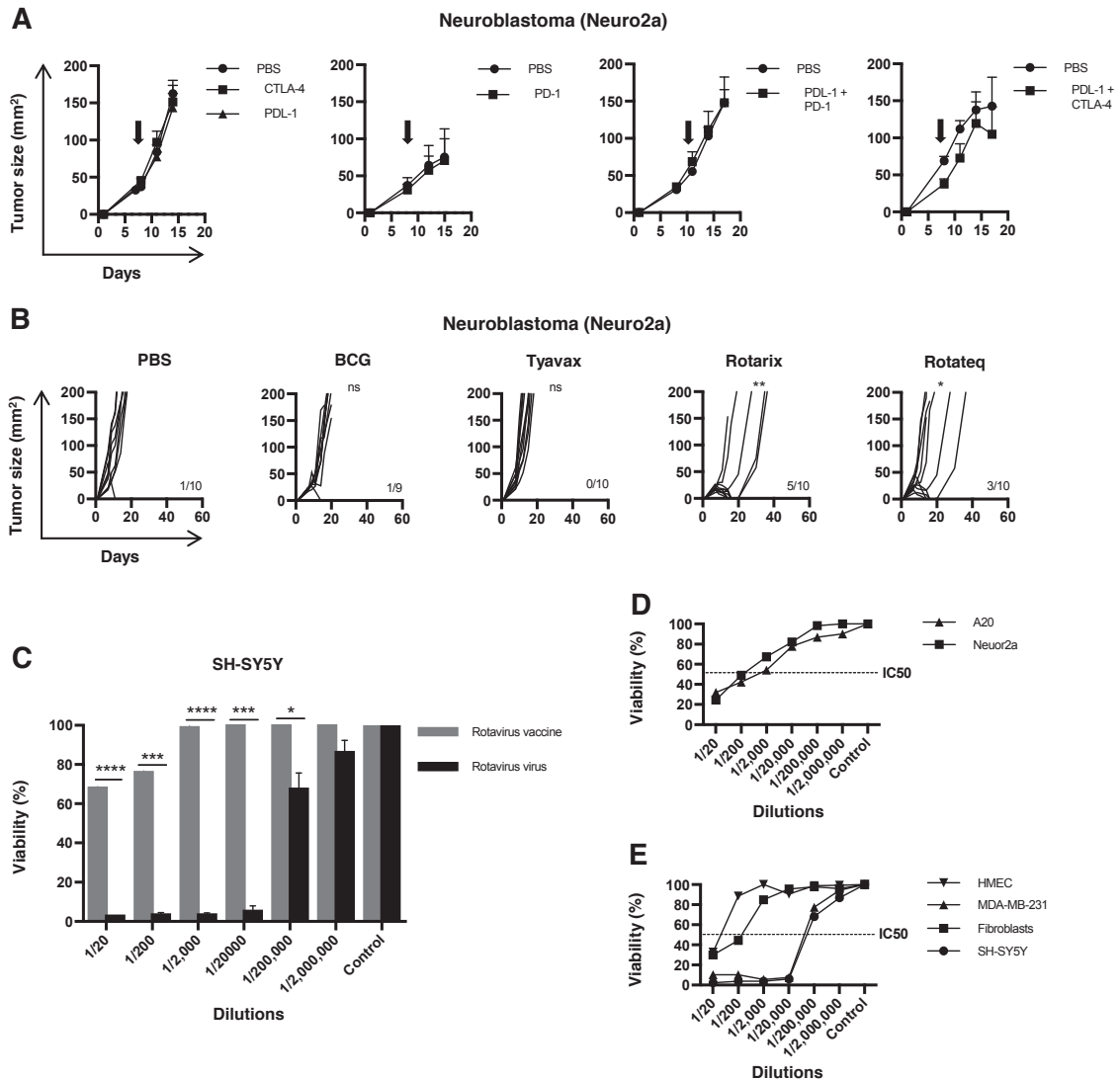


**Fig2) Rotavirus vaccines have antitumor activity against pediatric tumor models resistant to anti-CTLA-4 and anti-PD-1 (-L1):** **A**) Intraperitoneal (IP) injection of 200µg of αCTLA4 or αPD1/L1 alone or in combination in Murine Neuroblastoma model (Neuro2a). The mice were injected subcutaneously with 5x10<sup>6</sup> of Neuro2a murine cell line. The therapy started at Day 7 (black arrow) for 4 injections every 3 days. Data are (mean±s.e.m), n=10 mice per group. **B**) Intra-tumoral injection of NF-κB activating vaccine (Tyavax, BCG, Rotarix, Rotateq) in Neuro2a mice model. 3 consecutive intra-tumoral (IT) injections of (100 µl of the vaccines) every 3 days. n=10 mice per group, each group compared to PBS, (Unpaired one tailed t-test), ns=no significant, \*p<0.05 and \*\*p<0.005. **C**) Cytotoxic effect evaluated by Sulforhodamine B (SRB) assay of different components of Rotavirus vaccines: vaccine (~ 5,5x 10<sup>8</sup>pfu/ml), Rotavirus strain (virus) (100-1000x vaccine concentration; a mixture of 5,5x10<sup>7</sup> to 5,5x10<sup>8</sup> of 5 different Rotavirus strain) or excipient (see Fig S3) on Neuroblastoma human cell line (SH-SY5Y). (mean ± s.e.m), n=3 well per dilution, (Unpaired one tailed t-test) \*p<0.05, \*\*\*p=0.0001 and \*\*\*\*p<0.0001. **D**) IC50 of Rotavirus strain studied by SRB assay on NB murine cell line (Neuro2a) and Murine Lymphoma (A20). **E**) IC50 of Rotavirus strains studied by SRB assay, on normal cells (fibroblast and HMEC) compared to human triple negative breast cancer (MDA-MB-231) and human Neuroblastoma (SH-SY5Y). 1/10 serial dilution were performed from 1/20 to 1/2,000,000. The incubation time is 3 days on HMEC and MDA-MB231 or 5 days for SH-SY5Y, Fibroblasts, Neuro2a and A20.

**Fig 2**

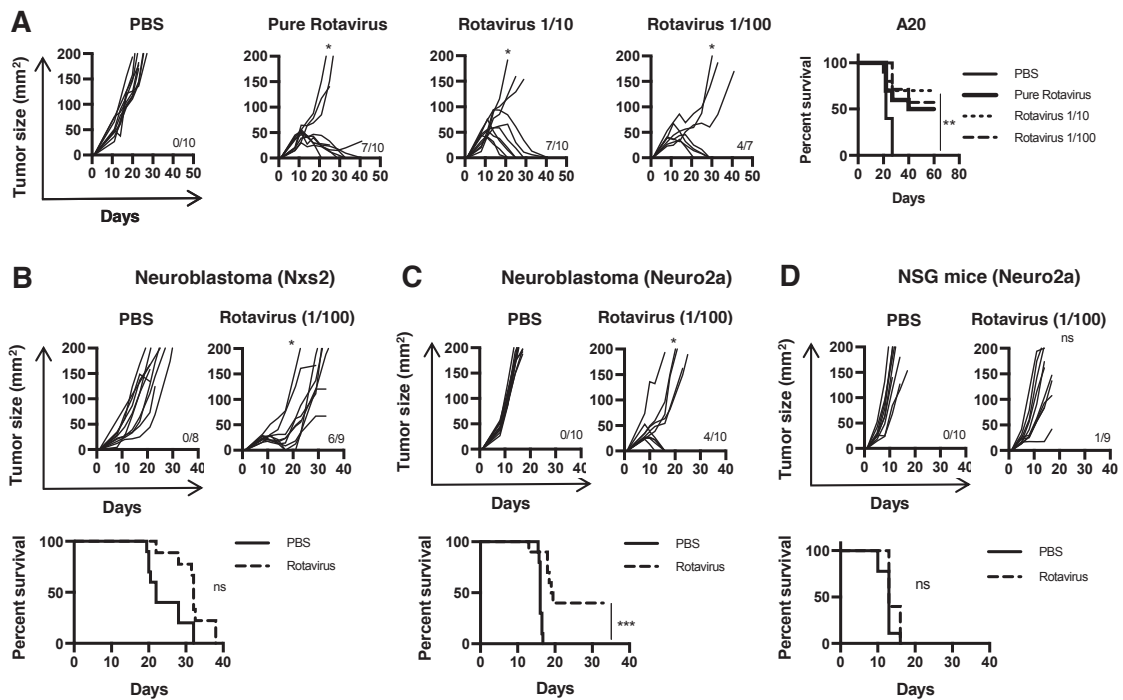


**Fig3) In vitro oncolytic properties of Rotavirus strains translate into in vivo anti-tumor immunity:** **A**) In vivo anti-tumor effect of the Rotavirus virus on A20 Lymphoma syngeneic mice model ( $5 \times 10^6$  tumor cell line were injected subcutaneously per mice for tumor graft), 3 injections of pure virus, 1/10 and 1/100 dilution were performed every 3 days (day 7, day10 and day 13) and tumor size was evaluated twice a week using formula surface = (length x width). n=10 mice per group, mean of different Rotavirus strain dilution compared to PBS, (Unpaired one tailed t-test), \* $p < 0.05$ , survival rate (log-rank test), \*\* $p=0.001$ . **B**) In vivo anti-tumor effect of 3 injections of 100 $\mu$ l of the 1/100 dilution of the vaccine, every 3 days in 2 murine syngeneic Neuroblastoma mice model NXS2, n=8 or 9 mice per group (paired one tailed t-test), \* $p < 0.05$ , Survival rate (log-rank test), ns=no significant, and **C**) Neuro2a, n=10 mice per group (Unpaired one tailed t-test), \* $p < 0.05$ , survival rate (log-rank test), \*\*\* $p=0.0001$ . **D**) In vivo anti-tumor effect of the same 3 injections of 1/100 Rotavirus virus in NSG immunodeficient mice, n=10 or 9 mice per group (Unpaired one tailed t-test), ns=no significant.

**Fig 3**

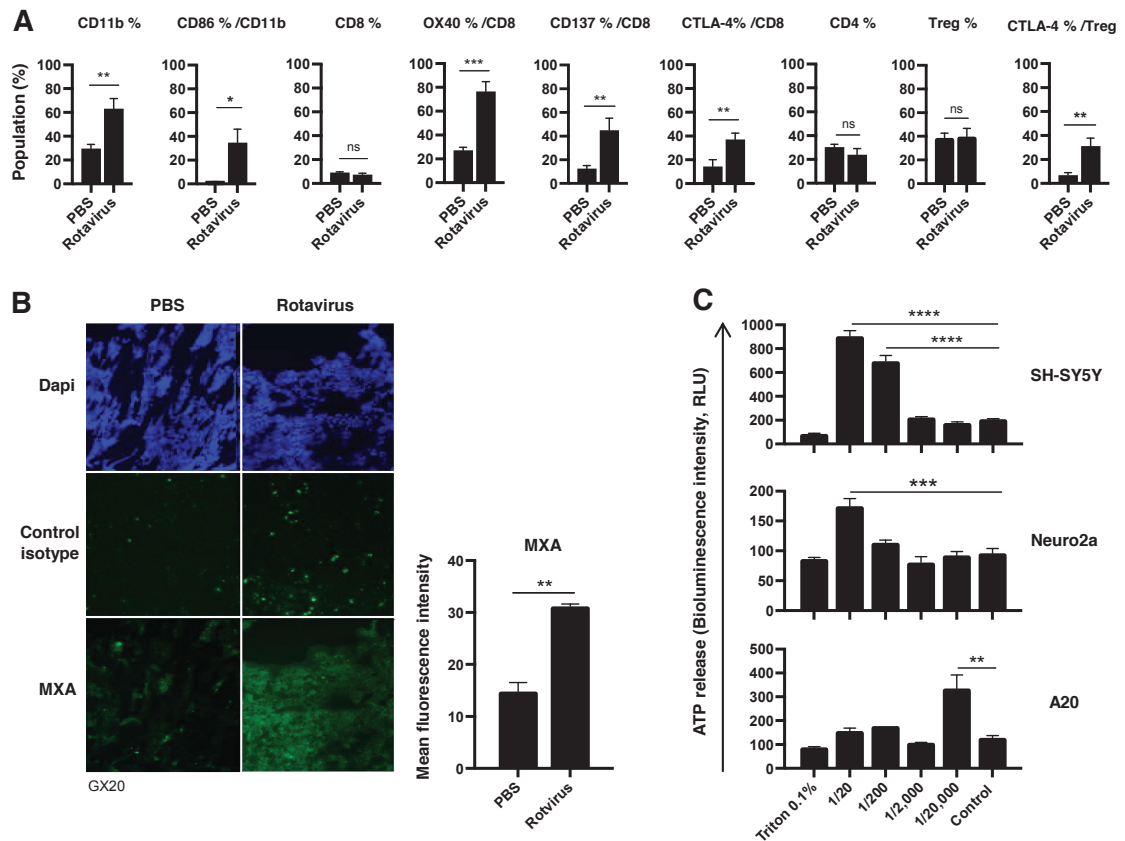


**Fig4) Immunostimulatory properties of intra-tumoral Rotavirus injection:** **A**) Tumor-infiltrating immune cells were studied 24 hours after the first intra-tumoral injection in Neuro2a tumor model by flow cytometry. Results are presented as % of CD11b/CD8/CD4 cells from CD45+ population and Tregs were gated as foxp3+ cell in the CD4+ population. Rotavirus injected tumors were compared to PBS injected tumor. Data are (mean± s.e.m), n=5 mice per group (Unpaired one tailed t-test), \*p< 0.05, \*\*p<0.005, \*\*\*p<0.0005. **B**) Immunofluorescence staining with anti-Mxa specific mAb on frozen tumor section from 24 hours Rotavirus or PBS treated mice bearing A20 tumors. Isootype control mAb was used as negative control for MxA detection (in green) after Dapi counterstaining (in blue). Typical pictures of MxA positive cells are presented demonstrating 100% of MxA positive cells 24 h after rotavirus treatment (left panel) and The mean of immunofluorescence intensity measured by image J software and presented in the right panel. Data are (mean± s.e.m), n=2 mice in each group with 3 tumor section (Unpaired one tailed t-test), \*\*p=0.005. **C**) ATP release measurement was performed by luminescence assay using CellTiter-Glo® Luminescent Cell Viability Assay kit on human (SH-SY5Y), murine Neuroblastoma (Neuro2a) and murine Lymphoma (A20) tumor cell lines, 48 hours after incubation with different dilution of Rotavirus. Results are reported as RLU intensity corresponding to relative ATP release intensity. Data are (mean± s.e.m), n=3 well per dilution (one way Anova test), \*\*\*\*p< 0.0001, \*\*\*p<0.0005, \*\*p<0.005.

**Fig 4**

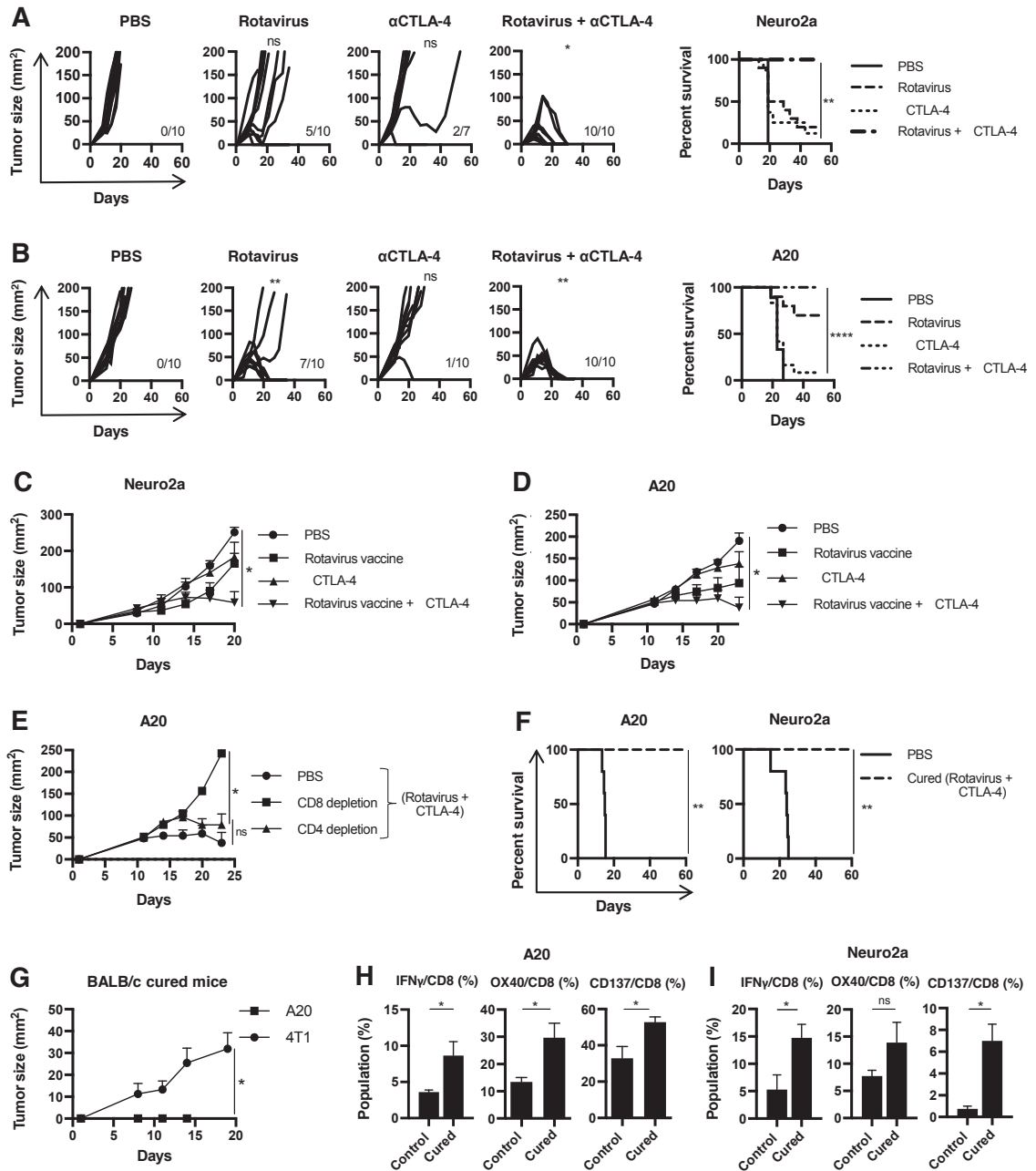


**Fig 5**

**Fig5) Rotavirus overcomes ICT resistance and synergizes with  $\alpha$ CTLA-4 to generate a CD8+ T-cell anti-tumor immune response:** Tumor measurement of combination of Rotavirus and  $\alpha$ CTLA-4, after 3 IT injection of 100  $\mu$ l Rotavirus (1/100) + 4 IP injection of 200 $\mu$ g of  $\alpha$ CTLA-4 with 3 days interval in **A**) Neuroblastoma (Neuro2a) and **B**) Lymphoma (A20). n=10 mice per group and each group compared to PBS (Unpaired one tailed t-test), \*p<0.05 and \*\*p<0.005, survival rate (rank-log test), \*\*p=0.002 and \*\*\*\*p<0.0001. **C**) Combination of Rotavirus vaccine with  $\alpha$ CTLA-4 in Neuroblastoma (Neuro2a) and **D**) Lymphoma (A20) with the same protocol. (mean $\pm$ s.e.m), n=10 or 9 mice per group (Unpaired one tailed t-test), \*p<0.05. **E**) Tumor measurement after CD8 and CD4 T cell depletion in mice treated with Rotavirus+ $\alpha$ CTLA-4. n=10 mice per group (Unpaired one tailed t-test), \*p<0.05. **F**) Survival rate of cured mice from Lymphoma and Neuroblastoma after injection with the same tumor. n= 5 mice per group, survival rate (log-rank test), \*\*p<0.005. **G**) Tumor measurement of cured mice from A20 lymphoma after injection with A20 lymphoma and 4T1 mammary tumor. (mean $\pm$ s.e.m), n= 3 mice per group, (Unpaired one tailed t-test), \*p<0.05. **H**) Splenocyte of cured mice from Lymphoma (A20) and control mice bearing Lymphoma (A20) treated by PBS, co-cultured with A20 tumor cell lines for 4 days, then CD8 T were stained for intracellular IFN $\gamma$  and surface activation markers. (mean $\pm$ s.e.m), n=3 mice per group (Unpaired one tailed t-test) \*p<0.05. **I**) The same experiment as described for Neuroblastoma (Neuro2a). (mean $\pm$ s.e.m), n=3 mice per group (Unpaired one tailed t-test) ns= no significant, \*p<0.05.

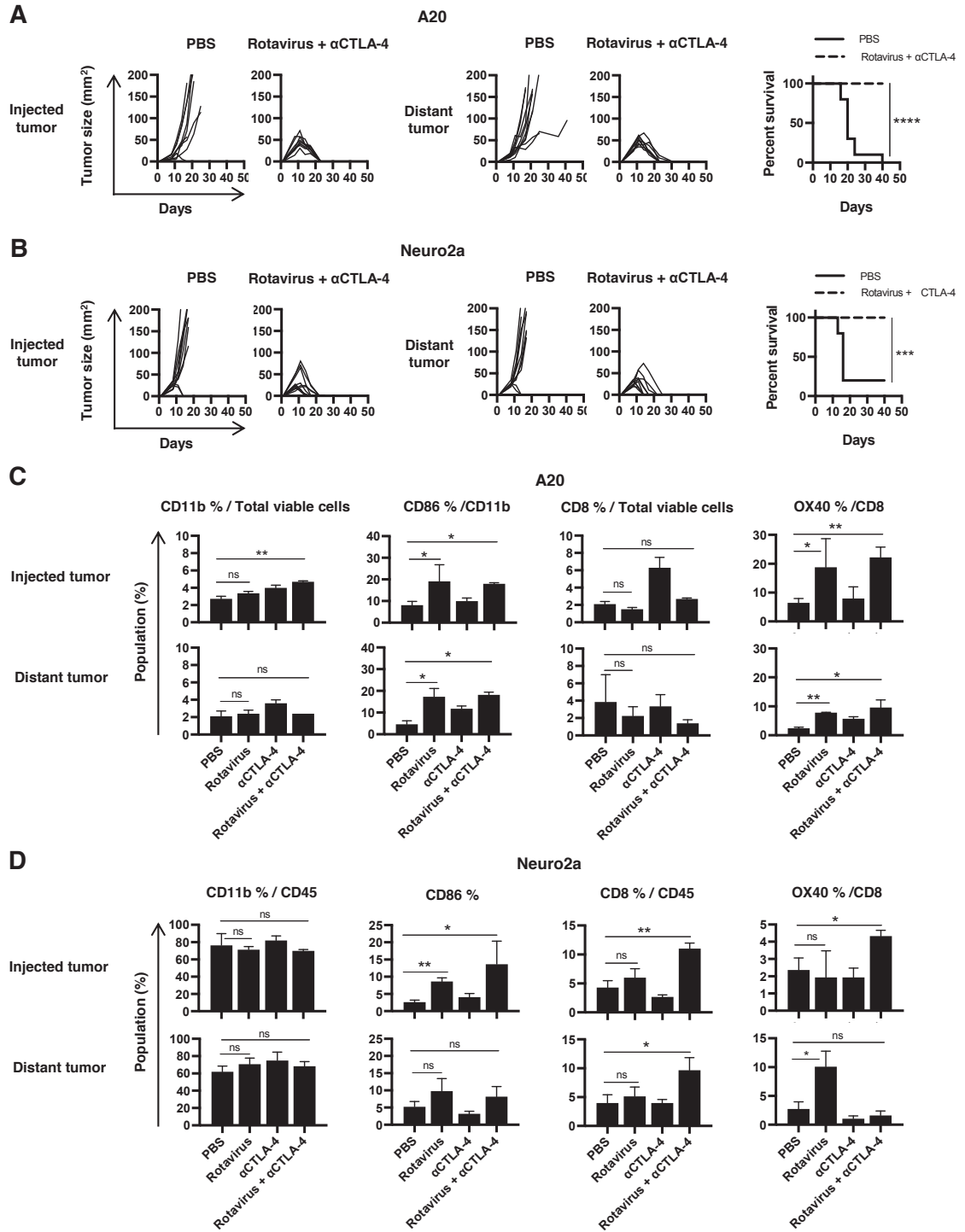
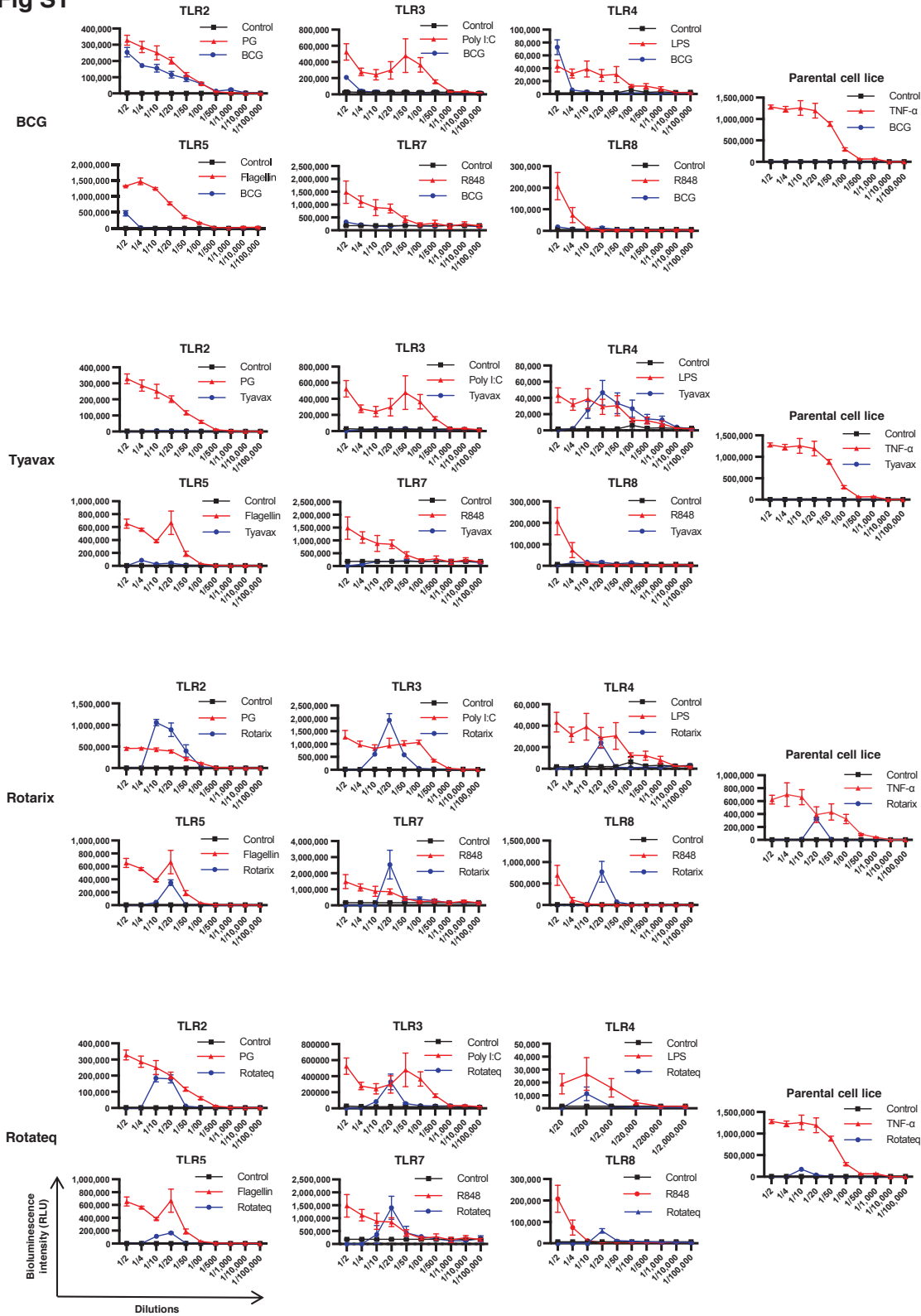


**Fig 6**

**Fig6) Intratumoral Rotavirus generates abscopal effect and durable tumor-specific immunity:** **A)** Lymphoma (A20) and **B)** Neuroblastoma (Neuro2a) mice model bearing 2 tumors. Rotavirus injection was done in one tumor and abscopal effect of Rotavirus and  $\alpha$ CTLA-4 combination was evaluated in distant tumor by tumor surface evaluation compare to PBS. Data are (mean $\pm$ s.e.m). n=10 mice per group, survival rate (log-rank test),\*\*\*p<0.0001, \*\*p<0.0005. **C)** Flow cytometry analysis of injected and distant Lymphoma (A20) tumors, excised 24 hours after second injection of Rotavirus and  $\alpha$ CTLA-4. CD11b and CD8 cells are gated from total lived cells (A20 tumor cells are CD45+ and cannot be excluded from immune infiltrating cell) for OX40 and CD86 marker analysis. n=3 mice per group data are (mean  $\pm$  s.e.m), Rotavirus and Rotavirus+ $\alpha$  CTLA-4 treated mice are compared to PBS treated mice (Unpaired one tailed t-test), ns=no significant, \*p < 0.05 and \*\*p<0.005. **D)** Flow cytometry analysis of injected and distant Neuroblastoma (Neuro2a) tumors, excised 24h after second injection of Rotavirus. CD11b and CD8 are gated from CD45+ cells, for OX40 and CD86 marker analysis. n=3 mice per group data are (mean  $\pm$  s.e.m), Rotavirus and Rotavirus+ $\alpha$  CTLA-4 treated mice are compared to PBS treated mice (Unpaired one tailed t-test) ns=no significant, \*p < 0.05and \*\*p<0.005.

**Fig S1**



**Supplementary data:**

**FigS1:** a) NF- $\kappa$ B activation capacities of different dilutions of Mycobacterium tuberculosis vaccine (BCG Pasteur<sup>®</sup>), the Typhoid Fever vaccine (Tyavax<sup>®</sup>), Rotarix and Rotateq vaccines in transgenic cell lines expressing specific TLR and NF- $\kappa$ B reporter system. Red line represents natural ligand of the TLR, blue line represents the vaccine and the black is negative control. (Normalization is done as described before in Fig.1e). Data are (mean  $\pm$  s.e.m), n=3 well per dilutions.

**Fig S2**

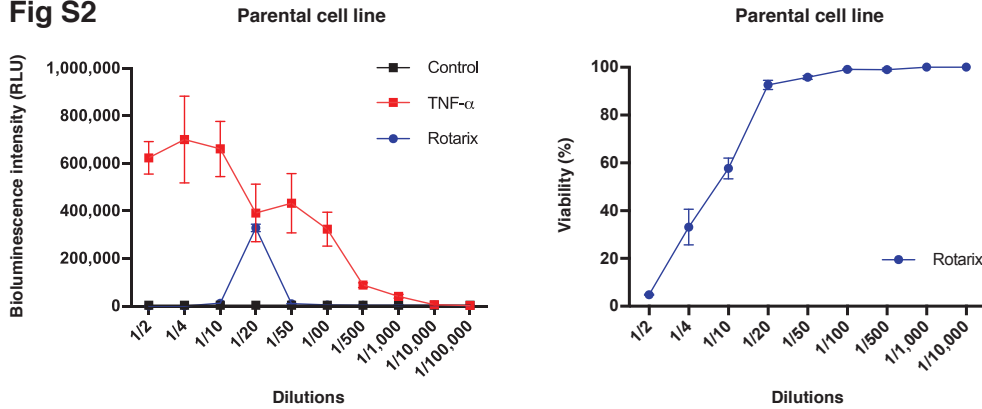


**Fig S3**

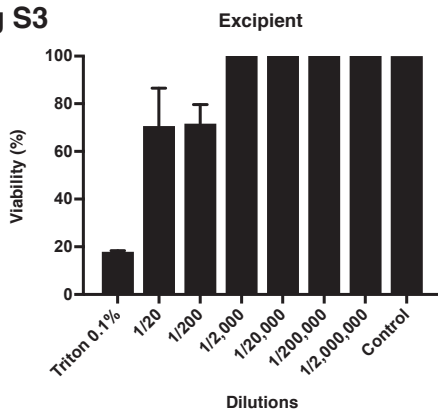
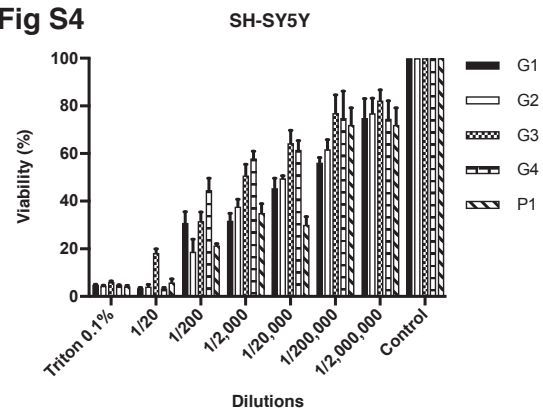


**Fig S4**



**FigS2:** In left figure, NF- $\kappa$ B activation by Rotavirus at 1/20 dilution in 293 T parental cell line. In right figure, cytotoxic analysis by SRB assay on 293 T parental cells line.n=3 well per dilution.

**FigS3:** Excipient cytotoxic effect analysis by SRB assay on SH-SY5Y after 5 days of incubation. . Data are mean  $\pm$  s.e.m.n=3 well per dilution.

**FigS4:** Sulforhodamine B (SRB) assay of each Rotavirus strain (G1, G2, G3, G4 and P1) individually on human Neuroblastoma cancer cell line (SH-SY5Y) (5 complete day of incubation). Data are mean  $\pm$  s.e.m, n=3 well per dilutions.